2023

Graphene-based biosensors for quantitative characterisation of DNA methylation

Safarzadeh, Mina

Copyright

UNIVERSITY OF
PLYMOUTH

Graphene-based biosensors for quantitative characterisation of DNA methylation

by

Mina Safarzadeh

A thesis submitted to the University of Plymouth
in partial fulfilment for the degree of

DOCTOR OF PHILOSOPHY

School of Engineering, Computing and Mathematics

January 2023

Acknowledgements

I would like to extend my sincere gratitude to my director of studies Professor Genhua Pan for his trust, patience and endless understanding and support. This experience has proven to be an invaluable step in my life and has improved me as a researcher and as a human being. Also I would like to express appreciation to my second supervisor, Dr. David Jenkins for his time and advises for my publications, as well as Mr. Nick Fry for his teachings in the lab. I would also want to appreciate Ms. Lorelei Robertson and Dr. Shaoliang Guan for performing certain measurements for my publications.

Furthermore I would also like to thank my colleagues and labmates, namely Dr. Jagriti Sethi, Dr. Ahmed Suhail, Dr. Benjamin O'Driscoll and future doctors: Mr. Theodore Bungon and Dr. Jonathan Bloor for their presence, comments and suggestions also for all of the talks, breaks and coffees we had together and for encouraging each other to go over PhD life. I also appreciate all of the AiPBAND ESRs especially Vanessa, Yagmur and Meenu, I learned a lot from them and we had so much fun together which I will never forget. I would like to thank my lovely friends in Plymouth especially Aira, Ahmed Ali, Ahmed Hammed, Hiba and Selin for all of the fun we had together and for making my time in the UK more lively and enjoyable. Special thanks to my best friends Nazanin, Foroozan, Maryam, Asma, Elli, Niloo and Monisha for all of the fun I had with them and all of the support I received from them even though I was far from them.

I am immensely grateful to my family, my parents, my brothers and my sisters in law for their love, motivation, encouragement and patience. I would like to express my love to my nieces and nephew Yekta, Hannah and Sina :-) and appreciate the love and happiness I received from them and hope that some day they will read my thesis. There are no words to express my gratitude to my husband, for his non-stop support, inspiration and encouragement. I am grateful for all that only he knows.

Authors declaration

At no time during the registration for the degree of Doctor of Philosophy has the author been registered for any other University award without prior agreement of the Doctoral College Quality Sub-Committee.

Work submitted for this research degree at the University of Plymouth has not formed part of any other degree either at the University of Plymouth or at another establishment.

Word count for the main body of this thesis: **21401**

Signed: 

Date: July 21, 2023

Abstract

Graphene-based biosensors for quantitative characterisation of DNA methylation

by

Mina Safarzadeh

DNA methylation is associated with various diseases including cancer, cardiovascular diseases and neurodegenerative disorders, making it a potential biomarker to diagnose and prognose these diseases. Hence, a tool to detect and quantify DNA methylation can be valuable to improve clinical tests. In this thesis, we report two different biosensors for the detection and quantification of methylated tumour suppressor gene, O-6-methylguanine-DNA methyltransferase (MGMT), which is a potential biomarker for brain tumours and breast cancer. Both of the reported biosensors in this thesis are based on screen-printed reduced graphene oxide electrodes (rGO SPEs) and are electrochemical biosensors.

In the Ab/ssDNA biosensor the rGO SPEs were first aminated by ammonium hydroxide chemisorption prior to their incubation in the anti-5-methylcytosine monoclonal antibody (anti-5mC) which acted as a methylation bioreceptor. After that, the target single-strand (ss) MGMT oligonucleotide is first recognised by its hybridisation with complementary DNA to form double-stranded (ds) MGMT, which is then captured by anti-5mC on the electrode surface due to the presence of methylation. The amination of the rGO electrodes were confirmed using XPS and Raman spectroscopy techniques. The assay development was tested via voltammetry techniques, namely CV and DPV. Furthermore, some of the preparation steps were optimized to achieve a better performance of the biosensor. Our validation studies showed that the peak current generated by the biosensor is proportional to the concentration of MGMT (both single stranded and previously hybridized double stranded) in the range of 50 fM to 500 pM, demonstrating the efficacy of the sensor. A selectivity experiment was also carried out in order to confirm that the biosensor is uniquely selective towards the methylated gene. Although, this biosensor is selective to the target biomarker when applied to previously hybridized dsDNA, it is not selective when detecting ssDNA because it responds to the methyl group regardless of the ssDNA sequence, so a hybridization step is needed to select the target ssDNA sequence from a mixture of strands. This drawback was the driving force behind the design and development of the second biosensor. To the best of our knowledge, this biosensor is the first report on the detection of MGMT genes, using rGO electrodes.

To achieve the ability to directly detect dsDNA as a biomarker without denaturating it to ssDNA, the PNA/Ab biosensor was designed. This biosensor is a sandwich assay based on gold nanoparticles (AuNPs) decorated rGO electrodes to achieve high conductivity and allow self-assembly of nucleic acids. Peptide nucleic acid (PNA) was used to form a self-assembled monolayer (SAM) on the surface via amine-AuNPs interaction. PNA acts as a bio-recognition layer for the target ds-MGMT gene sequence,

by invasion of the double strand and the formation of triple helix. The methylation was subsequently captured by biotinylated-anti-5mC which was then detected via amperometry. This results in a biosensor concept that is uniquely sensitive to both the target MGMT gene as well as its methylation. PNA has a high affinity to its complementary DNA relative to other natural nucleic acids and allows ds-DNA detection directly. Direct detection of double stranded DNA biomarkers removes the need for sample preparation (such as denaturation or hybridization) and makes the biosensor faster and easier to use. It may also result in a higher reliability of the biosensor due to the elimination of the risk of mistakes in the sample preparation step. To achieve this, the reduction of GO was performed in two ways: electrochemically (ErGO) and thermally (TrGO). XPS and Raman spectroscopy as well as voltammetry techniques showed that the ErGO was more efficiently reduced, had higher C/O ratio as well as smaller crystallite size of the sp^2 lattice and also was more stable during voltammetric measurements. It was also shown that the electro-deposition of AuNPs was more successful on the ErGO surface due to the higher At% of AuNPs. SEM images and EDS spectra also confirmed the presence of AuNPs on the surface. Therefore, the ErGO/AuNPs electrode was used to fabricate biosensors and to detect the ds-MGMT gene. To the best of our knowledge, this is the first report on using PNA to detect methylated DNA and the first report on the detection of double stranded methylated DNA.

Both of the above biosensor designs can be modified and tailor-made to detect other methylated genes, making them promising platforms to detect a variety of methylated biomarkers.

Abbreviations

Anti5-mC	Anti-5methylcytosine
AuNP	Gold nanoparticles
BBB	Blood Brain Barrier
BSA	Bovine Serum Albumin
cfDNA	Circulating free DNA
CNS	Central Nervous System
CNT	Catbon nanotube
CTC	Circulating Tumor Cells
ctDNA	Circulating tumor DNA
CSF	Cerebrospinal fluid
CV	Cyclic Voltammetry
CT	Computed Tomography
Denv-3	Dengue Virus-3
DNA	Deoxyribonucleic acid
DNMT	DNA methyltransferases
dsDNA	Double strand DNA
DPV	Differential Pulse Voltammetry
EDS	Energy-dispersive X-ray spectroscopy
EGOFET	Electrolyte-gated organic FET
EIS	Electrochemical Impedance Spectroscopy
ELISA	Enzyme-linked Immunosorbent Assay
EV	Extracellular Vesicles
FET	Field Effect Transistor
GBM	Glioblastoma
GCE	Glassy carbon electrode
GO	Graphene oxide
HRP	Horseradish peroxidase
LOD	Limit of detection
MB	Methylene Blue
MGMT	O-6-methylguanine-DNA methyltransferase
miRNA	microRNA
MS	Mass spectrometry
MRI	Magnetic Resonance Imaging
NA	Nucleic Acid
NMNP	Nobel metal nanoparticles
PBS	Phosphate buffered saline
PET	Positron Emission Tomography
PGE	Pencil Graphite Electrode
POC	Point of care devices
RNA	Ribonucleic acid
RSD	Relative standard deviation
rGO	Reduced graphene oxide
RT	Radiation Therapy
SAM	Self Assembled Monolayer

SEM	Scanning Electron Microscopy
SERS	Surface Plasmon Resonance
SPR	Surface-enhanced Raman spectroscopy
ssDNA	Single strand DNA
TJ	Tight Junction
TMB	Tetramethyl benzidine
TMZ	Temozolomide
WHO	World Health Organization
XPS	X-ray Photoelectron Spectroscopy

Contents

List of Figures

List of Tables

Chapter 1

Introduction

1.1 Cancer incidence and mortality

Cancer is one of the foremost causes of death worldwide and is expected to be the most important barrier for improving life expectancy in the 21st century (figure 1.1) (Bray et al., 2018; Siegel et al., 2019). Increases in cancer incidence and mortality along with uncertain prognosis after cancer diagnosis and treatment indicate the demand for new diagnosis techniques (Jayanthi et al., 2017). New biomarker-based diagnosis techniques are expected to improve early diagnosis of cancer which can result in improved prognoses and higher long-term survival rates (Kikuyama et al., 2018; Wang, 2017). Cancer biomarkers are biological molecules that are found in body and can be produced either by a tumour or the body in response to the presence of a tumour. Cancer biomarkers are typically present in the tumour environment, blood, urine or other bodily fluids, and the analysis of these biomarkers is one of the approaches in tumour detection (Rasooly and Jacobson, 2006; Tothill, 2009).

1.2 Brain tumor

1.2.1 Current status of brain tumor and classification

Brain tumors are the most fatal types of central nervous system (CNS) illnesses with low survival rate, high relapse rate and resistance to treatment, making it one of the most dreadful types of cancer. Brain cancer has an incidence rate of 28.57 per 100,000 population with 5-year survival rate of only 33% and average survival duration of 15 to 22 months (Miller et al., 2021; Sonali et al., 2018). Depending on the cell type from

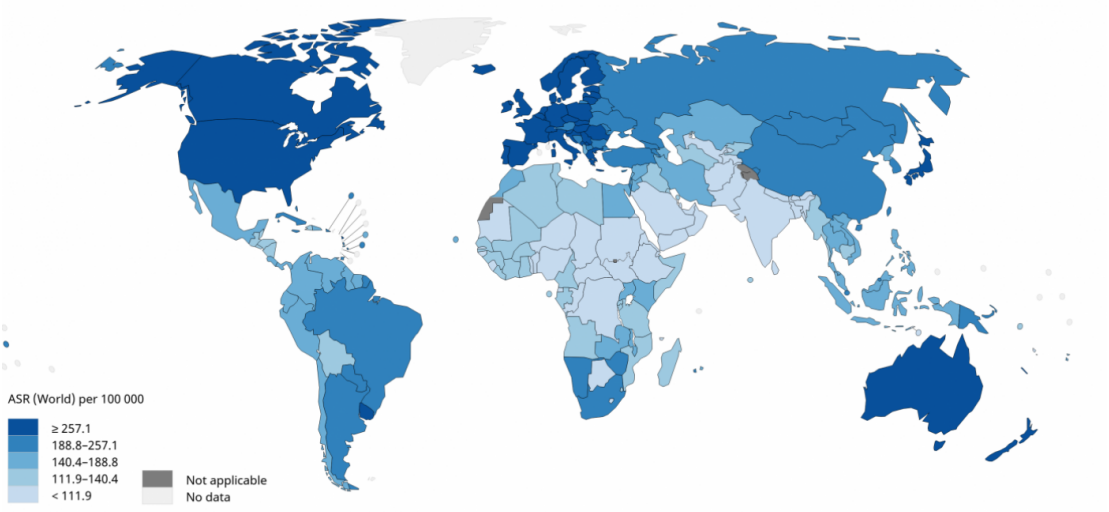

Figure 1.1: Estimated age-standardized incidence rates worldwide in 2020, all cancers, both sexes, ages 0-74. Adopted from WHO (2018).

which the tumor is originated, the position of the tumor and their tendency to grow, the brain tumor can be divided to 130 various types. Some of the classifications of the brain tumors are broad and some are more specific. Tables 1.1 and 1.2 feature the characteristics of primary and secondary brain tumors (Table 1.1) as well as their benign or malignant behaviour (Table 1.2) (Lather and Singh, 2020).

Glioma is the most common type of brain tumor with almost 200,000 new cases every year world wide. Based on the immunophenotypical similarities of the cell types, gliomas are subdivided into astrocytoma, oligodendroglioma, and oligoastrocytoma. Although gliomas usually tend to increase in their malignancy grade, they are appointed in malignancy grades by WHO (Kros et al., 2015). Table 1.3 showed the simplified clas-

Brain tumor	
Primary	**Secondary**
Stem in brain cells May proliferate to other parts of brain/ spine Rarely spread to other organs	Stem in other part of body/ proliferate to brain Named by the location where it stems Treated based on the place of origin More common than primary brain tumor

Table 1.1: Classification of brain tumor into primary and secondary tumors. Adapted from Lather and Singh (2020).

sification of gliomas and their WHO grade. Figure 1.2 shows the distribution of all brain and CNS tumors by behaviour and histology.

Glioblastoma (GBM), with occurrence of almost 50% of all primary brain malignancies and median survival period of only 15 months, is the most frequent and aggressive primary brain tumor in adults. GBM is classified as grade IV glioma in WHO classification (Lauko et al., 2021; Touat et al., 2015). Poor prognosis of GBM can be due to various reasons including: the invasion of tumor cells into the brain parenchyma, hypoxia (a hypoxic tumor microenvironment), the presence of cancer stem cells (CSCs), failure in penetration to the blood-brain barrier (BBB) by medications, and tumor cell heterogeneity and plasticity (Harder et al., 2018; Gimple et al., 2019; Colwell et al., 2017; Suter et al., 2020).

1.2.2 Importance of circulating biomarkers

Currently, the preliminary diagnosis of GBM is based on neuroimaging and resection or tissue biopsy and the prognosis is based on imaging techniques. However, taking a tissue biopsy, in case the tumor is accessible, is highly invasive and can cause serious risks to the patient such as brain swelling or affecting neurological functions. Furthermore, there is a possibility that the biopsy is not a correct representation of the whole tumour activity and therefore it fails to correctly predict the heterogeneity of

Brain tumor	
Benign	**Malignant**
Not cancerous	Cancerous
Slow growing cells	Rapidly growing cells
Marked with clear border	Not marked with clear border
Do not spread to other tissues	Can spread to entire brain and spine
Least destructive	Life threatening
Can be surgically cured	Can be cured with radiation and chemotherapy
Do not revert back once cured	May revert back after treatment

Table 1.2: Classification of brain tumor into benign and malignant. Adapted from Lather and Singh (2020).

Histology	Astrocytoma	Oligoastrocytoma	Oligodendroglioma
WHO grade			
Grade I (circumscript)	Pilocytic astrocytoma		
Grade II (low-grade)	Diffuse astrocytoma	Oligoastrocytoma	Oligodendroglioma
Grade III (diffuse, high-grade)	Anaplastic astrocytoma	Anaplastic oligoastrocytoma	Anaplastic oligodendroglioma
Grade IV (high-grade)	Glioblastoma		

Table 1.3: Classification of gliomas according to WHO grades. Adapted from Arcella et al. (2020).

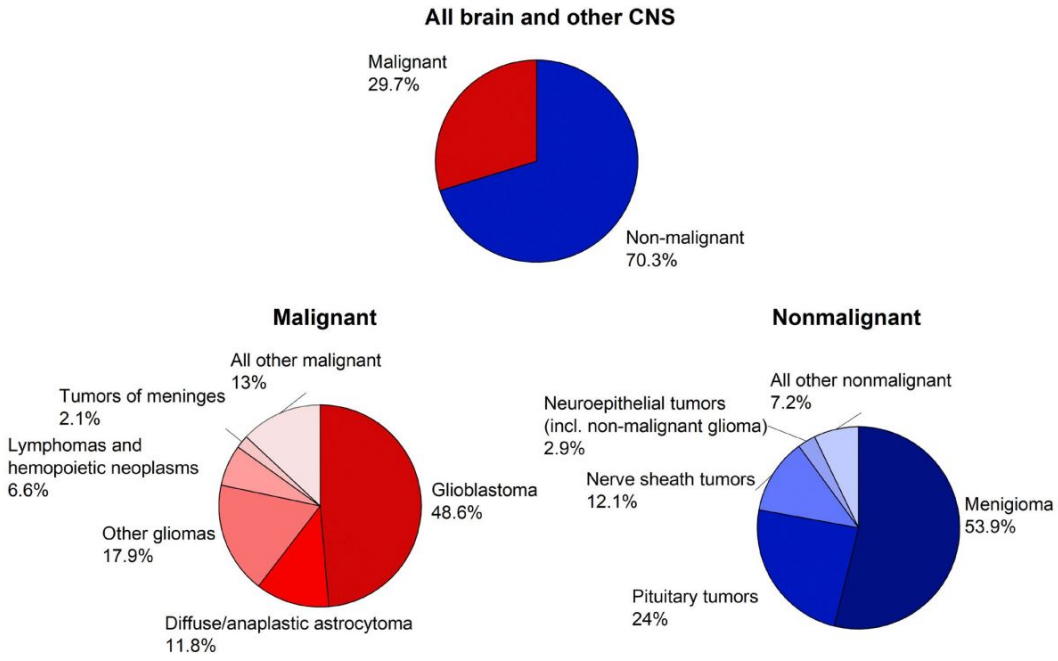

Figure 1.2: "Distribution of Brain and Other Central Nervous System (CNS) Tumors by Behavior and Major Histology Type, 2013 to 2017. Pilocytic astrocytoma is clinically considered nonmalignant but is included in the malignant category according to historical convention for cancer reporting. Data source: Central Brain Tumor Registry of the United States data provided by the Centers for Disease Control and Prevention's National Program of Cancer Registries and the National Cancer Institute's Surveillance, Epidemiology, and End Results Program, 2013 to 2017 (varying)." Adopted from Miller et al. (2021).

the entire tumour. Despite the great advantages of imaging techniques, they are unable to differentiate between pseudoprogression, which is caused by post-radiotherapy changes, and true progression (Kros et al., 2015; Müller Bark et al., 2020). Therefore a non-invasive or minimally-invasive solution for the diagnosis, monitoring the effect of treatment, prognosis, and assessment of the tumor progression is required. Circulating biomarkers or liquid biopsies are shown to be a considerable solution to this challenge.

Circulating biomarkers are the biomolecules found in the blood or other fluids of body, such as urine or CSF (Cerebrospinal Fluid) that provide information on the state of body and a condition or a disease. In oncology, a circulating biomarker is expected to facilitate differential (and early in some types of tumors) diagnosis, predict and examine the prognosis, follow the tumor evolution and provide molecular information on the tumor (Ludwig and Weinstein, 2005; Crowley et al., 2013). Using liquid biopsies in GBM is challenging due to the presence of BBB, which is a semipermeable barrier of endothelial cells between the blood and CNS. The BBB role is to protect the CNS from injury as well as circulating toxins or pathogens which would cause neurological diseases (Daneman and Prat, 2015; Abbott et al., 2010). The integrity of the tight junctions (TJs) between the endothelial cells, specifies the quality of a healthy BBB. It was shown that GBM can cause a mutation or a deficiency in the TJ proteins that can promote a proangiogenic and inflamed microenvironment, leading to a more permeable BBB (Chen and Hambardzumyan, 2018; Müller Bark et al., 2020). Also, hypoxia in the tumor environment is associated with the disruption of the BBB (Zhao et al., 2018). Furthermore, reports on the transmission of metastatic GBM from organ donors to transplant recipients confirms the presence of tumor cells in the circulation (Chen et al., 2008, 2009; Fatt et al., 2008). Figure 1.3 shows a schematic of transportation of biomolecules from a tumor through the BBB and into the blood. In this chapter, different categories of GBM associated biomarkers that can be detected in blood or CSF are reviewed. Various cancer biomarkers are reviewed in Table 1.4.

Biomarker	Advantages	Disadvantages	References
CTCs	• Information can be provided at the protein, DNA and RNA levels • Possibility of carrying out functional assays	• CTCs are rare (1 cell in 109 blood cells) • May represent only part of the tumour mass heterogeneity • Process to isolate them is challenging	Alix-Panabières and Pantel (2014); Ignatiadis et al. (2015); Shankar et al. (2017); Westphal and Lamszus (2015)
ctDNA	• There are new technologies in the development phase to isolate CTCs • Higher ctDNA levels compared with CTC • Levels correlate with disease stage	• Short half-life • Released mainly by cells undergoing necrosis or apoptosis	Westphal and Lamszus (2015); Ignatiadis et al. (2015); Wang and Bettegowda (2017); Bettegowda et al. (2014)
Exosomes	• Easy detection • Can be released by all cells, including tumour cells • Can carry proteins, DNA, RNA and miRNA • Present protection for their content	• The release is not exclusive from tumour cells • Possible presence of contaminants by current isolation methods	Westphal and Lamszus (2015); Xu et al. (2018); Santiago-Dieppa et al. (2014)

Table 1.4: An overview of various cancer biomarkers and their advantages and disadvantages. Adapted from Müller Bark et al. (2020).

Circulating Tumor Cells

CTCs are the cells that are secreted into the blood and the circulatory system from either primary or secondary tumours. CTCs are tumor-specific and their presence in

the circulatory system may be an indication to the existence of an undiscovered tumor (Touat et al., 2015; Müller Bark et al., 2020). CTCs are valuable biomarkers which provide key information and details on tumor cells, including morphology, molecular heterogeneity and immunocytochemical phenotype. These information are necessary for diagnosing tumors, In addition CTCs are also studied as biomarkers for tumors prognosis and therapeutic response (Pantel et al., 2008; Heitzer et al., 2013). CTCs can be found as individual cells and in cluster forms. Cluster CTCs are a group of two or more cells which have strong cell-cell connection. Clusters not only include tumor cells, but also non-tumor cells such as endothelial, platelets and fibroblasts. It has been shown that the CTC clusters have higher metastasic potential than individual CTCs and they comprise 5 - 20% of all CTCs (Rostami et al., 2019). Although the CTCs were discovered in 1869 and CTC clusters were first reported in 1954, GBM related CTC research is fairly new and inadequate. The first studies on GBM related CTCs as a single cell were published by Müller et al. (2014); Sullivan et al. (2014); MacArthur et al. (2014) in 2014 and the first article on GBM related cluster CTCs was published by Krol et al. (2018) only in 2018. Although isolation and detection of CTCs would greatly improve the early detection of tumors, technological obstacles have limited their clinical functionality (Heitzer et al., 2013).

Zhou et al. (2021) reported an electrochemical biosensor based on Platinum nanoparticles (PtNPs) which were decorated with hyperbranched PdRu nanospines (PdRu/Pt) for the detection of CTCs, using DNAzyme. In this work, super P carbon black and the AuNPs role was to improve electrical conductivity and to support the immobilization of antibody. The linear range for this biosensor was reported to be a wide range of 2 to 10^6 cellsmL^{-1} and LOD of 2 cellsmL^{-1}. Wang et al. (2021a) reported a colorimetric nanobioplatform for the detection of heterogeneous CTCs. This platform is based on aptamer-modified gold nanoparticles and two aptamer-functionalized dyes which are pH-sensitive. The AuNPs act as the capture unit and the dyes act as visual detection unit. The dynamic range of this sensor was 5-10^4 cellsmL^{-1} with LOD of 5 cellsmL^{-1}. Peng et al. (2022) developed a dual-recognition-controlled amperometric biosensor for

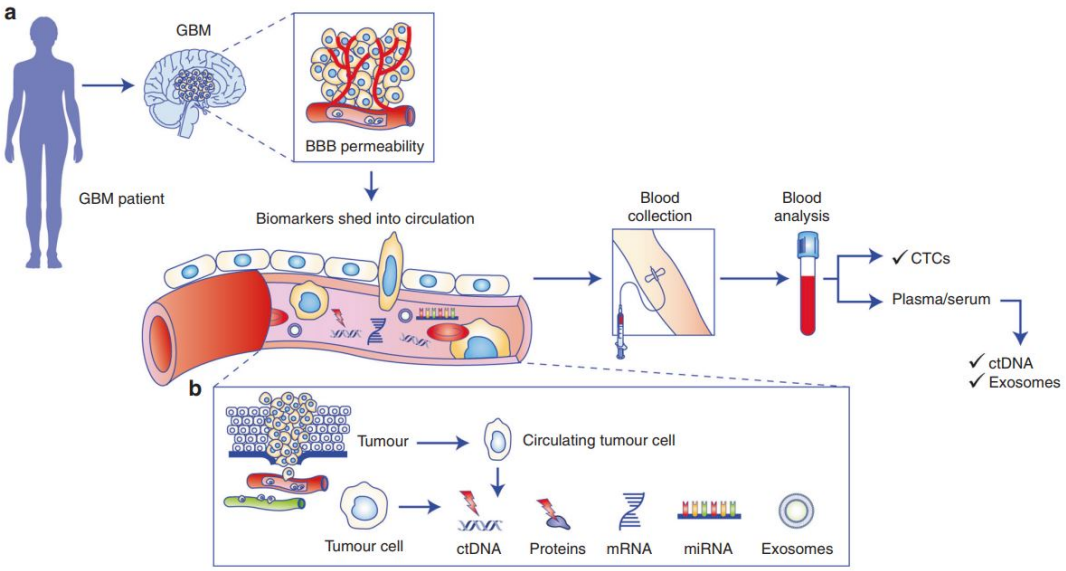

Figure 1.3: A schematic of the transportation of biomarkers from GBM to the blood and through BBB. (a) In patients with GBM the BBB is more permeable, which allows the biomolecules to enter the circulatory system and then be collected. (b) Several categories of tumor biomarkers can be detected in liquid biopsies. Adopted from Müller Bark et al. (2020).

detecting CTCs. In this work, two aptamer hairpin probes were seperately bound to two adjacent proteins on the cell membrane which triggered an amplification reaction leading to an electrochemical signal. The LOD was reported to be 3 cellsmL^{-1}. Jia et al. (2021) developed a CTC isolation approach based on N-cadherin recognition peptide functionalized on magnetic nanoparticles (NP@MNPs). In this work the CTCs were first captured by NP@MNPs, then the captured CTCs were isolated by an integrated microfluidic chip and finally they were sequenced. This method was reported to have a capture efficiency of 85%.

Extracellular Vesicles

EVs are vesicles that are discharged from normal and neoplastic cells into their microenvironment and therefore EVs can be present in various biofluids including blood, CSF and urine (Loo et al., 2019). EVs enhance cell-to-cell communication by carrying information (genomic and proteomic) from a host cell to other cells (figure 1.4). The EVs can be categorized depending on their sizes: 30-100 nm (exosomes), 50-2000 nm

(microvesicles), 50-4000 nm (apoptotic bodies) and >1μm (large oncosomes) (Yekula et al., 2020; Santiago-Dieppa et al., 2014; Whitehead et al., 2020). EVs contain information from the host cell which makes them valuable source of information on tumor progression and state. Also, EVs play a critical role in the migration and invasion of cancer cells as well as establishing a tumor-permissive microenvironment and drug resistance (Lv et al., 2014; Josson et al., 2015; Corcoran et al., 2012; Chen et al., 2014; Tadokoro et al., 2013).

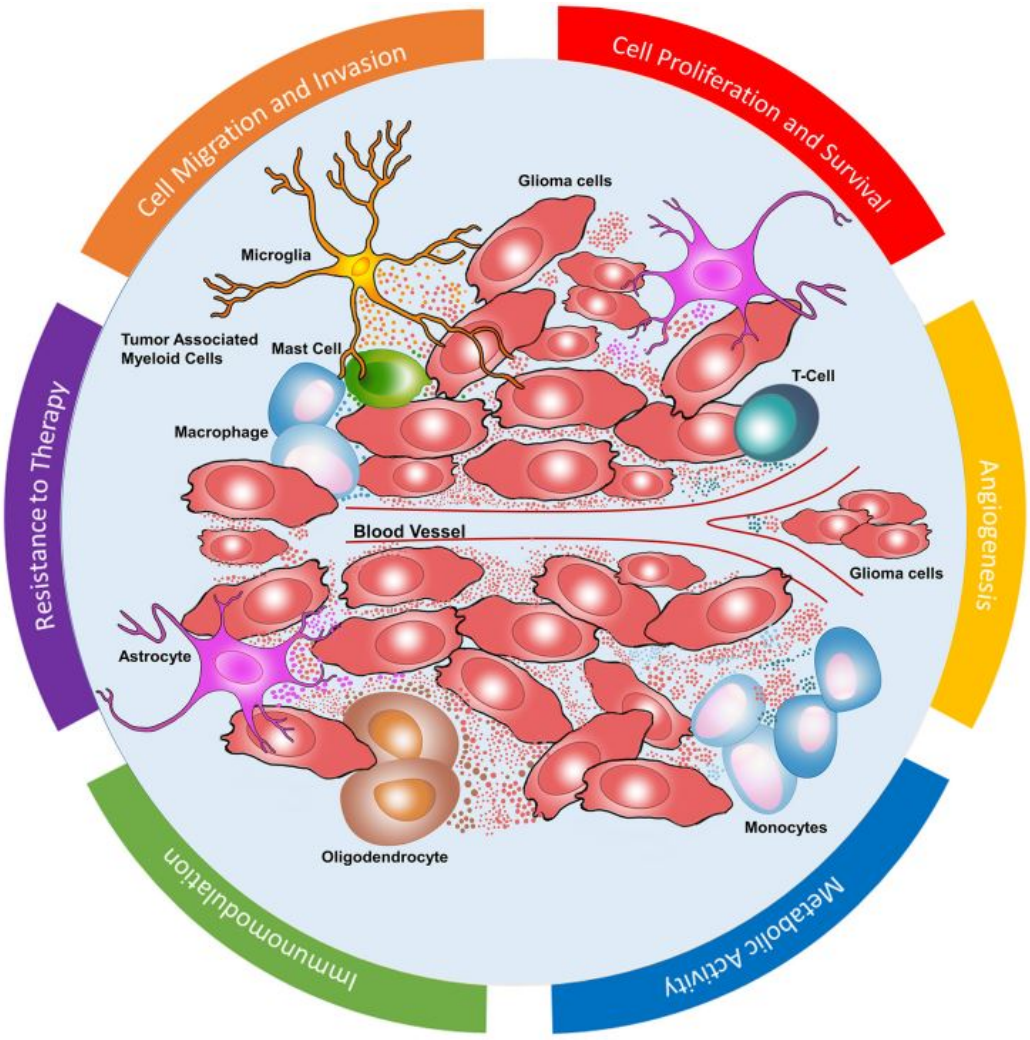

Figure 1.4: Glioblastoma microenvironment. EVs play an important role in cell proliferation and survival, cell migration and invasion, angiogenesis and metabolic activity. Adapted from Yekula et al. (2020).

Yildizhan et al. (2021) reported a bioassay to detect recombinant EVs (rEVs) using a fibre optic surface plasmon resonance (FO-SPR) spectrophotometer. In this work, six various combinations of EV-specific antibodies were tested to achieve the highest detection sensitivity of the sandwich bioassay, resulting in around 100 times higher sensitivity in human plasma for the best combination (anti-CD9/Banti-CD81 and anti-CD63/Banti-CD9). In addition to that, rEVs were successfully detected in cell culture medium without prior purification. Thakur et al. (2017) developed a SPR biosensor with self assembled gold nanoislands (SAM-AuNIs) which is able to detect EVs isolated from cells, serum, urine and tumor mouse models, using antibody-functionalised SPR. This sensor covered a linear range of 0.194 to 100 μM and a LOD of 0.194 μM. Jeong et al. (2016) developed an integrated magnetic-electrochemical exosome (iMEX) sensor for EV analyses. In this assay EVs are trapped on magnetic beads using a sandwich assay, followed by labelling the captured EVs with HRP to amplify the electrochemical signal. The dynamic range for this platform was reported to be 10^4 to 10^8 with LOD of 3×10^4 exosomes.

Circulating MicroRNA

miRNAs are short (18-22 nucleotides) non-coding single-stranded RNA molecules which are found in both healthy and cancerous tissues as well as almost all of the body fluids (Jelski and Mroczko, 2021; Santangelo et al., 2017). Researches support both down-regulation and up-regulation of various miRNA strands in both serum and tissues of GBM patients, making them a reliable and consistent biomarker for this type of cancer (Areeb et al., 2015; Dong et al., 2014). Although the potential miRNAs as glioma biomarkers still need to be researched and elucidated, mir-21 is known to be the most important and researched miRNA for the diagnosis of glioma so far.

Wang et al. (2022) developed an electrochemical biosensor for the detection of miR-21 in CSF. In this work, first the complementary miRNAs were immobilized on the AuNPs-coated glassy carbon electrode (GCE). After that, the capture miRNAs were partially hybridised with target miR-21 and partially with a long guanine-rich sequence which

would then adsorb methylene blue (MB) labels. The linear range for this biosensor was reported to be 0.5 to 80 pM with a LOD of 56 fM. Zhao et al. (2016) reported a visual and label-free colorimetric biosensor for the detection of miR-21 using graphene/AuNP hybrids and ssPNA-21. First, ssPNA was immobilized on the graphene/AuNP hybrid surface, hindering the oxidization of oxTMB in the presence of H_2O_2. Upon the addition of miR-21 to the solution and its hybridization to ssPNA-21, PNA/Ab duplexes were released from the hybrid surface, causing a change in the solution color. The dynamic range for this biosensor was reported to be 10 nM to 0.98 μM, with a LOD of 3.2 nM. Parchekani et al. (2021) developed an electrochemical assay using gold Nano-islands (Au-NIs) structures to capture miR-21 in both buffer and serum. For that, first fluorine doped tin oxide (FTO) electrodes were modified with Au-nanostructures, followed by immobilization of anti-miR-21 or cap-21 probes. After blocking the surface, the electrode was incubated in target miR-21 to allow the hybridization of the probe and target miRNA. The dynamic range for this biosensor was reported to be from 1.0 zM to 200 nM with a LOD of 0.12 zM.

Circulating Tumor Nucleic Acid

CtDNAs (Circulating tumor DNA) are pieces of the DNA in body fluids which originate from tumor cells (figure 1.5) (Wang et al., 2021b) and have been found in biofluids of patients with various diseases including cancer. CtDNAs are potential and promising targets for disease detection Kros et al. (2015). However, the abundance of cfDNA (circulating free DNA) in the body fluids makes the detection of the ctDNAs from cfDNA more challenging (Zachariah et al., 2018). The levels of ctDNAs in body fluids are affected by various determinants such as sex, age, tumor cell population, BBB permeability, clearance of the ctDNAs by liver and kidney, etc. (Kros et al., 2015). Therefore, ultrasensitive assays are required for the detection of ctDNA (Touat et al., 2015).

Rahman et al. (2020) reported an electrochemical sensing platform based on graphene oxide-wrapped gold nanostars (GO-AuNSs) for the detection of ctDNA. The target ctDNA was captured by its hybridization with the probe DNA, which resulted in the

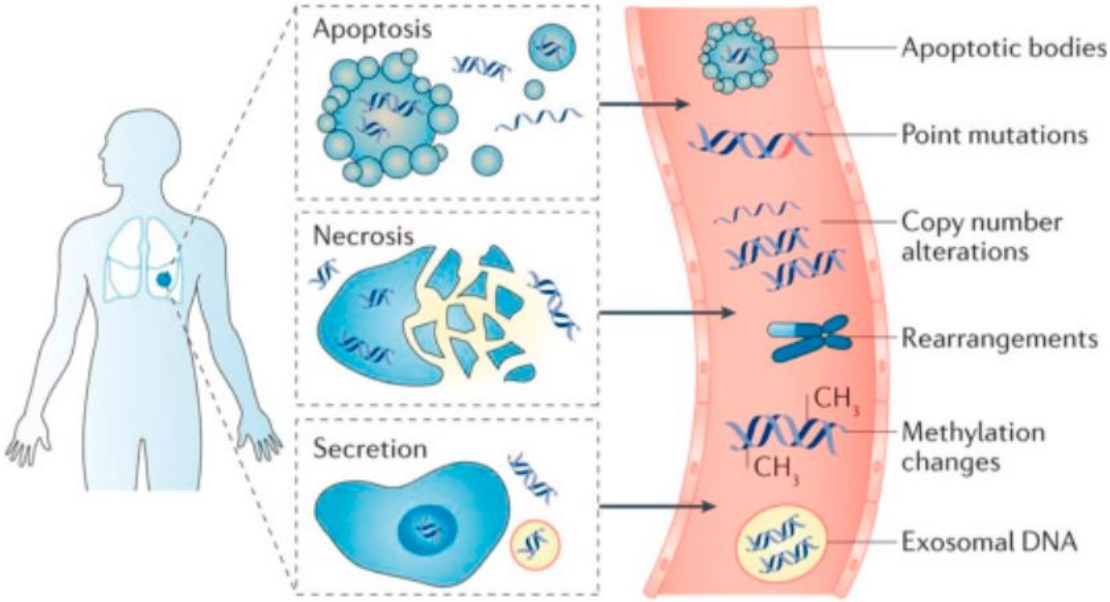

Figure 1.5: The potential sources of ctDNA originated by apoptosis, necrosis, or secretion of tumor cells. (Wan et al., 2017; Wang et al., 2021b)

formation of a helix structure. The linear range of this biosensor was reported to be 10^{-20} M to 10^{-12} M with a LOD of 10^{-20} M. Cui et al. (2022) fabricated an electrochemical biosensor utilising molybdenum disulfide (MoS_2) nanosheets for the detection of ctDNAs. First, a GCE was immobilized by a few layers of MoS_2, taking the advantage of their affinity towards ssDNA. This biosensor was then incubated in target ctDNA and was left to allow the hybridization of ssDNA probe and target ctDNA. MB was used as label to achieve higher sensitivity. The linear range was reported to be 1.0×10^{-7} to 1.0×10^{-16} M with LOD of 2.5×10^{-18} M. Ban et al. (2020) reported an electrical graphene FET, using a DNA-tweezer probe (DTP) for the detection of DNA methylation. The DTP promotes strand-specific displacement of methylated targets followed by electrical measurement of the source and drain electrode. The dynamic range for this sensor was 10pM to 10nM.

1.3 DNA methylation as a biomarker

DNA methylation is the most exhaustively characterized epigenetic modification of DNA that plays an important role in regulating cellular function. Epigenetic modifications are

the alterations in gene expressions without changing the DNA sequence (Davis and Uthus, 2004). It has been shown that changes in DNA methylation patterns may be associated with various diseases including cancer and may in the future be used in new screening methods prior to more advance clinical tests.

DNA methylation is the covalent binding of a methyl group (-CH_3) to the 5th carbon atom of a cytosine nucleotide (figure 1.6) that follows a guanine nucleotide (CpG sites), with the help of DNA methyltransferases (DNMTs) (Syedmoradi et al., 2016; Lam et al., 2016). The aberrant methylation of the CpG sites has the potential of being a diagnostic, prognostic, and predictive biomarker for various diseases (Mikeska and Craig, 2014; Das and Singal, 2004) including lung cancer (Usadel et al., 2002; Kersting et al., 2000), brain tumors (Esteller et al., 2000), breast cancer (Silva et al., 1999; Evron et al., 2001), and prostate cancer (Goessl et al., 2000; Lee et al., 1994).

Vrba and Futscher (2018) has analysed a cancer DNA methylation data set and identified sets of six markers for individual cancer types, which are expected to trace the majority of specific tumours with high sensitivity and specificity, making them suitable for non-invasive cancer detection and monitoring. Heller et al. (2018) identified 34 types of miRNA with increased methylation in the primary tumours of non-small-cell lung cancers, some of which are associated with certain molecular pathways. Georgopoulos et al. (2018) in their case-control study showed that DNA methylation in 5 various genes e.g. RASSF1, APC, RARβ, DAPK and hTERT are promising urine biomarkers for the diagnosis of bladder cancer. Majchrzak-Celińska et al. (2013, 2015) showed that aberrant methylation of a panel of genes is a marker for central nervous system cancer. Excitingly, they also revealed that the methylation of some specific genes such as MGMT, RASSF1A, RUNX3 etc. can be used as a tool to predict glioma aggressiveness.

1.3.1 Sensing DNA methylation

There are different techniques to detect DNA methylation. Conventional techniques which are based on molecular biology including bisulfite treatment, methylation-specific

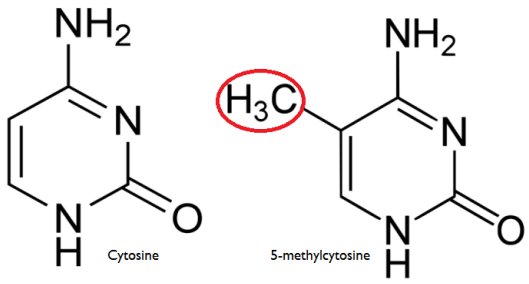

Figure 1.6: DNA methylation is the binding of a methyl group (-CH_3) to the 5th carbon atom of a cytosine nucleotide in a nucleic acid.

PCR (MSP), mass spectrometry (MS) and liquid chromatography (LC) have been used extensively. These techniques are sometimes used together and may rely on each other.

Bisulfite genomic sequencing is the standard technique to detect DNA methylation. In this technique, cytosine and 5-methylcytosine are converted to uracil and thymine respectively using sodium bisulfite. The advantage of this chemical reaction combined with PCR amplification and sequencing was first discovered by Frommer et al. (1992). Although the bisulfite conversion method is widely accepted as a reliable method, there are still some shortcomings such as requirement of acidic pH and high temperature causing DNA fragmentation, false negative readouts due to the slow 5-mC de-amination process, difficulties in DNA purification due to the presence of residual bisulfite and incomplete conversion of cytosine to uracil (Bhattacharjee et al., 2018; Laird, 2003).

MSP was introduced in 1996 by Herman et al. (1996) to detect blocks of CpG sites in CpG islands (regions which have a high number of CpG sites). This technique takes advantage of the bisulfite sequence conversion and is able to distinguish methylated DNA from non-methylated DNA as well as unmodified DNA or DNA that has incompletely reacted with bisulfite (Cottrell et al., 2004; Fackler et al., 2018; Fackler and Sukumar, 2018; Draht et al., 2016). This technique is limited by analysis time, occurrence of false-positive results due to the amplification of unconverted DNA and cost of labour and reagents (Shanmuganathan et al., 2013).

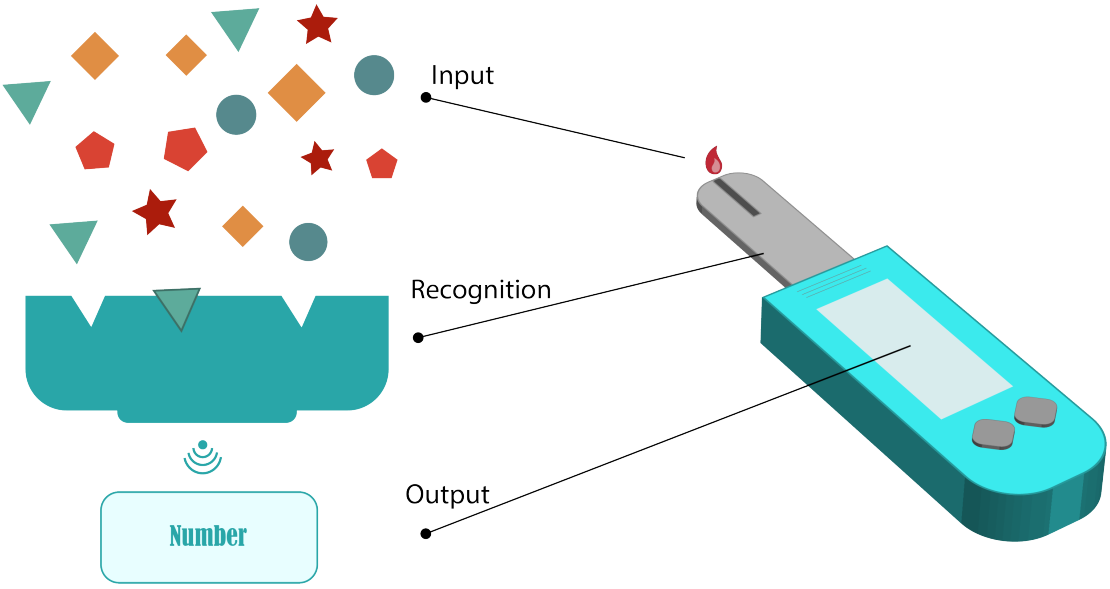

Figure 1.7: Illustration depicting the working process of a biosensor.

Other methods such as chromatography and spectrometry are either used individually or in tandem. Although they have advantages like high sensitivity and not being affected by DNA imperfections, these techniques require expensive equipment, large amounts of samples and specific expertise, making them less popular techniques to detect DNA methylation (Bhattacharjee et al., 2018; Kurdyukov and Bullock, 2016).

In recent years, considerable effort has been directed at the development of biosensors and DNA sequencing techniques that have the potential to overcome the limitations of aforementioned techniques, along with portability and amenability to miniaturization (Bhattacharjee et al., 2018). Biosensors can either be used to detect DNA methylation on their own, or combined with conventional techniques (Hossain et al., 2017).

1.4 Biosensors

Biosensors are bioanalytical devices used to detect the presence of biological analytes and convert it into a measurable signal (Bohunicky and Mousa, 2011). Recently, there is a growing interest and need in developing biosensors to facilitate faster diagnosis and efficient screening of various diseases, proven by COVID-19 pandemic. This is due to the biosensors ability to measure in real-time and being a point-of-care (POC) and easy

to use device. These features could make biosensors suitable for decentralized clinical applications such as bedside monitoring, emergency-room screening, GP check up, or self-testing by patients at home. All of these together with simplicity, low cost and reliability make biosensors a promising technique for the early detection of cancer in the near future (Tothill, 2009; Jayanthi et al., 2017; Wang, 2006; Nemati et al., 2022).

A biosensor is composed of three components: a biorecognition element, a transducer and a signal processor. The biorecognition element binds or recognizes the analyte. The transducer converts this recognition to an electrical signal and the signal processor processes and displays the signal (figure 1.7). Biosensors can be classified into four groups by the working mechanism of their transducer: electrochemical, optical, mass based, and calorimetric (figure 1.8 and 1.9).

Povedano et al. (2021) reported an electrochemical platform to detect the four most frequent methylations in DNA and RNA (5mC, 5-hmC, 6mA, and m6A). In this work, the target biomarkers were first captured on protein G-modified MBs (ProtG-MBs) using the corresponding capture antibody for each methylation (anti-5- mC, anti-5-hmC, or anti-m6A/6mA). Subsequently, the amperometric detections were performed using screen-printed electrodes with four carbon working electrodes (SP_4CEs) and streptavidin-HRP as the label. The linear ranges were reported to be 3.9×10^{-4} - 1.9 μM, 2.3×10^{-4} - 1.8×10^{-1} μM, 5.4×10^{-4} - 1.1×10^{-1} μM, 1.7×10^{-5} - 3.5×10^{-1} μM with LOD of 3×10^{-5} μM, 3×10^{-5} μM, 1×10^{-4} μM, 9×10^{-7} μM for 5-mC, 5-hmC, 6mA and m6A respectively. Bhattacharjee et al. (2019) reported an enzymatic bisulfite treatment and PCR amplification-free three step technique for the detection of DNA methylation. In their technique, the DNA was first isolated and denaturated from ovarian cancer cell lines before being adsorbed directly on a gold electrode surface. GO_x-5mC antibody was used to interrogate the DNA methylation sites and finally electrochemical detection was performed to obtain signals. In this technique, GO_x was used as a label to enhance the enzymatic catalytic electrochemical signals. With this technique they were able to detect 5% methylation level in 50 ng of total DNA input.

Lee et al. (2017) developed an electrochemical detection technique for DNA methylation using methyl CpG-binding protein and glucose dehydrogenase-fused zinc finger protein. This three step detection applied PCR amplification prior to electrochemical measurement.

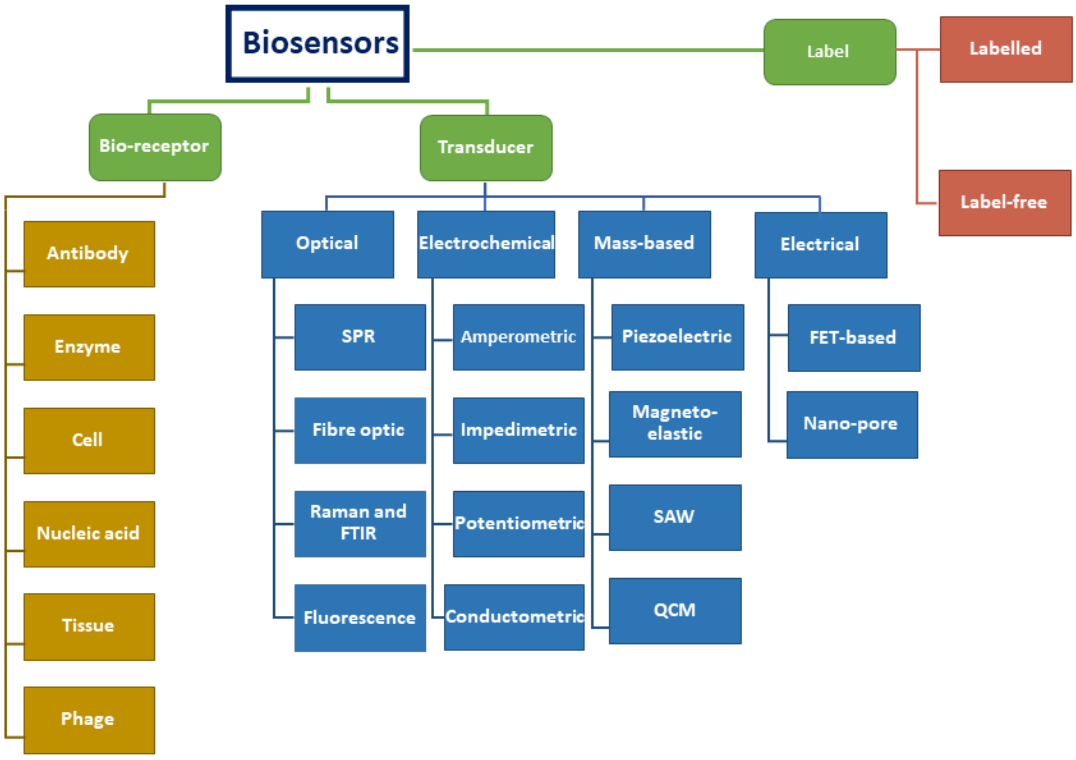

Figure 1.8: Classification of various types of biosensors.

Huertas et al. (2018) developed an optical biosensor which is based on SPR for the label free and real time detection of DNA methylation. In this technique they used apolypurine hairpins as probes and anti-5mC antibody to determine the cytosine methylation. The LOD was reported to be 115 pM. Ouyang et al. (2017) introduced a Surface-enhanced Raman spectroscopy (SERS) sensor using a Laser wrapped graphene-Ag array as a substrate. The LOD was reported to be 0.2 pgμ/L and the detection time was less than one hour. Wang (2017) developed an electrochemical assay for the detection of circulating methylated DNA based on a sequential discrimination-amplification strategy (SEDA). In this assay, the methylated DNA first underwent a bisulfite modification and then was identified and amplified using asymmetric MSP (AMSP). Finally, it

was hybridized with tetrahedral DNA probes that were decorated on a gold electrode. Avidin–HRP was used as the label for amperometric detection. The dynamic range for this assay was reported to be 3–150 pg and the LOD was one methylated DNA molecule in the presence of a 1000-fold excess of unmethylated alleles. Chen et al. (2019) developed an electrochemical biosensor for DNA methylation detection using tetrahedron DNA probes which were anchored to a AuNPs-coated gold electrode with avidin-HRP as the label. This biosensor showed a dynamic range of 1 aM to 1 pM, with the LOD of 0.93 aM.

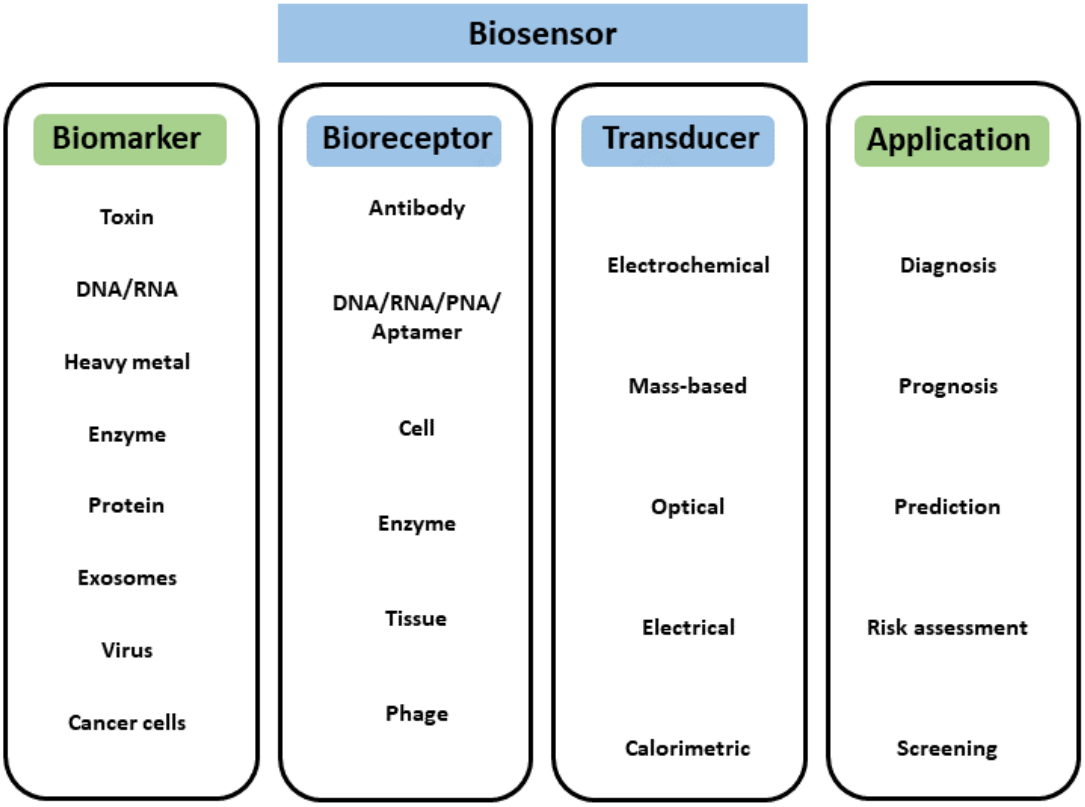

Figure 1.9: Classification of a biosensor biomarkers, elements and its applications.

Characteristics of a biosensor

A biosensor's performance is assessed based on its characteristics such as selectivity, limit of detection (LOD), linear dynamic range and reproducibility.

Selectivity is when the biosensor is able to capture, detect, and measure only the

analyte of interest in a sample which contains a mixture of contaminants and other biochemical species with minimal interference (Estrela et al., 2016).

Limit of detection (LOD) is the minimum amount of the analyte that can be distinguished from the absence of that specific analyte (a blank value) (Chakraborty and Hashmi, 2017).

Linearity is when the biosensor is able to produce a signal that is proportional to the concentration of the analyte of interest in the sample (Estrela et al., 2016).

Reproducibility is when the biosensor is able to produce identical response in a duplicated experimental set-up i.e. the precision between two experiments with varying operators and environments (Estrela et al., 2016).

Dynamic Range is the range in which the signal response of the biosensor can be used to indicate the concentration. (Prabowo et al., 2021)

1.4.1 Electrochemical Biosensors

Electrochemical biosensors have received considerable interest due to their portability, accuracy and in most cases disposability. The glucose biosensor is the most known and used example of such biosensors and the first commercially available biosensor (Tothill, 2009; Wang, 2006). This self-testing glucose meter is consists of a screen printed electrode and a pocket-size meter and has dominated the 5 billion/year diabetes monitoring devices market over the past decades and counts up to almost 85% of the world biosensors market (Newman and Turner, 2005). Although detecting cancer is a more complex assay than detecting glucose, recent advances in cancer-related biomarkers detection field showed a promising potential to develop a similar biosensor in the near future.

Electrochemical biosensors have been classified based on various criteria. However, the most commonly used categories are based on whether the sensor is amperometric or voltammetric (Table 1.5). In amperometric biosensors, changes in current is being monitored in time while the potential is kept constant, while in the voltammet-

Experimental methods	Checked property
Amperometry	Current (A)
Impedimetry	Impedance (Ω)
Potentiometry	Potential difference (V)
Conductometry	Resistance (Ω)

Table 1.5: Main electrochemical methods and their checked electrical properties.

ric technique, the potential is changing while the current response is being observed (Ronkainen et al., 2010). Another classification is with regards to using electro-active labels (such as nanoparticles, enzymes or organic dyes) , dividing the biosensors in labelled and label-free categories. Using labels increase the electrical signal and offer a high sensitivity electrochemical biosensor (Kerman et al., 2003; Wang, 2002).

Electrochemical biosensors for the detection of DNA methylation

Electrochemical measurement techniques offer interesting advantages for detecting DNA methylation, such as high accuracy and sensitivity, simplicity and portability along with low limits of detection and low cost instrumentation. Over the last decades, electrochemical biosensors have been a point of interest for the development of analytical tools for the detection of genes and genes mutation associated with human disease (Hossain et al., 2017; Krejcova et al., 2017). Povedano et al. (2018c) reported two different electrochemical affinity biosensors to detect the MGMT gene using anti-5mC antibody as a sensitive element. In the first method, the anti-5mC was used to capture the methylated DNA followed by another antibody conjugated with peroxidase as the detector element. In the second biosensor, a capture probe was immobilized on the surface and was used to hybridize with the DNA prior to the tagging of the methylated DNA by anti-5mC and using a secondary antibody conjugated with peroxidase as a detector element. In both sensors, the biological reactions took place on a streptavidin-modified magnetic beads surface which were then magnetically captured on a screen printed electrode followed by an amperometric detection of the target gene The reported LOD was 26 pM and RSD<4.3 for n=7.

In another paper Povedano et al. (2018b) developed an electrochemical biosensor by using magnetic beads modified with anti-5mC to detect DNA methylation followed by a two-step labelling prior to amperometric detection. Daneshpour et al. (2016) developed a chip format biosensor to detect DNA methylation using Fe_3O_4/Ntrimethyl chitosan/gold (Fe_3O_4/TMC/Au) nanocomposite which was used as a label for the DNA probe and polythiophene (PT) as immobilization substrate of anti-5mC as the sensing element. Huang et al. (2019) developed an electrochemical biosensor where the DNA probe was first assembled on the surface, followed by hybridization of the DNA probe using methylated complementary DNA. GO modified anti-5mC antibody was used to detect the methylation sites followed by utilizing HRP-labelled antibody to improve signals. The reported LOD was 1 fM. Chen et al. (2019) reported an electrochemical stem-loop-tetrahedron composite DNA-probe platform immobilized on a AuNPs-coated gold electrode. After the immobilization of the composite DNA probe on the electrode surface, complementary DNA was added and hybridization took place. Avidin-HRP was used to enhance the enzymatic reaction. This platform showed a broad dynamic range of 1 aM to 1 pM and the LOD was 0.93 aM. Khodaei et al. (2019) developed a voltammetric immunosensor using reduced graphene oxide and anti-5mC antibody to capture methylated DNA. Methylated DNA were then hybridized with ssDNA-conjugated Fe_3O_4 nanoparticle. The LOD for this biosensor was reported to be 9×10^{-5} ngmL^{-1}. Gao et al. (2018) reported an electrochemical method using a single stranded probe as the sensing element and anti-5mC antibody decorated with silver nanoparticles (AgNPs) and carbon nanotubes (CNCs) as a label. This biosensor showed a linear response from 0.05 to 120 Uml^{-1} with the LOD of 0.03 Uml^{-1}.

1.5 Application of Nanomaterials in Biosensors

Recently nanomaterials have received considerable interest and attention for the application in biosensors with the aim of improving both the sensitivity and limit of detection as well as decreasing the size of electrochemical biosensors (figure 1.10) (Sharifi et al., 2019). Nanomaterials can improve the biosensors performance and capabilities by ei-

ther surface modification or being used as a label (Maduraiveeran et al., 2018; Farka et al., 2017). Using nanomaterials in biosensors also resulted in stable system probes and allowed multiplex sensing (Yüce and Kurt, 2017). Various types of nanomaterials have been used including 0D nanomaterials such as nano particles (Li et al., 2017; Hashemi et al., 2020; Ferrari, 2023) and quantum dots (Iannazzo et al., 2021; Yang et al., 2020; Chung et al., 2021; Faridbod and Sanati, 2019), 1D nanomaterials including nanotubes (Alabsi et al., 2020; Zhou et al., 2019; Ferrier and Honeychurch, 2021) and nanowires (Li et al., 2020; Leonardi et al., 2021), 2D materials such as graphene and its derivatives and graphene-like nanomaterials (Han et al., 2012; Li et al., 2022; Magesa et al., 2019; Bai et al., 2020) and finally 3D nanomaterials including nanospindles and nanodendrimers (Bieniek et al., 2021; Idris et al., 2020; Thakare et al., 2022; Osman et al., 2019). Noble metal nanoparticles (NMNPs) and carbon based nanomaterials are the most widely used nanomaterials in the biosensors field. NMNPs hold advantages such as similar dimensions with biological molecules, large surface area, conductivity, stability and biocompatibility, making them beneficial for the fabrication of electrochemical biosensors (Wang, 2012). Carbon based nanomaterials also have advantages including high surface to volume ratio, conductivity, chemical durability and biocompatibility along with unique morphology (Yang et al., 2015a). Below, two types of nanomaterials used in this study will be explained in detail.

1.5.1 Graphene

Graphene has been studied for over sixty years, however it was after the 2010 Nobel Prize by Giem and Novoselov that this two-dimensional material started to attract more attention. Graphene is a monolayer of carbon atoms, packed in a two dimensional atomic-scale hexagonal lattice which has applications in various fields such as electronics, energy storage and bioscience/biotechnology (Geim and Novoselov, 2010; Shao et al., 2010).

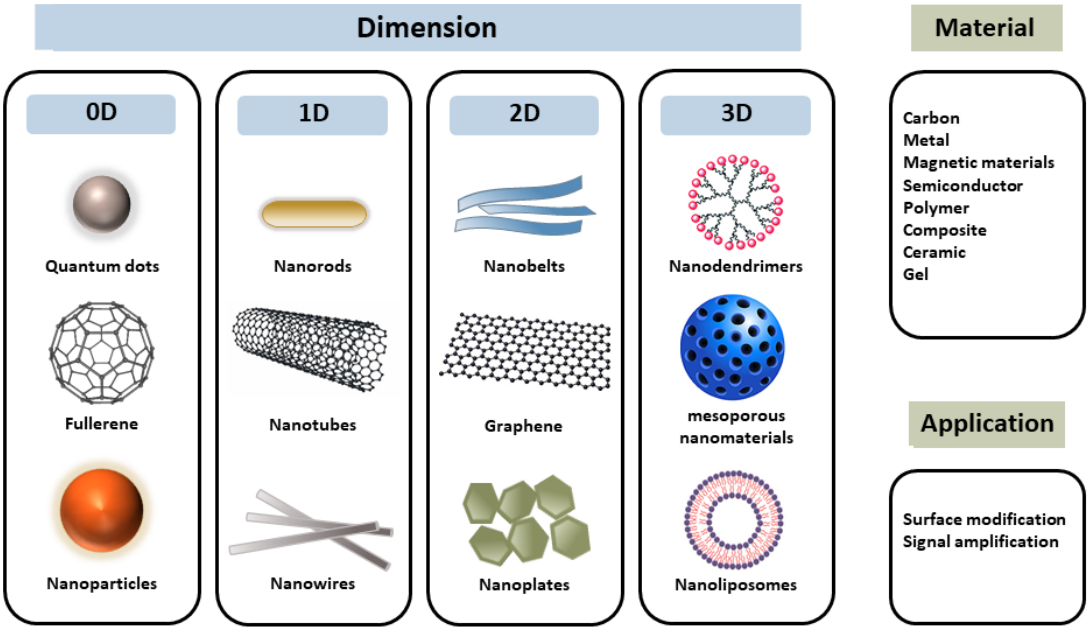

Figure 1.10: Classification of nanomaterials based on their dimension, material and their application in biosensors.

Graphene and its derivatives

Graphene has specific electrical, mechanical and optical properties due to its unique structure. The electron configuration of carbon is $1s^2 2s^2 2p^2$, providing four available valence electrons for chemical bonding. Graphene's atoms have four covalent bonds each, three σ bonds with other neighbours and one π bond which is oriented out of the plane in the z-direction (figure 1.11) (Zhu et al., 2010; Balaji and Zhang, 2017). Graphene shows high mobility for charge carriers, high electrical conductivity and large surface area (2630 m^2/g) (Suvarnaphaet and Pechprasarn, 2017; Yang et al., 2010). The room temperature mobility has been measured at 15000 cm^2/Vs for graphene with one to three layers. Moreover, the electrochemical performance of graphene and it's derivatives such as graphene oxide (GO) and reduced graphene oxide (rGO) is shown to be higher, compared to other electrodes such as glassy carbon (GC), graphite and carbon nano tubes (CNTs) (Yang et al., 2010). The electron transfer behaviour of graphene showed well-defined redox peaks using cyclic voltammetry (CV) in redox active solutions such as $[Fe(CN)_6]^{3-/4-}$ and $[Ru(NH_3)_6]^{3+/2+}$. Also, the apparent electron

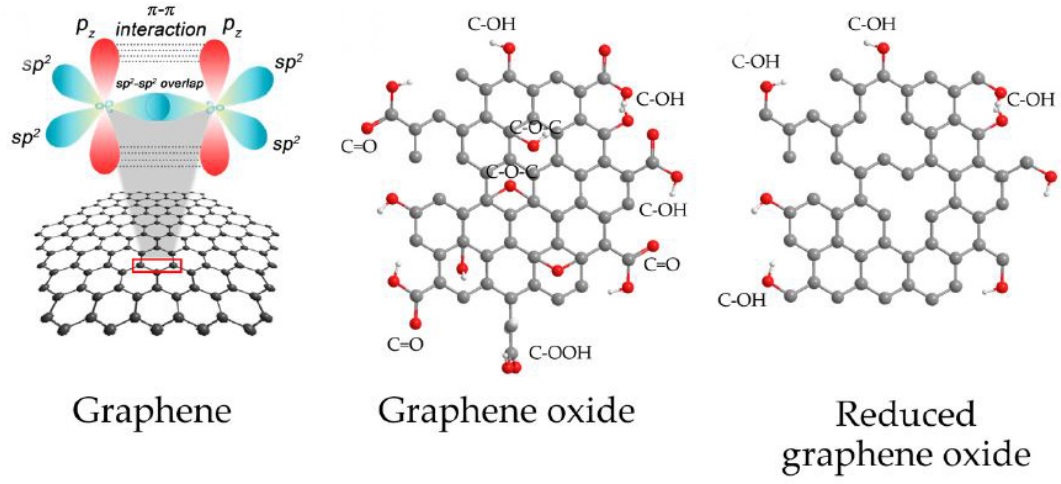

Figure 1.11: Structures of graphene based materials. Adapted from Suvarnaphaet and Pechprasarn (2017).

transfer constant (k^0) was shown to be higher in graphene than GC, which indicates a faster electron transfer (Shao et al., 2010). The aforementioned properties along with the presence of defects, disorders and functional groups on the surface of graphene, GO and rGO makes them suitable for biosensing (Suvarnaphaet and Pechprasarn, 2017): Defects provide active sites for electron transfer and oxygen containing functional groups to help the oxidation reaction by reducing the overpotential voltage (Kuila et al., 2011; Szunerits and Boukherroub, 2018). Li et al. (2015) developed a novel graphene-rGO double layer biosensor for the detection of a DNA sequence. The reported electrochemical biosensor is label free and requires no signal enhancement and complicated immobilization. It showed a linear range from 10^{-7} to 10^{-10} M and a LOD of 1.58×10^{-13}. Munief et al. (2019) introduced a reproducible process to fabricate rGO-based FET on wafers, which can be used to measure N-terminal pro-brain natriuretic peptide (NT-ptoBNP) in human serum. Their rGO sensor showed a LOD of 1-10 pgmL^{-1}.

Tahernejad-Javazmi et al. (2018) reported a label free DNA biosensor for the detection of dasatinib in aqueous solutions in the concentration range of 0.03-5.5 μM. In this study, they used rGO and AuNPs to modify the GCE surface, followed by immobilizing of DNA on the surface. They then detected the presence of dasatinib using the DPV

technique. Tian et al. (2019) developed a 3D nitrogen doped rGO/AuNPs platform for the detection of miRNA-155. In this paper, they used tetrahedral DNA structure as the biorecognition element and gold and silver nanorod/thionine/complementary DNA for signal amplification. The electrochemical response was proportional to miRNA-155 concentration in the range of 1×10^{-11} to 1×10^{-4} M and the detection limit was 1×10^{-12} M. Zhou et al. (2019) designed a biointerface for graphene field-effect transistors (GFETs) using nano-denatured bovine serum albumin (nano-dBSA) and antibody (anti-CEA mAb) for the detection of carcinoembryonic antigen (CEA). They reported a sensitivity of 337.58 fgml^{-1}, good specificity toward CEA targets and offered their multifunctional nano-dBSA functionalization as a promising method for biosensing, nanomedicine and drug delivery. Kovalska et al. (2019) showed that multi-layer graphene (MLG) are beneficial as electrode material in e-nose engineering for real time detection of specific lung-cancer biomarkers (CMs) in exhaled human breath. Their research showed that both flat and patterned MLGs have high selectivity and sensitivity and a potential for future lung cancer biosensors. Meng et al. (2019) developed an electrochemical biosensor to detect prostate specific antigen (PSA). In this technique graphene oxide (GO) was used to be immobilized on the peptide-modified electrode in the absence of PSA. Further the GO triggered the formation of silver nanoparticles (AgNPs). In the presence of PSA, cleavage of peptide avoids the immobilization of GO and thus formation of AgNPs. The LOD was calculated to be 0.33 pgmL^{-1} with the detection range of 5 pgmL^{-1} to 20 ngmL^{-1}. Gazze et al. (2018) fabricated a label-free detection platform through the deposition of a polyaniline layer on the screen printed graphene electrode surface. The sensor was then used to detect ovarian cancer in stage 1 or 2 through detection of the CA125 biomarker. The dynamic range was reported to be 0.92 pg/μL to 15.20 ng/ μL with a LOD of 0.923 ng/ μL. Sethi et al. (2020) designed a label-free electrochemical biosensor for the detection of beta-amyloid biomarkers. In this work which was conducted in our group, A-β_{1-42} biomarker was detected by using a graphene and reduced graphene oxide dual-layer screen printed electrode (SPE). This biosensor showed excellent performance in both

human and mice plasma and showed high specificity towards A-β_{1-42} over other interfering biomarkers such as A-β_{1-40} and ApoE $\varepsilon 4$. The LOD was 2.398 pM with the detection range of 11 pM to 55 nM. Ahmadi and Ahour (2020) developed a biosensor based on a graphene oxide modified pencil graphite electrode and PNA to electrochemically detect dsDNA in plasmid samples. GO was first casted on to the pencil graphite electrode and then the PNA probes were immobilized on the modified electrode. Upon incubation of the biosensor in the target ds-DNA, PNA probes detached from the electrode surface, resulting in a guanine oxidation signal, decreasing linearly with the target concentration. Under optimized conditions, the linear range was from 30 pM to 10 nM and the LOD was reported to be 1.3 pM.

1.5.2 Gold Nanoparticles

Gold nanoparticles (AuNPs) are one of the most widely used and studied nanomaterials in electrochemical biosensors to enhance their analytical performance. AuNPs provide a stable foundation for the immobilization of biomolecules which allows them to retain their bioactivity (figure 1.12) (Yanez-Sedeno and Pingarron, 2005; Pingarrón et al., 2008). In addition, AuNPs size and morphology can simply be controlled by adjusting the preparation conditions and synthesis method, allowing the optimization of the microenvironment on the electrode surface (Yanez-Sedeno and Pingarron, 2005; Pingarrón et al., 2008; Putzbach and Ronkainen, 2013). Furthermore, conjugation of biomolecules with AuNPs does not alter the biochemical activity of the biomolecules due to the AuNPs high biocompatibility (Rasheed and Sandhyarani, 2017). Immobilization of biomolecules on AuNPs can mostly be achieved in one of these three methods: Chemical adsorption, physical adsorption, self assembled monolayers (SAM) (Putzbach and Ronkainen, 2013).

Zhang et al. (2019) reported an electrochemical biosensor for the detection of miRNA-21. In this sensor AuNPs and horseradish peroxidase (HRP) were used in combination with duplex-specific nuclease (DSN)-assisted target recycling to gain a triple signal amplification. The reported LOD was 43.3 aM with the linear range of 0.1 fM to 100 pM.

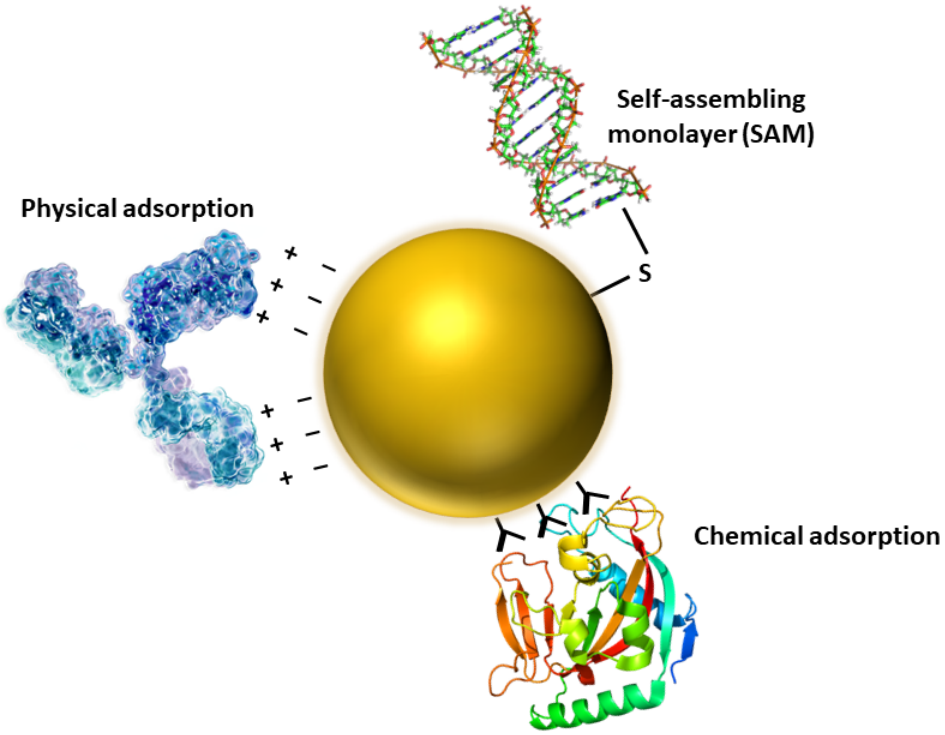

Figure 1.12: Various immobilization methods of biomolecules on the AuNP surface.

Saeed et al. (2017) reported two sandwich and amperometric assays for the detection of ERBB2 and CD24c, which are breast cancer biomarkers and a control biomarker. In this work, first the glassy carbon electrode (GCE) was modified with a mixture of AuNP and GO. Later, the modified electrode was incubated in the complementary probes for each target and then in the target DNA strands. Using HRP label as a reporter probe, LODs were reported to be 1.6×10^{-10} M and 2.3×10^{-10} M for ERBB2 and CD24, respectively. Su et al. (2016) reported an electrochemical aptasensor for the simultaneous detection of thrombin and adenosine triphosphate (ATP). The Biosensor is based on AuNPs-decorated-MoS_2. This aptasensor was able to simultaneously detect ATP and thrombin as low as 0.74 nM ATP and 0.0012 nM thrombin, respectively. Jolly et al. (2017) reported a dual-mode impedimetric and amperometric aptasensor platform to detect prostate specific antigen (PSA). In this label free biosensor AuNPs was attached to a gold planar surface in order to improve the limit of impedimetric detection. The LOD was reported to be 10 $pgmL^{-1}$ with a dynamic range from 10 $pgmL^{-1}$

to 10 ngmL^{-1}. Suresh et al. (2018) reported an immunosensor based on a SPE which was coated with AuNPs and a chitosan (CHI) nanocomposite film and MB was used as redox mediator. This biosensor was designed for the detection of PSA biomarker and was able to detect this biomarker over the range 1–18 ngmL^{-1} with a LOD of 0.001 ngmL^{-1}.

1.6 Overview of this thesis

Aims

This study is a part of AiPBAND network which stands for An Integrated Platform for Developing Brain Cancer Diagnostic Techniques. AiPBAND is funded by the Marie Skłodowska Curie Action Initial Training Networks ("MSC-ITN") under Horizon 2020. Because the focus of AiPBAND is on gliomas, a broad category of brain tumours, the target methylated gene for this study was chosen accordingly. Glioma is the most frequent and malignant type of brain tumour which has higher incidence in developed countries. Glioma has a very poor prognosis with less than 3% of 5 years survival rate (Ohgaki, 2009). Glioma can be either primary or metastatic. Primary tumours start in the brain cells while metastatic begin in other part of the body and spread to the brain (Jain et al., 2007). Nowadays gliomas are diagnosed by neurological exams and imaging tests (CT scan and MRI) of the head followed by Positron Emission Tomography (PET) scan and Cerebral Angiography as complementary tests. A biopsy is later taken via surgery to assess the type of tumour (Tidy, 2018). Glioma treatment is complex and includes surgical resection, radiation therapy (RT) and concurrent Temozolomide (TMZ) chemotherapy (Tamimi and Juweid, 2017).

The aim of this study is to develop a graphene based, electrochemical biosensor for quantitative characterisation of DNA methylation. With this biosensor we will develop a new point of care screening technique prior to MRI and CT scan which is less invasive and more time and cost effective. To fabricate a biosensor two various assays were developed and their performance for the detection of MGMT gene, one of the most reliable golima's biomarkers, were tested. These techniques will be promising for the

detection of brain tumours and potentially making the subsequent treatment easier and more effective. Both of these sandwich assays can be tailor-made to detect other methylated genes, revealing them as a basis for clinical applications in diagnostics and making them promising platforms for detecting methylated biomarkers.

Outline

This thesis has four chapters. Chapter 1 reviewed the current status of the brain tumors and its circulating biomarkers, with focus on methylated biomarkers. In addition, background knowledge on biosensors and their capabilities were reviewed as well as the state of the art biosensors for the detection of DNA methylation. Application of nanomaterials in biosensors, mainly graphene and gold nanoparticles (AuNPs) were also discussed in this chapter.

Chapter 2 will include various measurement and characterization techniques such as electrochemical techniques (voltammetry and amperometry), Raman spectroscopy, X-ray Photo electron Spectroscopy (XPS), Energy-dispersive X-ray spectroscopy (EDS) and, Scanning Electron Microscopy (SEM) as well as a list of the materials that were used throughout this project. In addition, immobilization techniques for various bioreceptors will also be briefly discussed in this chapter.

Chapter 3 will present the concept, the optimization process and the results of the designed sandwich biosensors: the Ab/ssDNA biosensor and the PNA/Ab biosensor. The former is based on aminated rGO electrodes and uses antibody and ssDNA to detect ss-MGMT gene and its methylation. The latter is based on ErGO/AuNPs electrodes and utilizes PNA to capture ds-MGMT gene following by the detection of methylation by antibodies. The dynamic range, LOD and sensitivity results of both of the biosensors can be found in this chapter as well.

Chapter 4 will summarize and conclude the major progress and the results of this PhD project and will highlight the contribution of this thesis to knowledge together with recommendations for future studies based on this work. Furthermore, there will be a list of publications, presentations in conferences and network events (talks and posters),

awards and self-development activities which were done during the time of this project at Plymouth University.

1.7 State of the art (2019 - 2023)

Table 1.6 shows an overview of the biosensors which were developed between 2019 and 2023, to detect the MGMT gene.

Biomarker	Platform	Detection Technique	LOD and Dynamic Range	References
MGMT	Gold electrodes modified with 11-mercaptoundecanoic acid (11-MUA) SAM	Electrochemical Impedance Spectroscopy (EIS)	0.24 $\times$ 10^{-12} mol L^{-1}, 1.0 $\times$ 10^{-11} to 1.0 $\times$ 10^{-6} mol L^{-1}	Carr et al. (2020)
MGMT	Streptavidin–magnetic microbeads (Strep–MBs) modified with a complementary DNA capture probe	Amperometry	23.0 and 13.2 pM, N/A	Povedano et al. (2020)
MGMT	Graphene oxide-magnetic nanoparticles-β-cyclodextrin (GO-Fe3O4-β-CD) nanocomposite and anti-5mC	Voltammetry	0.0825 pM, 0.001 - 1000 nM	Yang et al. (2022)
MGMT	Aminated rGO	Voltammetry	12 fM, 50 fM- 100 pM	This work
MGMT	AuNPs decorated ErGO and PNA	Amperometry	0.86 pM, 1 pM - 50 μM	This work

Table 1.6: An overview of various biosensors developed from 2019 - 2023 to detect MGMT gene.

Chapter 2

Materials and methods

2.1 Introduction

This chapter covers the details about the immobilization of biorecognition elements on the electrode surface, as well as electrochemical techniques used for both detection and characterization. Moreover, principles of other characterization techniques e.g. Raman, XPS, SEM and EDS are also explained.

2.2 Immobilization of bioreceptors

The biochemical specificity of the bioreceptor as well as the quality of the transducer determine the performance of a biosensor. The bioreceptor selection mainly depends on the analyte, however, other factors like stability, shelf life and enduring in certain conditions can also affect the selection process (Asal et al., 2018; Prieto-Simon et al., 2008). Various types of biomolecules have been used as a bioreceptor for biosensing purposes as listed in figure 1.8. However, antibodies and nucleic acid based probes are the most extensively used bioreceptors. Bioreceptor immobilization techniques includes covalent binding (including chemisorption and self assembled monolayer (SAM)), physical adsorption (physisorption), entrapment or encapsulation and affinity. Table 2.1 summarizes these techniques and their advantages and disadvantages. A proper immobilization technique will lead to an enhanced orientation of the bioreceptor and a higher reactivity and availability of the bioreceptor to capture the biomarker (figure 2.1) (Rashid and Yusof, 2017). This thesis will only focus on adsorption and chemisorption of antibodies and nucleic acid probes.

Immobilization method	Interaction	Advantages/Disadvantages	References
Physical adsorption	Van der Waals, electrostatic, hydrophobic/ Reversible	**Advantages:** Low cost, rapid, simple. **Disadvantages:** Random orientation, Sensitive to ionic strength and pH, short usage time, poor reproducibility.	Lemeshko et al. (2001); Du et al. (2012)
Covalent binding	Chemical bonding, chemisorption, SAM/ Irreversible	**Advantages:** Good stability, high binding strength, high sensitivity, good orientation, good reproducibility. **Disadvantages:** High cost, slow, use of linker molecules.	Li et al. (2012); Wang et al. (2004)
Affinity	Streptavindin or avidin with biotin interactions/ Reversible	**Advantages:** Good orientation, high specificity. **Disadvantages:** High cost, slow.	Ma et al. (2013); Zhang et al. (2013)
Entrapment/ encapsulation	Trapping probes within a polymer like chitosan, pyrrole, etc/ Irreversible	**Advantages:** High thermal stability, well controlled polymer growth, high entrapment of probes. **Disadvantages:** Biomolecule leakage, mass transfer limitations.	Jolly et al. (2016); Teles and Fonseca (2008)

Table 2.1: An overview of various immobilization techniques, their type of interaction as well as advantages and disadvantages.

2.2.1 Antibody immobilization

Antibodies are Y shaped biopolymers with molecular mass of approximately 150 kDa and size of about 10 nm. Antibodies are consist of two variable regions which bind to antigen (F_{ab}) and a constant fragment or a tail region (F_c) which are joined together by a flexible hinge (Davies and Chacko, 1993; Reth, 2013). Physical adsorption or physisorption of the antibodies onto the surface is the simplest attachment method; however, there would be no control over the orientation of the antibodies and also, they can be removed by washing steps (Shen et al., 2017). Chemical adsorption or chemisorption is the formation of chemical bonds between a sorbent (solid surface) and a sorbate (an ion, atom, or molecule). Chemisorption of antibodies provides high

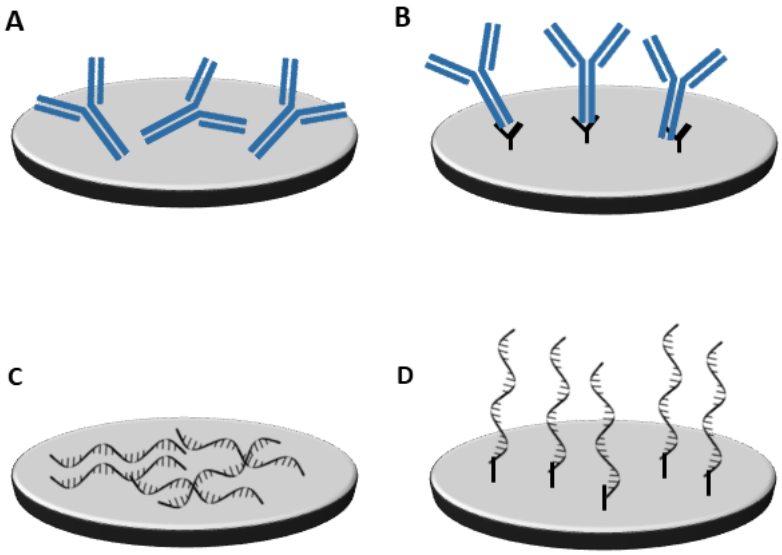

Figure 2.1: Immobilization technique of the biorecognition layer influences the orientation of the biomolecules and their availability to detect the target biomarker. A & C) The biorecognition layers were immobilized on the surface without considering the orientation of the biomolecules. In these cases, the antigen binding sites are not available to bind. B & D) The biorecognition layers were aligned in the desired orientation, leaving the antigen binding sites available for binding to the target antigen.

stability of the antibodies and improved orientation and therefore better reproducibility (Ruthven, 2003; Zhang et al., 2020). Although chemisorption of antibodies has shown to improve their orientation and density, still unfavourable orientation can happen (Welch et al., 2017).

Protein G and protein A, are immunoglobulin-binding bacterial membrane proteins which have specific binding affinity for the F_c regions of antibodies. These proteins can be immobilized on the sensor surface to capture the F_c regions of the antibody, leaving the F_{ab} domains free to attach to the antigen (Fowler et al., 2007; Lu et al., 1996; Trilling et al., 2013). Elshafey et al. (2013) reported an electrochemical impedance immunosensor for the detection of epidermal growth factor receptor (EGFR), based on AuNPs-protein G scaffold. In this work, they first electrodeposited AuNPs on the gold electrode, followed by immobilization of protein G, using linkers. Protein G layer was then used to orient the EGFR antibodies immobilization. The dynamic range was re-

ported to be from 1 pgmL^{-1} to 1 μgmL^{-1} with LOD of 0.34 pgmL^{-1} in PBS and 0.88 pgmL^{-1} in human plasma. Gohring et al. (2010) developed an opto-fluidic ring resonator (OFRR) biosensor for the detection of HER2 protein biomarker. In this work a layer of protein G was first immobilized on the inner surface of OFRRs, which then oriented the HER2 antibodies. The results showed that the OFRR was able to detect HER 2 in serum, in 30 minutes with a dynamic range of 13 to 100 ngmL^{-1} with a LOD of 10 pgmL^{-1}. Duan and Xi (2020) reported a biosensor based on localized surface plasmon resonance (LSPR), silver nanoparticles and protein G to detect HE4, a biomarker of ovarian carcinoma in urine. In this study, first the silver nanoparticles were synthesized on a glass substrate, then the substrate was incubated in protein G and finally, the anti-HE4 was immobilized on the surface. The dynamic range was reported to be 1 to 10×10^3 pM with a LOD of 1 pM.

2.2.2 Nucleic acid based probes immobilization

Depending on the target biomarker, various types of nucleic acid (NA) based probes can be used in developing biosensors. SsDNA, miRNA and PNA are amongst the most intensively used probes. Adsorption is a common technique to immobilize the probes on the electrode surface, taking the advantage of electrostatic forces between the NA and the electrode surface. Although this technique is the simplest immobilization technique, there are some disadvantages such as a high risk of desorption from the electrode surface in certain conditions and immobilization in random orientations. On the other hand, chemisorption which is the covalent bonding of the NA-based probes on the metal surface using functional groups, has shown a higher stability and a better orientation (Rashid and Yusof, 2017). The chemisorption of the NA-based probes on the electrode surface will lead to the formation of self assembled monolayers (SAM). SAM is one of the most extensively reported techniques to immobilize NA-based probes, specially on gold electrodes or AuNPs covered surfaces. Some functional groups (-CN, -NH_2 or -SH) have demonstrated high affinity towards gold and gold nanoparticles, enabling the formation of SAM-modified electrode surface (Putzbach and Ronkainen,

2013). Feng et al. (2006) reported a CeO_2/chitosan (CHIT) nano-porous film as a modification matrix on GCE surface for immobilization of DNA probes. The matrix showed an enhanced signal compared to the chitosan modified GCE by increasing the loading of DNA probes. The dynamic range for this sensor was 1.59×10^{-11} to 1.16×10^{-7} mol L^{-1}, with LOD of 1×10^{-11} mol L^{-1}. Oliveira et al. (2015) reported an electrochemical biosensor for the detection of a DNA biomarker of dengue virus (DENV-3). Prior to the immobilization of the DNA probes, the pencil graphite electrode (PGE) were pretreated by applying potential in an acetate solution for 5 min. The developed biosensor showed the dynamic range of 10 - 100 nM with LOD of 3.09 nM. Thevendran et al. (2022) developed a biosensor for the FLT3-ITD mutations using electrode IDE sensor chips covered by gold-sputtered zinc oxide (ZnO) nanorods. Thiolated ssDNA probes were immbobilized on the Au-ZnO nanorods and were then incubated in the target biomarker. The dynamic range for this biosensor was reported to be 1 nM to 1 μM with LOD of 1nM. Hamidi-Asl et al. (2013) reported a PNA-based biosensor for the electrochemical detection of the point mutation of the p53 gene. In this work, first, thiolated PNA probes formed a SAM on a gold electrode surface and then the electrode was incubated in the ds-target gene to form triplex structures. Methylene blue (MB) was used as the label to enhance the electrochemical signal. The linear range was reported to be 10 pM to 5 × 107 pM with an LOD of 4.15 pM. Ahour et al. (2013) reported an electrochemical biosensor for the detection of the double-stranded plasmid (ds-PI) using PNA probes and a gold electrode. The PNA oligomer probes were first immobilized on the surface before capturing the ds-PI target, forming a PNA/ds-PI structure using MB as the label. The dynamic range was from 10 to 300 pgμL^{-1} with an LOD of 9.5 pgμL^{-1}.

Approach	Most usage	Advantages/Disadvantages	Sensitivity
Potentiometric	Enzymatic activity	**Advantages:** Low cost, reproducibility, rapid measurements, reusable, and suitable for placement of enzymes. **Disadvantages:** Sensitive to the environment and temperature.	Achieve up to pg/mL
Amperometric	Commercial activity such as diagnosis of blood glucose, nucleic acid, antigens, pesticides, food quality and so on.	**Advantages:** Low cost, reproducibility, rapid measurements, reusable, suitable for placement of enzymes, no need for calibration and more appropriate for mass production. **Disadvantages:** Need redox elements to enhance the current production, time consuming, sensitive to the environment.	Achieve up from ng/mL to pg/mL
Impedimetric	Widely used to detect DNA hybridization, direct monitoring of antibody-antigen connected reactions, and enzyme reactions	**Advantages:** Enabled label-free recognition, ease of detection for genomics and proteomics, upper signal-to-noise ratio, cost-effective, short period of assessment. **Disadvantages:** Sensitive to the environment, bulky devices required, require theoretical stimulation for data analysis.	Achieve up to μg/mL to pg/mL
Conductometric	Many enzyme reactions, many biological membrane receptors, clinical analysis, detect foodborne pathogens, drug detection and pollutant detection	**Advantages:** Inexpensive, reusable, insensitive to light, without any reference electrode, possibility of miniaturization, and reducing power consumption due to voltage reduction.	Achieve up to µg/mL to pg/mL

Table 2.2: An overview of various electrochemical biosensors and their advantageous and disadvantages. adapted from Sharifi et al. (2019).

2.3 Characterization techniques

2.3.1 Electrochemical measurements

Electrochemistry

Electrochemical detection is used by many researchers due to its ease of use and simplicity. Electrochemistry studies the relation between the flow of electrons (electrical properties) and chemical changes. In electrochemistry, the target reaction generates either a measurable current, a charge accumulation (potential), changes in the conductivity of a medium or resistance and reactance. The techniques to monitor these properties are called amperometry, potentiometry, conductometry and impedimetry respectively. Electrochemical experiments typically need a small sample volume, which is an advantage over some other detection methods. Electrochemistry was shown to be able to achieve low limits of detection (LOD) with minimum sample preparation (Ronkainen et al., 2010; Elgrishi et al., 2017). Different electrochemical methods, their usage, advantages and disadvantages as well as their sensitivity limit is listed in Table 2.2. Yang et al. (2018) developed a DNA-labeled sandwich electrochemical biosensor for the detection of MCF-7 breast cancer cells based on a GCE modified with 3D graphene and a hybrid of Au nanocages and amino-functionalized multi walled carbon nanotubes. This biosensor showed a LOD of 80 cells/mL. Shahrokhian and Salimian (2018) reported a label-free electrochemical biosensor based on conducting polymer and rGO for the detection of BRCA1 gene which is a biomarker for breast cancer. For the fabrication of this sensor, first rGO was deposited electrochemically on the GCE surface followed by electro-polymerization by P3CA polymer. ssDNA probe was immobilized on the surface overnight and finally the probe was hybridized by the target DNA. The quantitative determination of BRCA1 gene was reported in the range of 10 fM to 0.1 μM and the LOD was 3 fM. Akbari jonous et al. (2019) designed a sandwich biosensor for the detection of total and free prostate specific antigens (PSA) based on rGO and AuNPs. In this paper, anti-total PSA and anti-free PSA antibodies were first immobilized on AuNPs modified GO. These nanoprobes were used to capture to-

tal and free PSA antigens in a sandwich order on a GCE. The LOD was reported to be 0.2 and 0.07 ng/mL for total and free PSA antigen respectively. In another paper, Cardoso et al. (2016) developed a simple electrochemical biosensor for the detection of miR-155, which is a biomarker of breast cancer. For the aim of this project, thiolated anti-miR-155 was immobilized on the gold electrode, followed by the hybridization of the probe and the target miRNA. The reported LOD was 5.7 aM.

Electrodes and electrolyte

An electrochemical reaction is carried out by placing at least two conductive materials (electrodes) in an electrolyte solution, in an electrochemical cell. As shown in figure 2.2, the electrochemical cell consists of a working electrode (sensing or redox electrode), a reference electrode, usually a counter (auxiliary) electrode and a conductive electrolyte solution. A potentiostat is also required to control and run the experiment.

The electrodes provide a place where a charge can be transferred or its effects can be measured. Since the reactions are detected in close vicinity of the electrode surface, the electrode material, its dimensions and surface modification play a crucial role in detection ability and performance of the electrochemical biosensor (Anik, 2017; Grieshaber et al., 2008).

The working electrode is the electrode at which the reactions or transfers of interest take place. The working electrode can be made of elements, such as gold, carbon or platinum, composites like carbon-based composites or nanomaterials such as graphene electrodes. The reference electrode provides a constant potential which is required for electrochemical reactions. The most common reference electrodes are silver/silver chloride (Au/AuCl) and saturated calomel electrodes. The auxiliary electrode which usually is used in voltammetric and impedimetric measurements, establishes a connection to the electrolyte to apply current to the working electrode. platinum and graphite are the most common auxiliary electrodes used. All the three electrodes should be conductive and chemically stable in order to provide enable a suitable electrochemical reaction (Anik, 2017; Grieshaber et al., 2008; Kounaves, 1997).

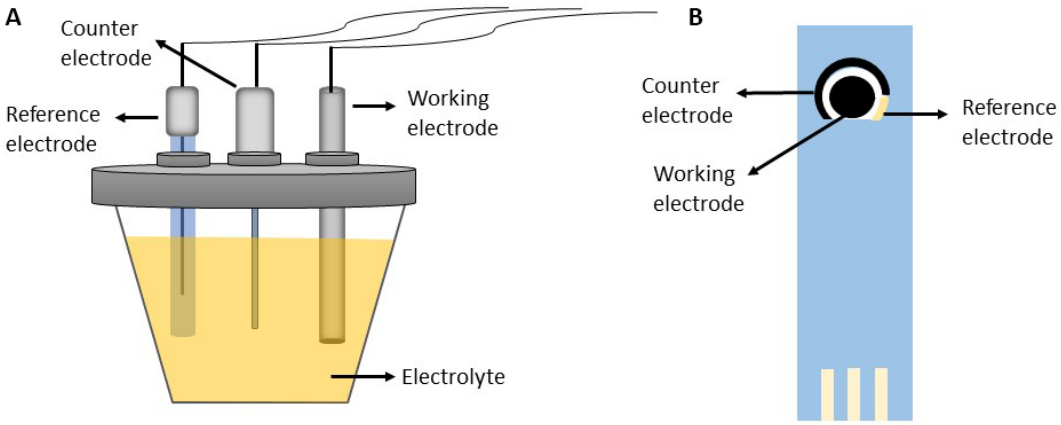

Figure 2.2: A schematic of A) an electrochemical cell, consisting of three electrodes (namely: reference electrode, counter electrode and working electrode) and electrolyte. The electrochemical reactions are carried out in the cell and are measured with a potentiostat which connects to the electrodes through wires. B) on a screen printed electrode the three electrodes are printed on a substrate and a small amount of the electrolyte is needed to cover all of the electrodes.

The supporting electrolyte solution is ionic and conductive and contains salt or acid. The electrolyte carries the current, balances the charge and completes the circuit. A good electrolyte substance should be highly soluble in the chosen solvent and be both electrochemically and chemically inert in the experiment's conditions. The most common electrolyte substances are $[Fe(CN)_6]^{3-/4-}$ and $[Ru(NH_3)_6]^{2+/3+}$ (Elgrishi et al., 2017; Scott, 2016). The potentiostat is used to maintain the working electrode's potential at a constant level as a function of the reference electrode's potential by adjusting the current at the auxiliary electrode (Elgrishi et al., 2017).

Voltammetry

In voltammetry, information about an analyte is obtained by varying the applied potential (E) to the working electrode which changes with time (T) and the current (I) that flows through working electrode is recorded as a function of the applied potential. Therefore voltammetry falls into the category of potentiometric techniques. The outcome of voltammetry is a plot of response current versus applied potential which is known as a voltammogram. There are various forms of voltammetry, such as square

wave voltammetry (SWV), linear sweep voltammetry (LSV), differential pulse (DPV) and cyclic voltammetry (CV). The differences between these techniques are in the way the potential is varied. Voltammetric techniques have various analytical advantageous such as: high sensitivity over concentration, various types of useful solvents and electrolytes, fast analysis time, simultaneous determination of several analytes, measurement of small current and possibility to detect in a wide range of temperatures (Grieshaber et al., 2008; Compton and Banks, 2018; Simões and Xavier, 2017). It is very common in sensor development to use CV and DPV together. CV is normally used for the exploratory purposes such as determination of adsorption processes in surfaces and the study of electron transfers. However, DPV is a more sensitive technique and is normally used for the analytical determination (Simões and Xavier, 2017).

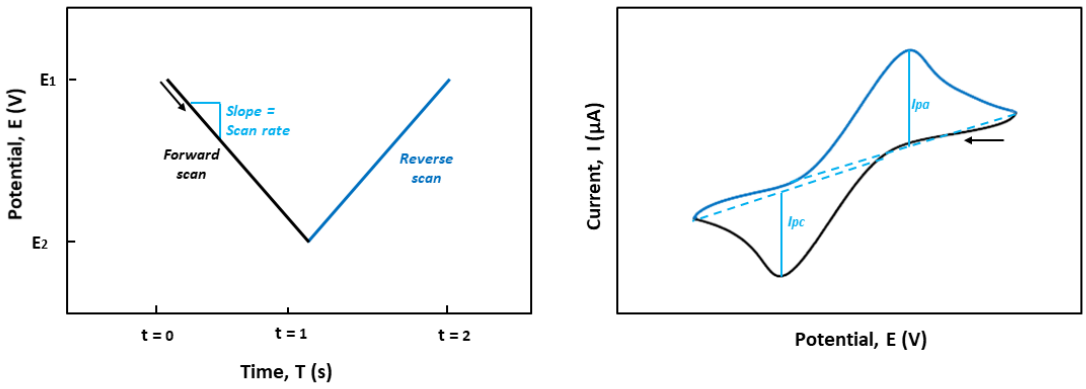

Figure 2.3: CV measurement: The waveform of the applied potential as a function of time (left) and a cyclic voltammogram (right), where I_{pa} shows the anodic peak current and I_{pc} shows cathodic peak current.

Cyclic Voltammetry (CV): CV is a versatile and the most widely used electroanalytical measurements to study electroactive behaviour of an analyte. In this technique, the applied potential at the working electrode is swept linearly versus time in both forward and reverse directions. The fixed rate at which the potential is swept between two potentials is known as experiment's scan rate. The current is monitored and recorded. For example, the voltage is swept from E_1 to E_2 and then the scan is reversed and the voltage is swept back to E_1 (figure 2.3). In the case of $[Fe(CN)_6]^{3-/4-}$ electrolyte, the

resulting electrochemical changes are due to the following oxidation/reduction reaction:

$$[Fe(CN)_6]^{3-} + e^- \rightleftharpoons [Fe(CN)_6]^{4-} \tag{2.1}$$

The voltage is measured between the working and the reference electrodes while the current is measured between the working and the counter electrodes. The obtained current is then plotted as a function of the scanned potential. The peak current and peak potential of the cyclic voltammograms are important parameters and can be further studied together with other parameters such as scan rate or concentration (Elgrishi et al., 2017; Scott, 2016).

Differential Pulse Voltammetry (DPV): In DPV, the potential is applied in a series of regular pulses increasing along a linear baseline. The applied base potential is the potential value at which there is no reduction or oxidation reaction. The potential increases between pulses and this increase in constant. The current is measured just before the potential is applied (I_1) and before the end of each pulse (I_2). Then the difference between the two current measurements ($I_2 - I_1$) is plotted as a function of potential (figure 2.4). Like in CV, the potential is applied between the working and the reference electrodes, while the current is measured between the working and the counter electrodes (Kounaves, 1997; Simões and Xavier, 2017).

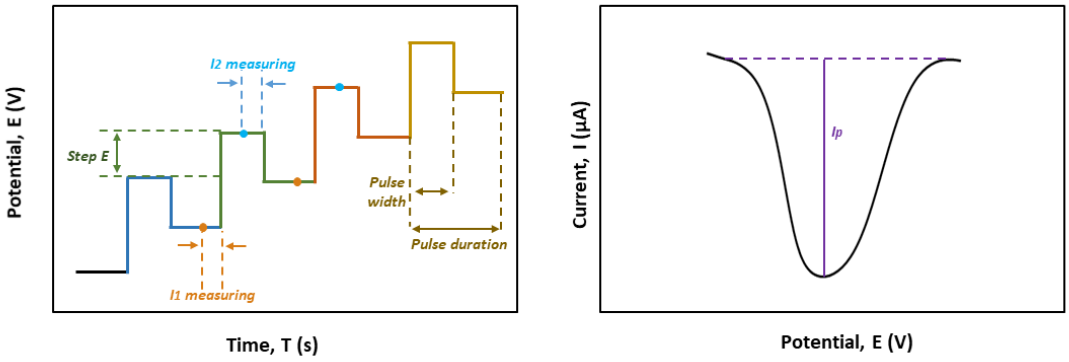

Figure 2.4: DPV measurement: Pulse sequence detail (left) and a Differential Pulse Voltammogram (right), where I_p shows the peak current.

Amperometry

In amperometric measurements potential is maintained constant at the working electrode while current, which is generated by an electrochemical oxidation or reduction, is measured. Most of the biomolecules do not have redox properties and therefore require electroactive labels as well as redox mediators, Oxygen and H_2O_2 being the most widely used mediators (Luppa et al., 2001; Grieshaber et al., 2008; Chaubey and Malhotra, 2002). A well known example of amperometric biosensors is the glucose biosensor which is the first commercialized biosensor. Figure 2.5 shows the principle of the amperometric detection.

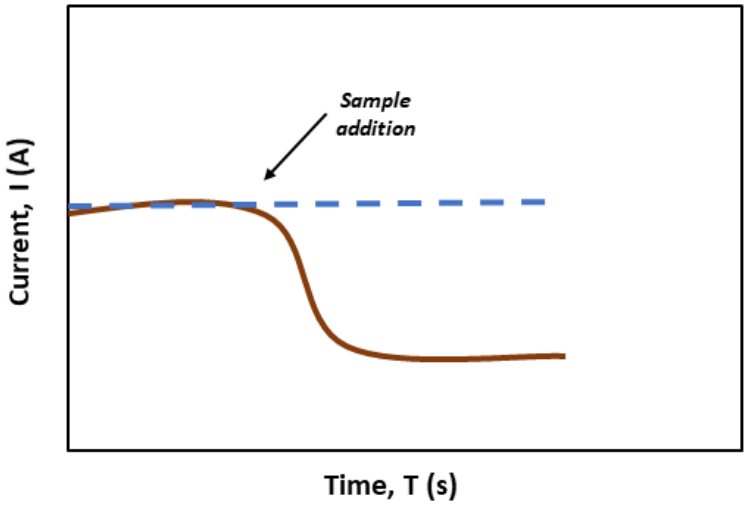

Figure 2.5: Amperometric measurement: Upon addition of the sample (mediator), the oxidation reaction starts which causes a decrease in current.

Electrochemical measurements

Electrochemical measurements were performed with Dropsens (Spain) μStat ECL BiPotentiostat/Galvanostat using DropView 8400 software. The reduced graphene oxide (rGO) screen printed electrodes (DRP-110RGPHOX) were purchased from Dropsens. The electrodes had rGO as the working electrode, carbon as the counter electrode and silver as the reference electrode. All of the electrochemical measurements were performed at room temperature. The μStat ECL BiPotentiostat/Galvanosta and a SPE is

Figure 2.6: A μStat BiPotentiostat/Galvanostat and a screen printed disposable electrode, both from Dropsens (Spain). The potentiostat is used to maintain the working electrode's potential at a constant level and adjusting the current. The electrode is a three electrode system printed on a substrate and can be connected to the potentiostat. The principles are explained in section 1.4.1.

shown in figure 2.6.

Electrochemical measurements (CV and DPV) were carried out for the bare electrode and after each incubation step using a μStat BiPotentiostat/Galvanostat. All of the measurements were performed in 100 μL of 10 mM PBS pH 7.4 solution containing 10 mM $K_3[Fe(CN)_6]$ and 1M KCl as electrolyte agents. For the Ab/ssDNA biosensor measurements, the CV signals were obtained in the scan potential range of -0.2 and 0.55 V with the scan rate of 100 mV/s. While DPV measurements were performed in the scan potential range of -0.15 and 0.45 V, a pulse duration of 40 ms and scan rate of 100 mV/s (Li et al., 2015). For the PNA/Ab biosensor measurements, the the CV and DPV voltammograms were obtained in the same scan potential range as the Ab/ssDNA biosensor while the scan rate of the CV measurements was changed to 50 mV/s. Amperometric measurements were performed in PBS containing 1 mM HQ under agitation at -0.2 V. Once the background current was stabilized, 0.1 M H_2O_2 solution was added and the current was recorded until the steady-state current was reached. The entire measurement was done in 150 s. A schematic of the electrochemical measurement setup is shown is figure 2.7.

Figure 2.7: A schematic of a measurement setup, using a galvanostat and a software interface.

2.3.2 Raman Spectroscopy

Raman spectroscopy is an essential tool in nanotechnology and specially in single/ multi layer graphene systems due to its high resolution and sensitivity to the chemical and physical properties of materials as well as its non-destructive nature (Jorio et al., 2011; Ferrari and Basko, 2013). In Raman Spectroscopy, a laser beam is used for the excitation and polarization of the surface atoms and moving them to a new vibrational and rotational state. After the photon is emitted, most of the atoms go back to their initial state (Rayleigh Scattering) and the photons are elastically scattered. However, a small portion of the photons are inelastically scattered and experience a Raman shift. These atoms either go back to a lower (Anti-Stokes Raman Scattering) or higher (Stokes Raman Scattering) vibrational states. This phenomenon gives various types of information, in this case about the present molecules and chemical bonds in graphene based materials (figure 2.8) (Cialla-May et al., 2019; Ferrari, 2007).

Raman spectrum of GO and rGO normally show two major peaks, which are caused by the laser excitation. The D bands which are at around 1330 cm^{-1} for GO and 1350 cm^{-1} for rGO, is due to the out-of-plane vibration of the disordered structures. The G bands which are at around 1592 cm^{-1} and 1570 cm^{-1} for GO and rGO, respectively are caused by in-plane vibrations of the sp^2-bonded graphitic carbon atoms. Two minor bands of 2D and D + G, which are more significant in rGO are attributed to the restoration of the graphite structures. The relative intensity ratio (I_D/I_G), is normally used to assess the defect and disorder levels and increases after reducing the GO to

rGO which is due to the increase of the defects in the structure, decrease in the average size of the sp^2 due to the removal of the oxygenated functional groups as well as more isolated domains of graphene (Lee et al., 2018; Le et al., 2020; Wu et al., 2018; Konios et al., 2014; Hidayah et al., 2017; Childres et al., 2013).

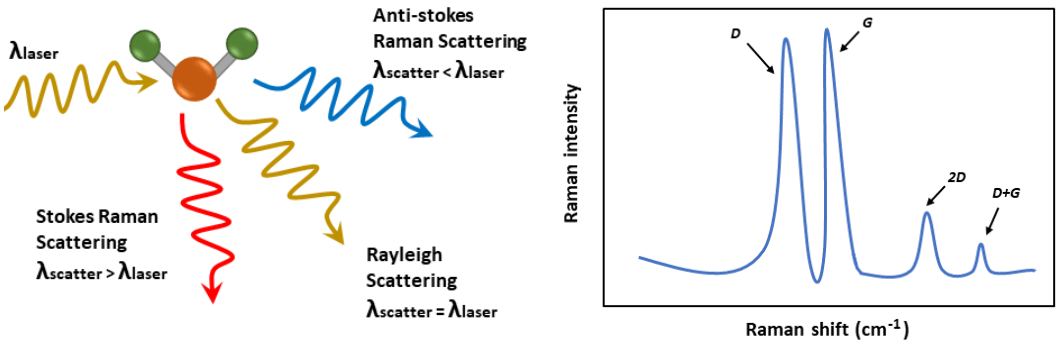

Figure 2.8: A schematic of the different possible scattering processes which happens in a Raman Spectrometer after a photon is emitted and atoms are excited (left). The most common Raman peaks of graphene-based materials (right).

Raman measurements

Raman spectra were obtained using a XPLORA HORIBA system combined with an Olympus BX41 microscope (equipped with 10X, 100X objective lenses and 10 X eyepieces). The XPLORA HORIBA system and a schematic of the Raman setup are shown in figure 2.8. A 532 nm green laser source with the power of 100 mW, 100X objective lens, a scan range of 1100 to 3000 cm^{-1} and an exposure time of 5-60 s were used to characterise graphene and reduced graphene oxide electrodes. A graphene electrode was used to compare the spectrographs with rGO electrode.

2.3.3 X-ray photoelectron spectroscopy

X-ray photoelectron spectroscopy (XPS) is a widely used surface sensitive tool which is used to identify the elemental composition and chemical states of a specimen. In a XPS measurement the sample is bombarded by X-rays, which lead to electron emission from the surface and can then be used to determine the presence of elements (except hydrogen and helium) on the surface (Fadley, 2010; Stevie and Donley, 2020). XPS

spectra can be obtained in two modes: wide scan and high resolution scan. The wide scan gives an overview of the elements present on the surface where the high resolution scan reveals a more in depth profile of the elements such as bonding state. Figure 2.9 depicts a schematic of working principle of XPS as well as examples of a wide scan and a high resolution spectra. In this study, XPS was used to ensure the presence of required molecules on the surface of GO and rGO electrodes. Both wide scan and high resolution scans were used in this study.

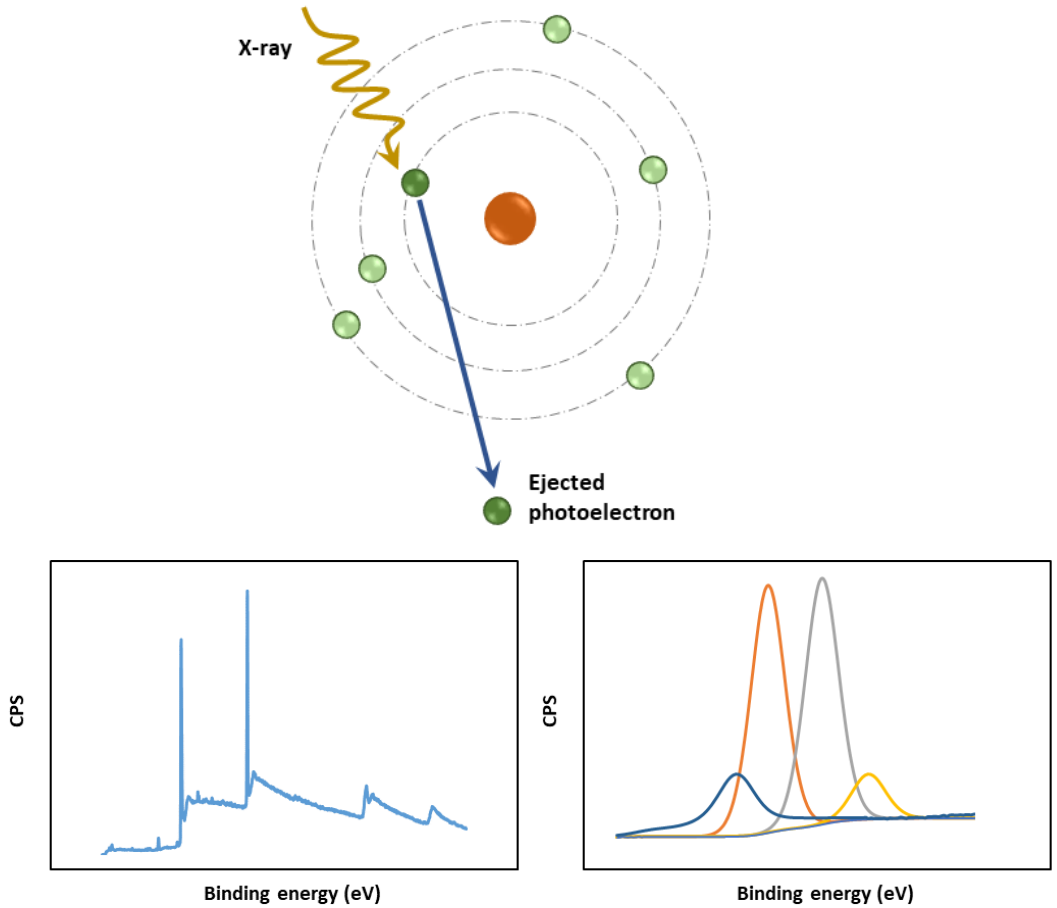

Figure 2.9: A schematic of the working principle of XPS where an electron is ejected from its orbit by an X-ray (top). Samples of a wide scan spectrum (left) and a high resolution spectrum (right).

XPS measurements

A Thermo Scientific Nexsa X-Ray Photoelectron Spectrometer System was used to carry out the XPS analysis using a monochromatic Al Kα X-ray source (1486.68 eV).

The pass energy for wide scans was 200 eV with an energy step size of 1 eV and 10 scans. The pass energy for high resolution scans was 40 eV with an energy step size of 0.1 eV and 20 scans.

2.3.4 Electron Microscopy and Energy Dispersive Spectrometry

The scanning electron microscope (SEM) is a versatile instrument which can provide information about the morphology, surface topography and chemical composition of a specimen. In SEM the light source of a microscope is replaced with an electron beam. SEM has various advantages over a light microscope such as: larger depth of field, higher magnification as well as providing compositional data (Zhou et al., 2006; Ul-Hamid, 2018; Vernon-Parry, 2000). In addition to that, an energy dispersive x-ray spectrometer (EDS) detector can be attached to the SEM for further analysis of the surface. EDS uses a beam of electrons to shift an electron from its shell and creating an electron hole after which an electron from a higher energy shell fills the electron hole resulting in a X-ray emission (Shindo and Oikawa, 2002). EDS gives information about the chemical state of a sample as well as the relative abundance of elements. Figure 2.10 shows a schematic of the working principle of EDS and an example of a spectrum obtained from EDS. In this work both SEM and EDS were used to study the morphology and the chemical state of the GO and rGO electrodes before and after different modification steps. This was to confirm the structural changes after modifications as well as the presence of desired molecules on the surface.

SEM measurements

Scanning electron microscopy (SEM) was performed using a JEOL 6610LV SEM using Accelerating Voltage of 30 kV. The SEM was equipped with a OI X-Max 80mm^2 EDX with the beam adjusted to 15.0 kV.

2.4 Materials and Suppliers

All of the reagents used in this project were of analytical grade. Tris-EDTA (TE) pH 8.0, phosphate buffered saline (PBS) pH 7.2, bovine serum albumin (BSA), sodium

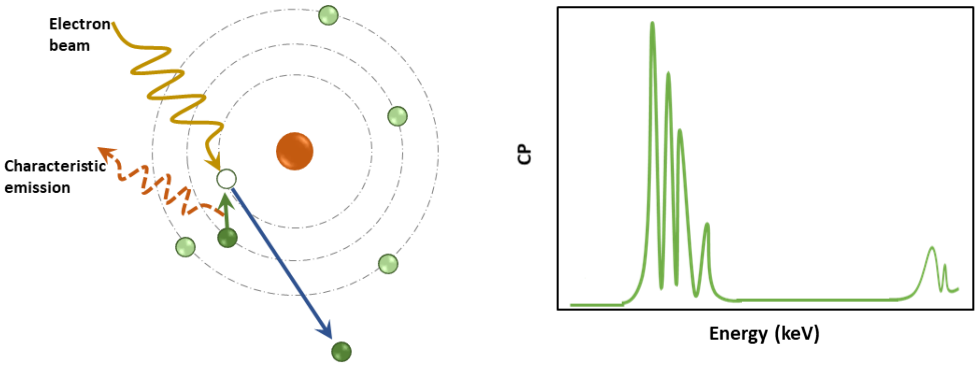

Figure 2.10: A schematic of the working principle of EDS where an electron is shifted from its orbit and an electron from a higher energy shell fills the electron hole, resulting in an X-ray emission (left). A sample spectrum of EDS (right).

chloride (NaCl), potassium ferricyanide ($K_3[Fe(CN)_6]$), potassium chloride (KCl), ammonium hydroxide solution 28% ($NH_3(aq)$), hydroquinone (HQ), hydrogen peroxide solution 30% (H_2O_2), Nuclease-Free Water, gold(III) chloride trihydrate ($HAuCl_4$), Sulphuric Acid (H_2SO_4) and 6-Mercapto-1-hexanol (MCH) were purchased from Sigma-Aldrich (UK). PBS tablets pH 7.4 were purchased from Fisher Scientific (UK) and the PBS buffer solution was prepared in Milli-Q water. Recombinant protein G was obtained from ThermoFisher (UK). Single layer graphene oxide solution (GO) was ordered from Graphene Supermarket (USA). Mouse anti-5-methylcytosine monoclonal antibody (anti-5mC) was purchased from Zymo research (USA). Biotinylated anti-5mC and Streptavidin-HRP were ordered from abcam (UK). PNA was obtained from Cambridge Research Biochemicals (UK) and its sequence was N-AEEA-AEEA-CACCAAGT CGCAAACGGTGC-C. All other nucleic acids were purchased from Integrated DNA Technologies (USA). The purchased single stranded (ss) DNA sequence of the MGMT gene was GTCC C_M GA C_M GCC C_M GCAG GTCCT C_M GCGGTGCGCACCGTTTGC-GACTTGGTG, where C_M was methylcytosine. The complementary sequence was CACCAAGTCGCAAACGGTGCGCACCGCGAGGACCTGCGGGCGTCGGGAC. All of the solutions and biomolecules used in this study were prepared freshly before or during the experiments.

2.5 Data Collection and Data Analysis

Voltammetric and amperometric measurements were perfromed using Dropview 8400 software which was provided by Dropsens. A python code was developed to collect the peak potentials of both CV and DPV voltammograms. Raman spectroscopy data were collected and analyzed using LabSpec 6 software. XPS data were analyzed using CasaXPS. SEM and EDS data were collected and analyzed using AzTec software. All of the graphs were plotted in Sigmaplot software and the two tailed T-test analysis for the selectivity studies were also performed by Sigmaplot. All of the error bars are the standard deviation of at least 3 replicates.

Chapter 3

Results and discussions

3.1 Ab/ssDNA sensor

3.1.1 Background

This section introduces an electrochemical biosensor for label-free detection of DNA methylation. In order to develop the biosensor to detect DNA methylation as a biomarker associated with glioma, the MGMT gene was chosen to be the specific target of this biosensor as it is shown to be a relevant biomarker for this category of brain tumor (Majchrzak-Celińska et al., 2013, 2015). The biosensor is based on aminated reduced graphene oxide electrode, which is achieved by ammonium hydroxide chemisorption

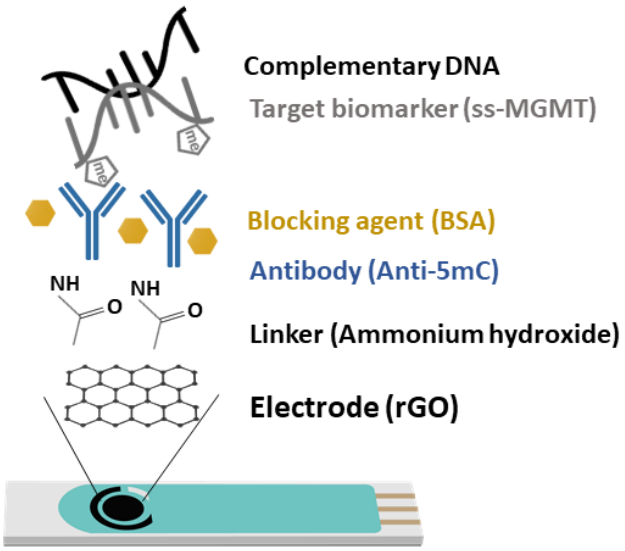

Figure 3.1: Illustration of various layers of the Ab/ssDNA biosensor.

and anti-5-methylcytosine (anti-5mC) as a methylation bioreceptor. The target single-strand (ss) MGMT oligonucleotide is first recognised by its hybridization with complementary DNA to form double strand (ds) MGMT, which is then captured by the anti-5mC on the electrode surface due to the presence of methylation. For the purpose of simplicity, this biosensor is named Ab/ssDNA sensor which shows that Ab and ssDNA were the biomolecules that were used in this sensor to detect the target methylated gene. Raman spectroscopy, XPS and SEM techniques were used to characterize the electrode surface. CV and DPV techniques were used for electrochemical measurements. Under optimized conditions, the proposed biosensor is able to quantify a linear range of concentrations of MGMT gene from 50 fM to 100 pM with a limit of detection (LOD) of 12 fM. The sandwich design facilitates the simultaneous recognition and quantification of DNA methylation and the amination significantly improves the sensitivity of the biosensor. This biosensor is label, bisulfite and PCR-free and has a simple design for cost-efficient production. The various layers of this sensor is illustrated in figure 3.1.

3.1.2 Biosensor concept and preparation

In this immunoassay ammonium hydroxide solution was chosen to provide the functional groups that facilitate the immobilization of antibodies on the surface. For that, the rGO SPEs were first incubated in ammonium hydroxide solution (28.0-30.0% NH_3 basis) for 2 hours at room temperature. Subsequently, the aminated electrodes were dried with nitrogen and were kept in vacuum for further use. Anti-5methylcytosine monoclonal antibody (anti-5mC) was chosen as the bioreceptor agent, which was used by many other groups (Cai et al., 2018; Chowdhury et al., 2014; Povedano et al., 2018c). Anti-5mC is able to capture DNA methylation targets and is methylation-specific. Protein G was used together with the anti-5mC, in order to orient the antibodies and prevent them from binding to the surface through their antigen binding sites (the regions in the antibody which bind to the antigen-Fab regions). Protein G is a bacterial membrane protein which is known for its affinity to the non-antigenic (Fc) regions of antibodies, leaving the antigen binding sites available to bind to their target antigen (Elshafey

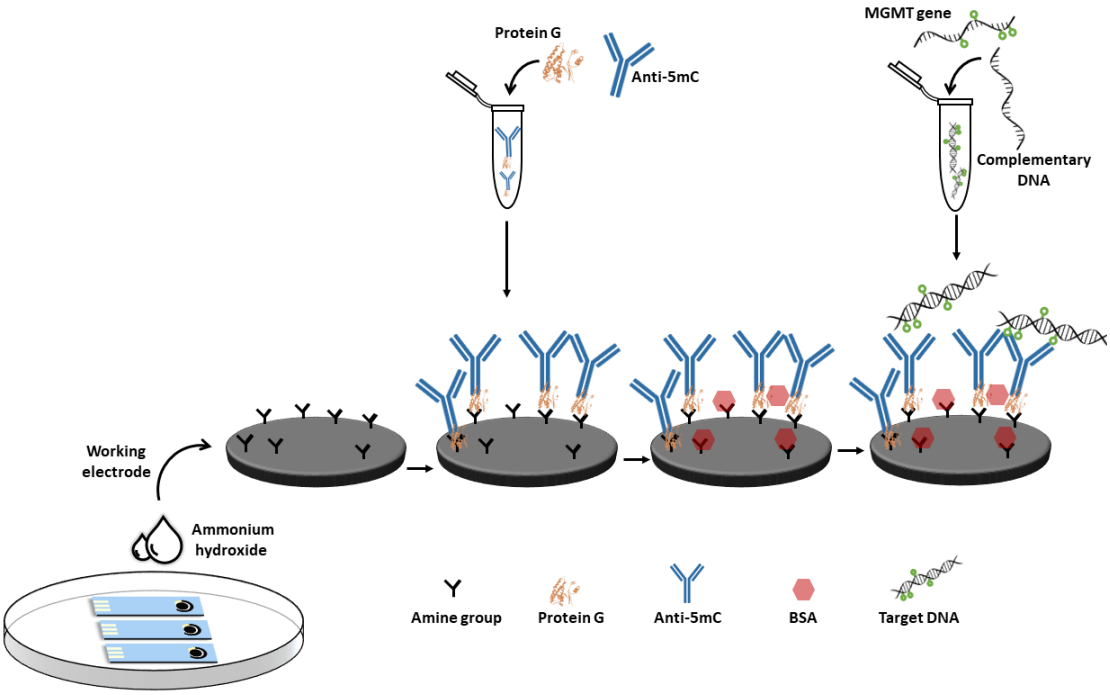

Figure 3.2: A schematic of the Ab/ssDNA assay.

et al., 2013; Fowler et al., 2007). The electrode was incubated in a mixture of anti-5mC and protein G (70:30) both diluted in PBS pH 7.2. After immobilization of antibody and protein G mixture, 1% BSA in PBS pH 7.4 was used as a blocking agent to block unbound functional groups that remain after incubating the bioreceptor molecules. Finally the sensor was incubated in various concentrations of single stranded target gene as well as hybridized target gene. The single stranded gene was diluted in TE buffer. The hybridization process was done as follows: first both the single stranded (ss) MGMT target gene and its complementary strand were diluted to a concentration of 1μM using TE buffer containing 50mM of NaCl (TE-NaCl). Then, 200μL of each gene was mixed together into a vial and the mixture was heated at 65°C for five minutes. The mixture was then diluted with TE-NaCl to desired concentrations and kept at 4°C for short term use. The electrode was washed with 300μL of PBS after each incubation step to remove unbound molecules and after each measurement to clean the surface and prepare for the next incubation step. Various preparation steps was optimized to achieve better repeatability and LOD. The optimizations are explained in detail in sec-

tion 3.1.3. The preparation steps are shown in figure 3.2. All of the incubation steps were carried out at room temperature and in a clean room to keep the moisture and the temperature constant throughout the study.

3.1.3 Optimization

Various preparation steps of this biosensor was optimized in order to achieve the most effective assay which leads to the best LOD and selectivity. The steps which were optimized for this biosensor are the following: understanding the effect of BSA, as blocking agent and protein G, BSA incubation time, antibody and antigen incubation times. For the all optimization steps, the normalization was done by dividing the peak current for each concentration with the peak current obtained with buffer containing no DNA (i.e. blank buffer) and the error bars are the standard deviation of at least three replicas.

The effect of BSA

For most biosensors, it is essential to block unbound functional groups on the surface prior to the incubation in the target biomarker to avoid non-specific binding to the sensor surface (Ronkainen et al., 2010). Here, the importance of the usage of BSA as the blocking agent was investigated for the detection of 100 pM of the target MGMT gene with both CV and DPV techniques. For the purpose of this experiment, two groups of electrodes were used. The electrodes of the first group were incubated in 100 pM of the target MGMT gene, after immobilizing the antibody on the surface. The electrodes of the second group were additionally incubated in 1% BSA for 15 minutes prior to the incubation in 100 pM of the target MGMT gene. The results for this experiment are shown in figure 3.3 where the normalized peak current is plotted with and without usage of BSA. The results show that without using the BSA the error bars are large and the CV and DPV results are not consistent, while the error bars are much smaller after using BSA and both CV and DPV techniques yielded consistent normalised peak currents. Thus, BSA was used as a blocking agent in further experiments.

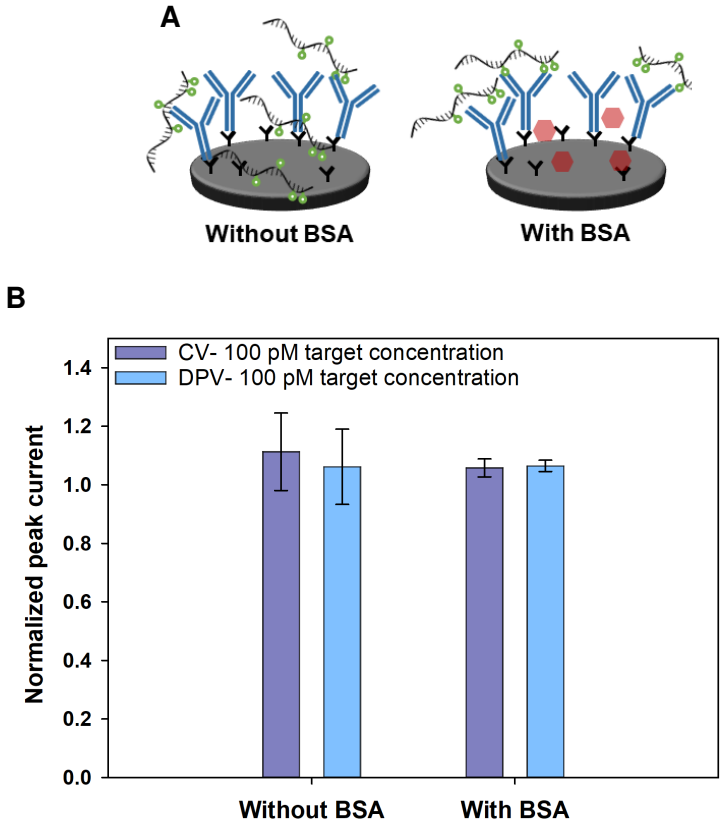

Figure 3.3: A schematic of BSA functionality tests (A) and their results (B) where 100 pM of the target gene was detected without (left) and with (right) usage of BSA, using both CV (purple) and DPV (blue) techniques.

The effect of protein G

Protein G was shown to be able to orient the antibodies on the surface through Fc (non-antigenic) region, leaving the Fab regions (antigen binding regions) available to bind. Here, the effect of protein G on the orientation of anti-5mC was investigated, using both CV and DPV techniques for the detection of 100 and 1000 pM of target gene concentrations. In this experiment, two groups of electrodes were used. The first group was incubated in anti-5mC with the concentration of 20 μg/ml prior to the incubation in 1% BSA. While the second group was incubated in a mixture of anti-5mC and protein G (70:30) with a concentration of 20 μg/ml (both diluted in PBS pH 7.2) before being incubated in 1% BSA. Finally both groups of the electrodes were incubated in 100 and 1000 pM of the target gene. As shown in figure 3.4, in the case of

both techniques, after using protein G the error bars decreased compared to not using protein G and the target concentrations became more distinguishable for the biosensor as the error bars of both concentrations do not overlapped. These results are due to the fact that the presence of protein G acts to preferentially align the antibodies on the electrode surface, resulting in an increased antigen binding capacity of the antibody Elshafey et al. (2013). Consequently, protein G was used in a mixture with antibody in the upcoming experiments.

BSA optimization time

The first optimization of incubation time was the optimization of the BSA incubation time by incubating three groups of electrodes in BSA for either 5, 15 or 30 minutes, followed by the detection of 100 and 1000 pM of the target gene. The CV (left) and DPV (right) (figure 3.5) results showed that among these three, an incubation time of 15 minutes was optimal, as the error bars are the smallest and the increase in the normalized peak current between 100 and 1000 pM in both techniques are consistent. In contrast, the normalized peak currents for both 15 and 30 minutes BSA incubation time showed larger error bars which can be due to remaining unbound functional groups for the shorter 5 min incubation time, and conversely, saturation of the electrode surface with BSA molecules for the longer 30 minute incubation time. Therefore, the incubation time of 15 minutes was selected as the optimized time and used in future experiments.

Amination incubation time

The second incubation time optimization step was optimizing the time that the electrodes were incubated in ammonium hydroxide. The rGO electrodes were divided into 5 groups and each group was incubated in ammonium hydroxide for a specific duration (either 30, 60, 120, 180 or 240 minutes). After that all of the electrodes were gone through the same procedure as follows: incubation in a mixture of antibody and protein G, incubation in BSA and finally incubation in 100 and 1000 pM of the MGMT gene. As shown in figure 3.6, there was an increase in the average normalised value from 100 pM to 1000 pM for all of the cases in both CV and DPV techniques. However, only in

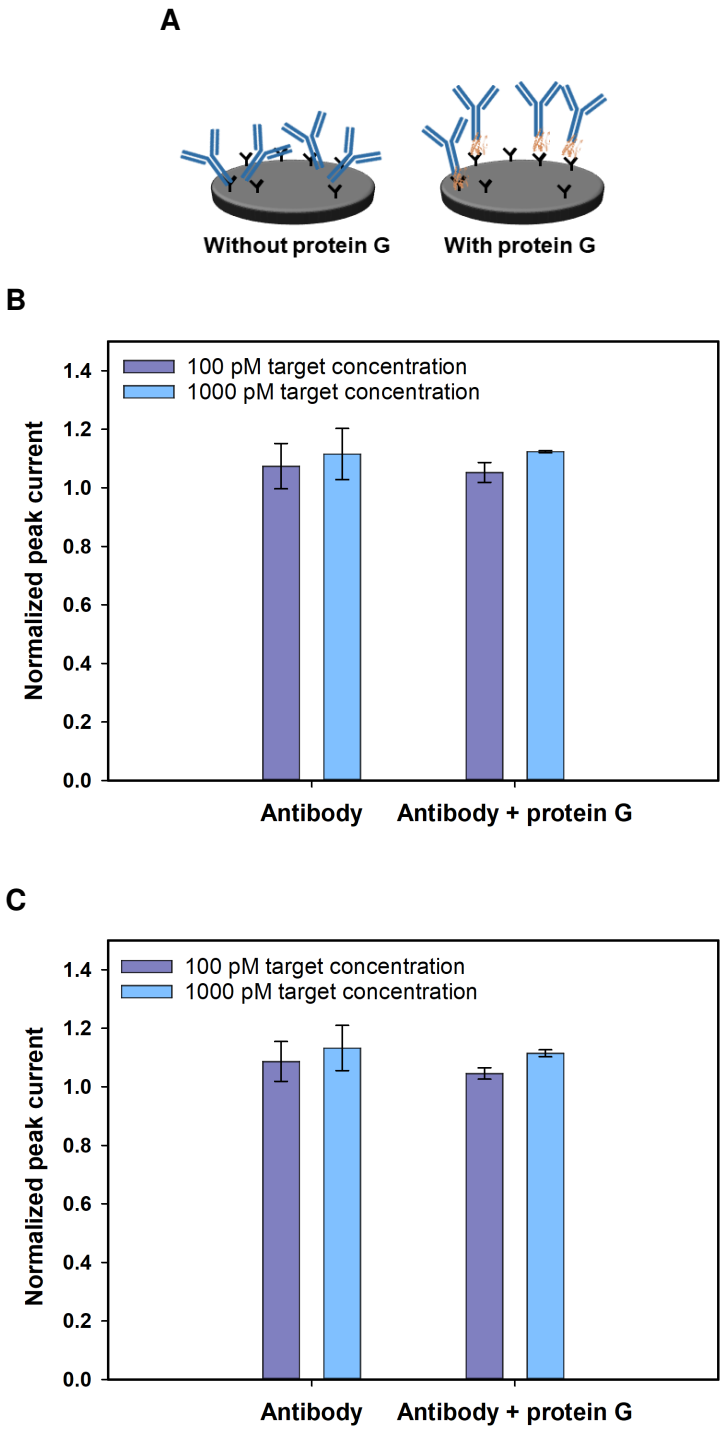

Figure 3.4: A schematic of protein G functionality tests (A) and their results where 100 (purple) and 1000 (blue) pM of the target gene was detected without (left) and with (right) usage of protein G for both the CV (B) and the DPV (C) techniques. In both figures the normalized peak currents are plotted as a function of concentration

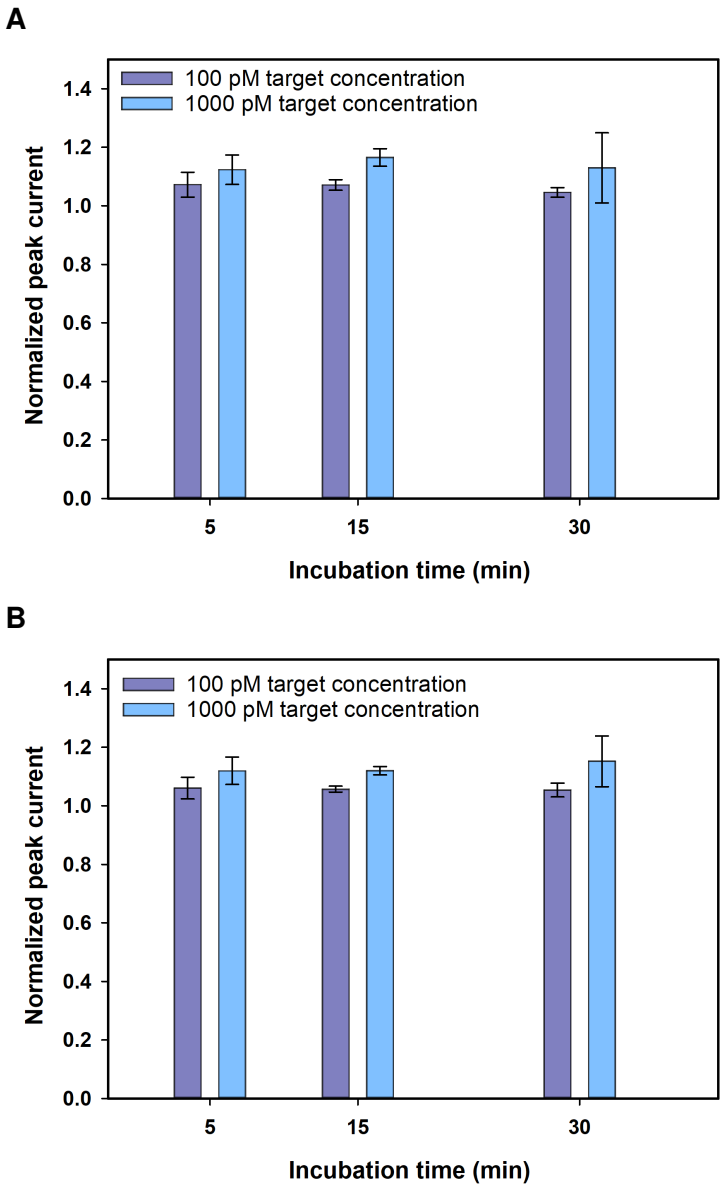

Figure 3.5: Detection of 100 (purple) and 1000 (blue) pM of the target gene with various BSA optimization times (5, 15 and 30 minutes) using both CV (A) and DPV (B). In both figures the normalized peak currents are plotted as a function of concentration.

the 120 minutes incubation time the error bars did not overlap which means all of the electrodes in this group showed an increase from 100 pM to 1000 pM. Also, the error bars were smaller in the case of 120 minutes which means the results obtained from this incubation time were more consistent that other incubation times. The incubation time of 120 minutes was chosen as the optimized linker incubation time and was used

in further experiments.

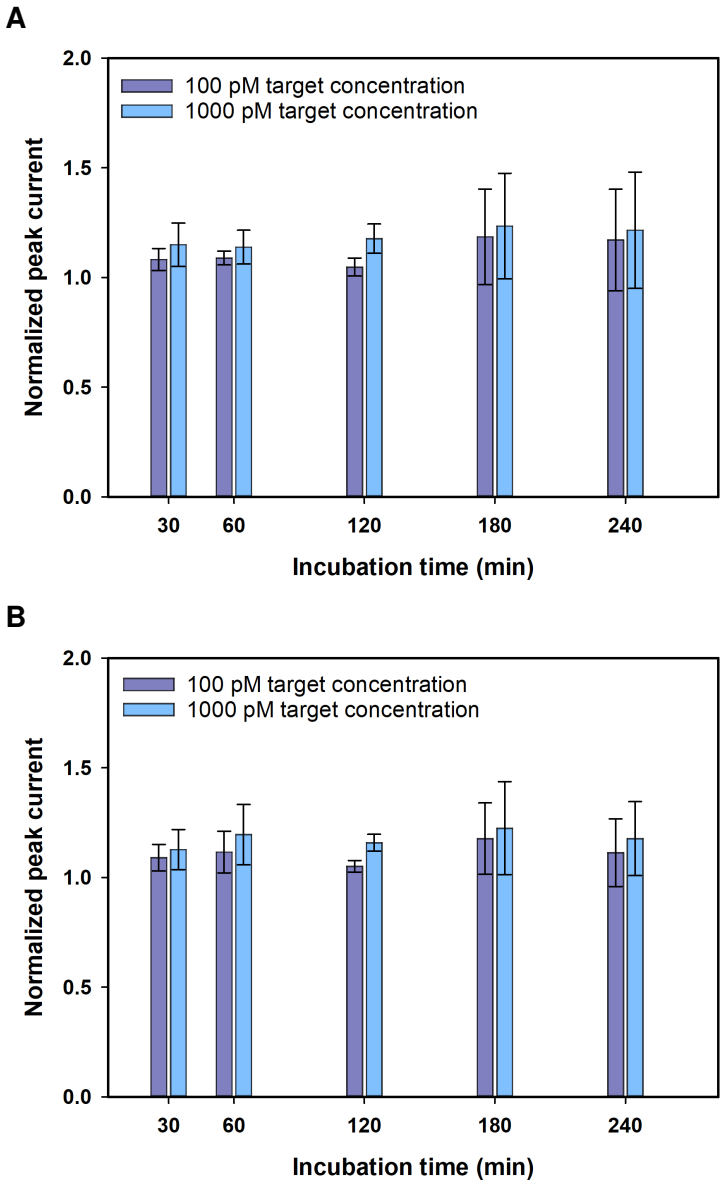

Figure 3.6: Detection of 100 (purple) and 1000 (blue) pM of the target gene with various amination (linker) optimization times (30, 60, 120, 180 and 240 minutes) using both CV (A) and DPV (B). In both figures the normalized peak currents are plotted as a function of concentration.

Antibody incubation time

The third incubation time optimization step was the antibody incubation time. After incubating in the linker, the electrodes were divided in to seven groups and each group was incubated in the anti-5mC for a specific incubation time (1, 2, 3, 4, 5, 6 and 8

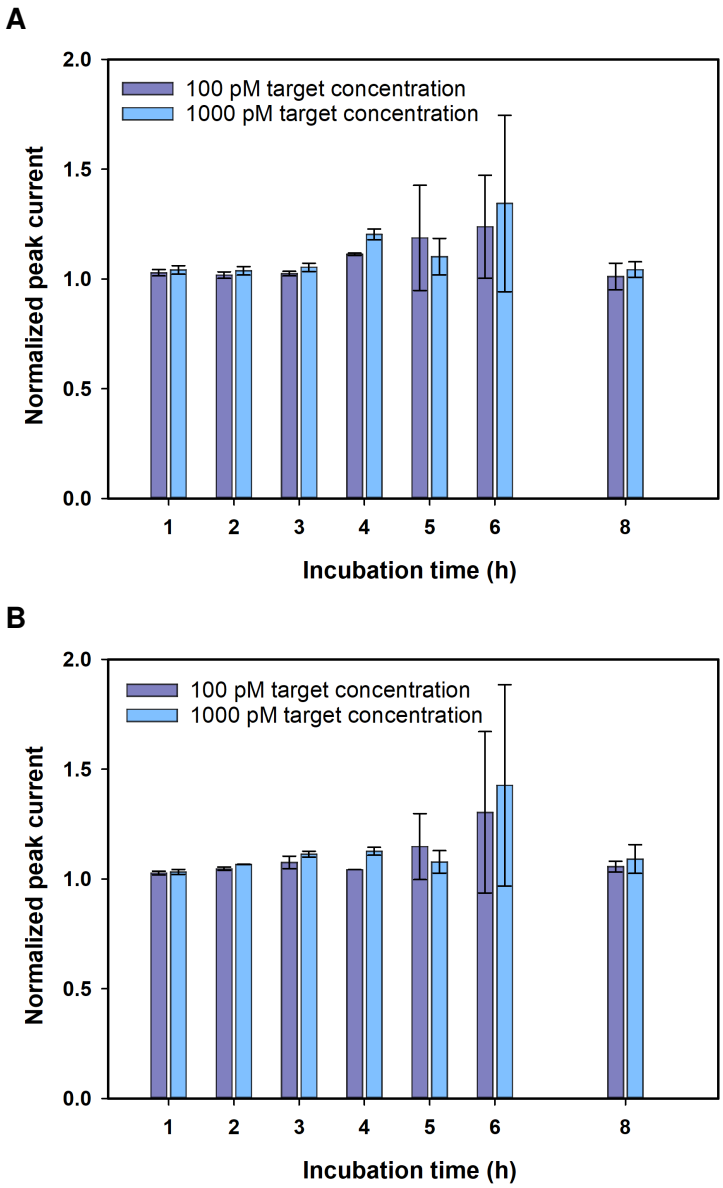

Figure 3.7: Detection of 100 (purple) and 1000 (blue) pM of the target gene with various antibody incubation times (1, 2, 3, 4, 5, 6 and 8 hours) using both CV (A) and DPV (B). In both figures the normalized peak currents are plotted as a function of concentration.

hours). Later all of the electrodes were incubated in 1% BSA, followed by the detection of 1000 and 1000 pM of the target gene. As can be seen in figure 3.7 only in the incubation time of 4 hours the error bars did not overlap for 100 and 1000 pM which means there was an increase in the peak current of all of the electrodes used for this group. Also, the normalized peak current shift as well as the error bars were

consistent in the both measurement techniques. However, in less incubation times (1, 2 and 3 hours) there was a small shift between 100 and 1000 pM which shows that the sensor is unable to distinguish between these two concentrations. Also, for longer incubation times (5, 6 and 8 hours) the error bars are larger, meaning that the result of the biosensor is not reproducible. Hence, 4 hours incubation time was selected as the optimized antibody incubation time and was used in the future experiments.

Target DNA incubation time

The last incubation time optimization was the antigen incubation time. For this experiment the sensors were divided in to four groups and each group was separately incubated in antigen for either 30, 60, 90 or 120 minutes. The results for this experiment are shown in figure 3.8 where the normalized peak current is plotted as a function of incubation time (minutes). These results show that although there was a shift between 100 and 1000 pM in all of the groups, the error bars were large and overlapped in almost all of the cases except for the group which was incubated in antigen for 60 minutes. Consequently, 60 minutes was chosen to be the optimized incubation time for antigen. All of the optimization steps, the checked ranges and the selected values are summarized in table 3.1

Experimental variable	Range	Selected value
The effect of of BSA	With-without BSA	With BSA
The effect of protein G	With-without protein G	With protein G
Amination incubation time	30-240, minutes	120
Anti-5mC incubation time	1-8, hours	4
BSA incubation time	5-30, miuntes	15
MGMT gene incubation time	30-120, minutes	60

Table 3.1: Optimized preparation steps of the Ab/ssDNA biosensor and selected values.

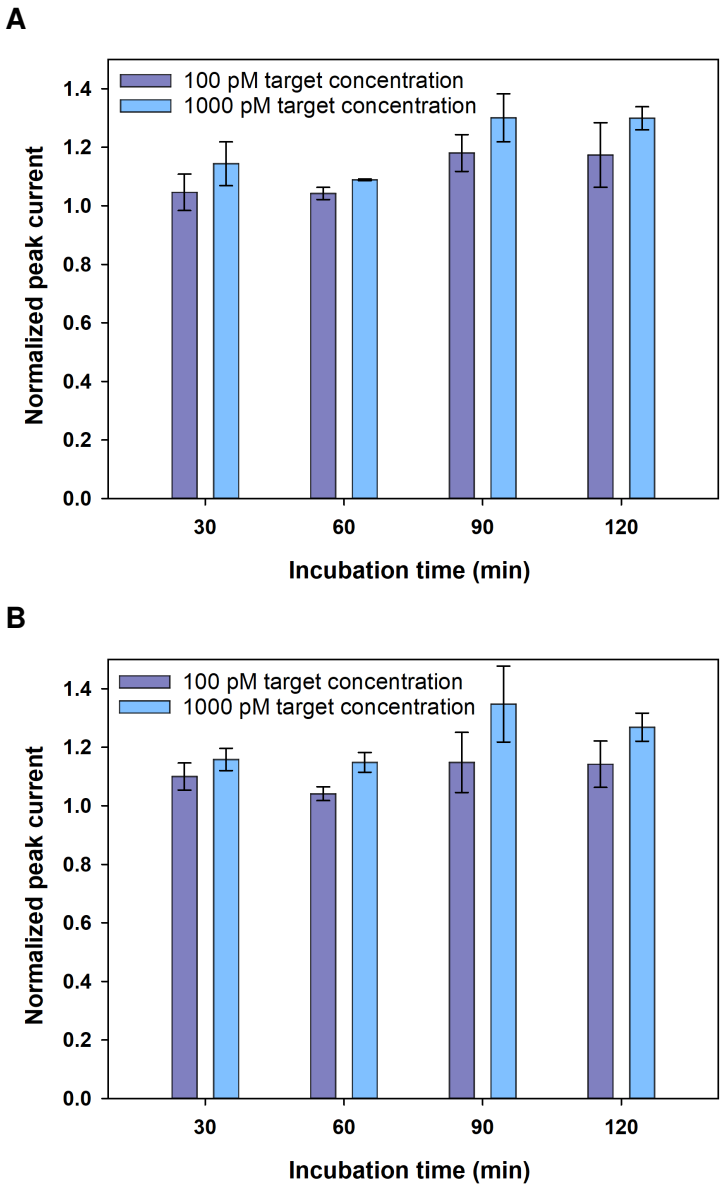

Figure 3.8: Detection of 100 (purple) and 1000 (blue) pM of the target gene with various antigen incubation times (30, 60, 90 and 120 minutes) using both CV (A) and DPV (B). In both figures the normalized peak currents are plotted as a function of concentration.

3.1.4 Surface Characterisation

Electrochemical

After each incubation step, the electrochemical response was evaluated via the voltammograms changes according to structural changes of bio-functional surface of the electrode. Figure 3.9 shows the various preparation steps of the biosensor (top) as well

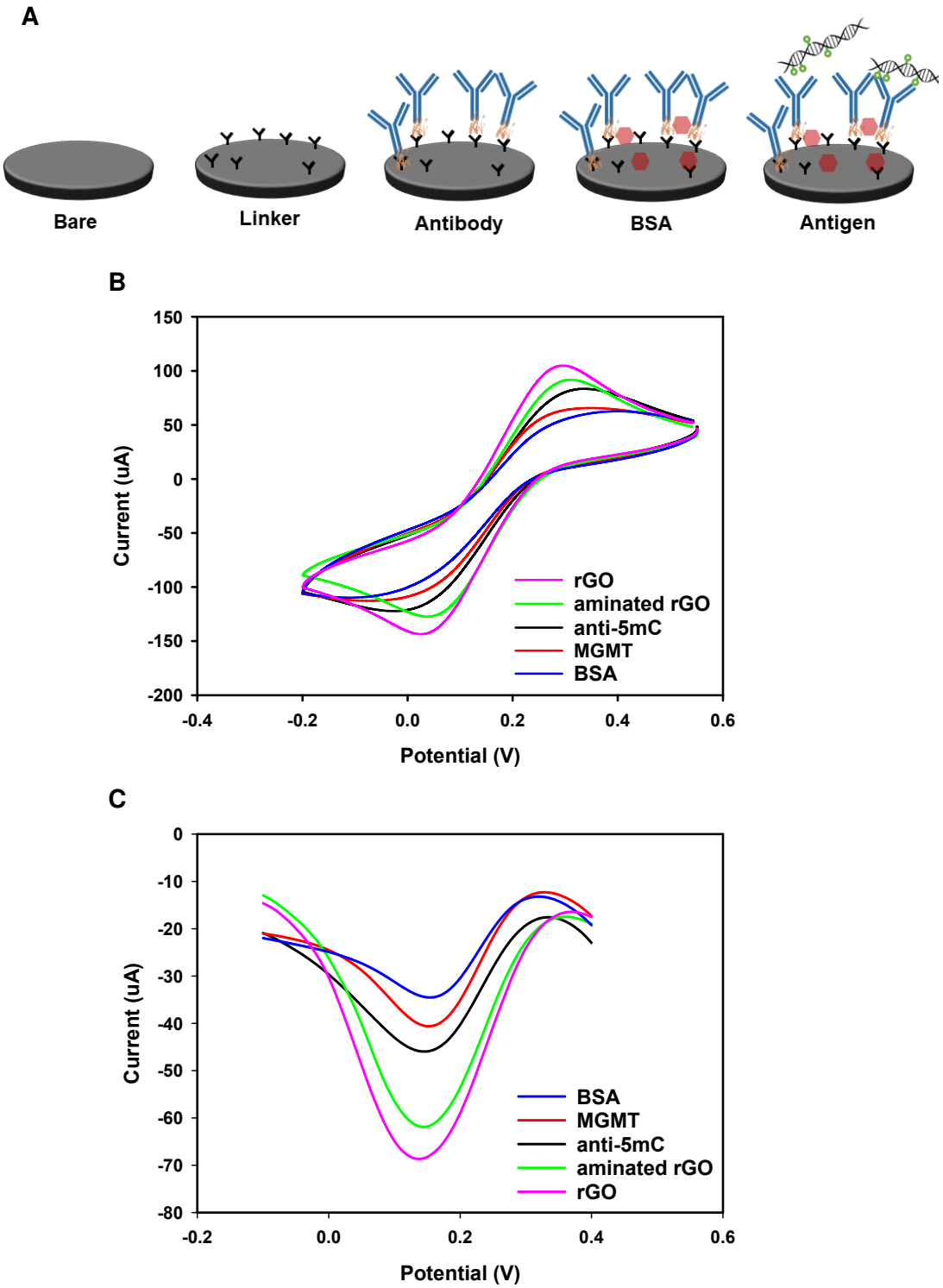

Figure 3.9: Various steps of developing the biosensor (A) after which the surface changes was measured electrochemically. Variation in the behaviour of the voltammograms after each incubation step in both CV (B) and DPV (C).

as measured voltammograms for the bare electrode (rGO) (purple), aminated rGO (green), antibody (black), BSA as the blocking agent (blue) and 100pM of antigen (red) for both CV (middle) and DPV (bottom) measurement techniques at a scan rate of 100 mV/s.

According to the CV voltammograms, first the positive anodic peak current (i_{pa}) of the bare electrode is at 106.5 μA, which is due to the electrical conductivity, electron mobility and the available electroactive sites on the rGO surface which enable the electron transfer (Benvidi et al., 2015; Li et al., 2015). After amination of the electrode, the peak current decreased to 91.7 μA which is attributed to the presence of amine functional groups on the surface. The peak current decreases once more to 83.4 μA after immobilization of antibody on the surface, which indicates the formation of a layer of the antibody on the surface and reducing the number of active sites for electron transfer. The peak current further decreases to 55.8 μA after immobilizing BSA on the surface, which is due to the fact that BSA is an inert layer and blocks the surface, impeding electron transfer (Huang et al., 2011; Liu and Ma, 2013). Finally, after the biosensor is incubated in the target MGMT gene, the peak current rises to 65.6 μA which can be ascribed to ionic conductance and π-π interaction of DNA which leads to increased charge transfer (Singh et al., 2013). Although the peak current slightly grew after DNA incubation, it was still smaller than bare, linker and antibody peak currents which indicates the formation of immunocomplex and the presence of DNA (Liang et al., 2012). Also, after immobilization in antibody a slight positive shift in the peak potential was observed which represents the spatial blockage of the surface and impeded electron transfer (Azimzadeh et al., 2016). The negative cathodic peak currents (i_{pc}) of the CV voltammograms showed the same trend with the positive peak current after each incubation step. Also, a negative shift in the peak potential was observed.

The DPV voltammograms for various preparation and detection steps were in agreement with the CV voltammograms. First, the peak current magnitude of DPV for the bare electrode was 71.7 μA , then after incubating in linker, it decreased to 61.8 μA

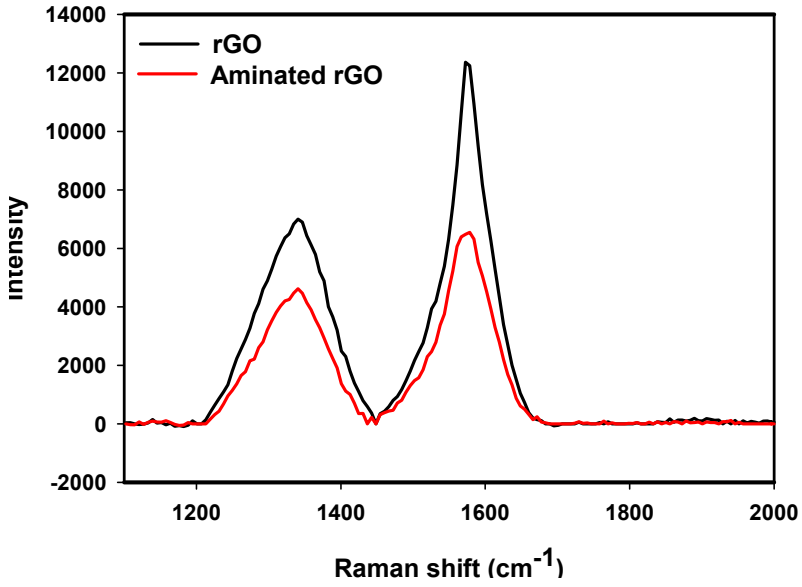

Figure 3.10: Raman spectra of both bare rGO (black) and aminated rGO (red).

followed by a decrease to 45.9μA after immobilizing antibody on the surface. The peak current magnitude further decreased to 34.5 μA after incubation in BSA and finally it slightly grew to 40 μA after the detection of target gene with the biosensor and forming immunocomplexes. In addition, there was also a positive shift in the peak potential of the DPV voltammograms which is due to the hindered electron transfer.

Raman spectroscopy

Raman spectroscopy was used to achieve a structural fingerprint of the rGO electrode. figure 3.10 shows a comparison of Raman spectra obtained from both bare rGO and aminated rGO electrodes.

The peak at 1578 cm^{-1}, G (stands for graphitic) band, characterise the in-plane vibrations of sp^2-bonded graphitic carbon atoms. The weak peak at 1340 cm^{-1}, D (stands for defect or disorder) band, represents the out of plane vibration of disordered structures (Childres et al., 2013). In Raman spectra, the peak intensity ratio (I_D/I_G) is generally used to evaluate the disorder level or the ratio of structural defects in the rGO layers (Childres et al., 2013). Here, the I_D/I_G was increased from 0.6 for the bare electrode to 0.7 for the aminated electrode, as expected. This indicates the presence of

more defect sites in the aminated rGO sample which is consistent with the results from Wei et al. (2018) and Baldovino et al. (2016) where higher intensity ratios are reported in the carbon structure after GO and rGO were exposed to nitrogen atoms. Additionally, the full width at half maximum (FWHM) of the G peak of the Raman spectra is used along with the I_D/I_G ratio to give further information about the defects level. The FWHM of the G peak was 60.5 for the bare electrode, which increased to 78.2 after the amination of rGO, confirming the presence of N atoms on the surface which is in agreement with results from Baldovino et al. (2016). Moreover, no shifts were observed in the G and the D band after amination, meaning that no strain or doping happened in the aminated rGO lattice (Zafar et al., 2013; Ni et al., 2008; Das et al., 2008).

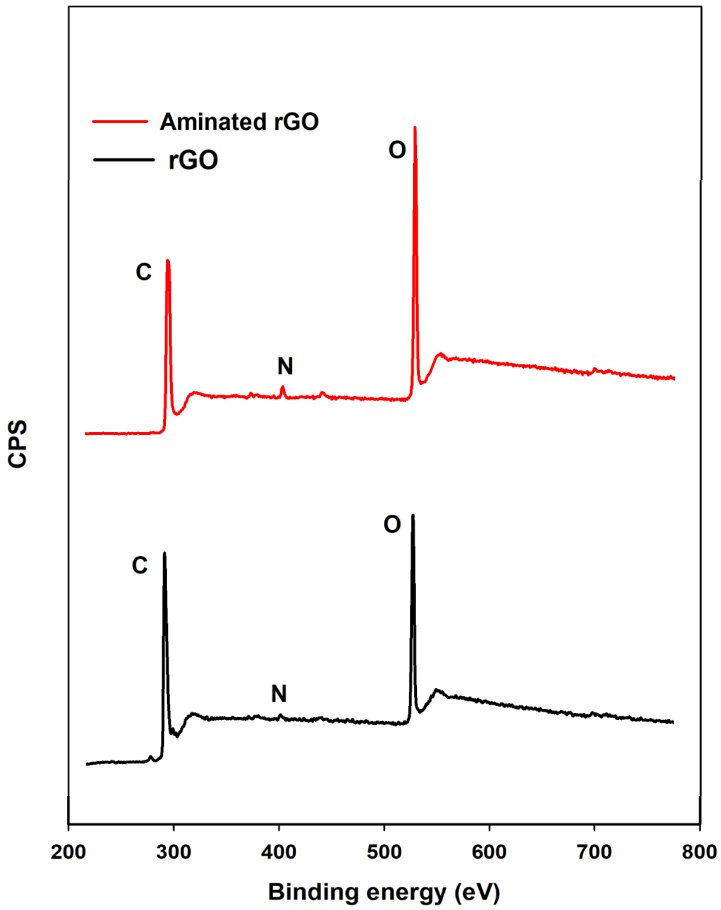

Figure 3.11: Survey scans of bare rGO electrode and aminated rGO electrode obtained by XPS.

X-Ray photoelectron spectroscopy

XPS measurements were carried out in order to quantitatively characterize the chemical state of the both bare rGO and aminated rGO sample electrodes and to confirm the findings from Raman spectra. As can be seen in the survey scans of the bare and the aminated rGO electrode in the bottom figure in 3.11, a nitrogen (N) peak was observed at 400 eV in the survey scan of the aminated rGO which confirms the presence of nitrogen bearing molecules on the surface. However, a small N peak was also observed in the spectrum of bare rGO sample (figure 3.11, top) which is due to the reduction process of GO and was also reported by Li et al. (2015). The atomic ratio (%A) of nitrogen was 2.09% for the aminated rGO sample while it was only 0.61% for the bare rGO sample. Moreover, the integrated peak areas of N and C were used to calculate the N/C ratio for both samples. The N/C ratio was 3.07% for the aminated sample which was 0.83% for the bare sample. The increment in the amount of nitrogen atoms on the surface is in agreement with results from Raman spectra which shows the presence of more defects on the surface of aminated rGO electrode.

The high resolution scans of N1s of the bare rGO and the aminated rGO are shown in figure 3.12, in the top and the bottom respectively. The N1s spectra showed asymmetrical profile for both bare and aminated rGO samples.

The N1s spectrum of the bare rGO electrode can be deconvoluted into two components at 399.9 eV and 4.1.8 eV. The former peak can be attributed to C-NH_2 and the latter can be assigned to C-NH_4^+ (quaternary nitrogen) (Ederer et al., 2017; Chen et al., 2012; Petit et al., 2009). Similarly, the N1s spectrum of aminated rGO can be deconvoluted into two peaks at the same positions as the peaks from the N1s spectrum of the bare electrodes, which can be assigned to the same features, C-NH_2 and C-NH_4^+. However, comparing the N1s spectra of both samples showed that the C-NH_2 peak height doubled after amination, while the C-NH_4^+ peak height showed no significant change. This means that C-NH_4^+ was already embedded in the rGO lattice during the reduction process while the amination process only resulted in increasing the amount

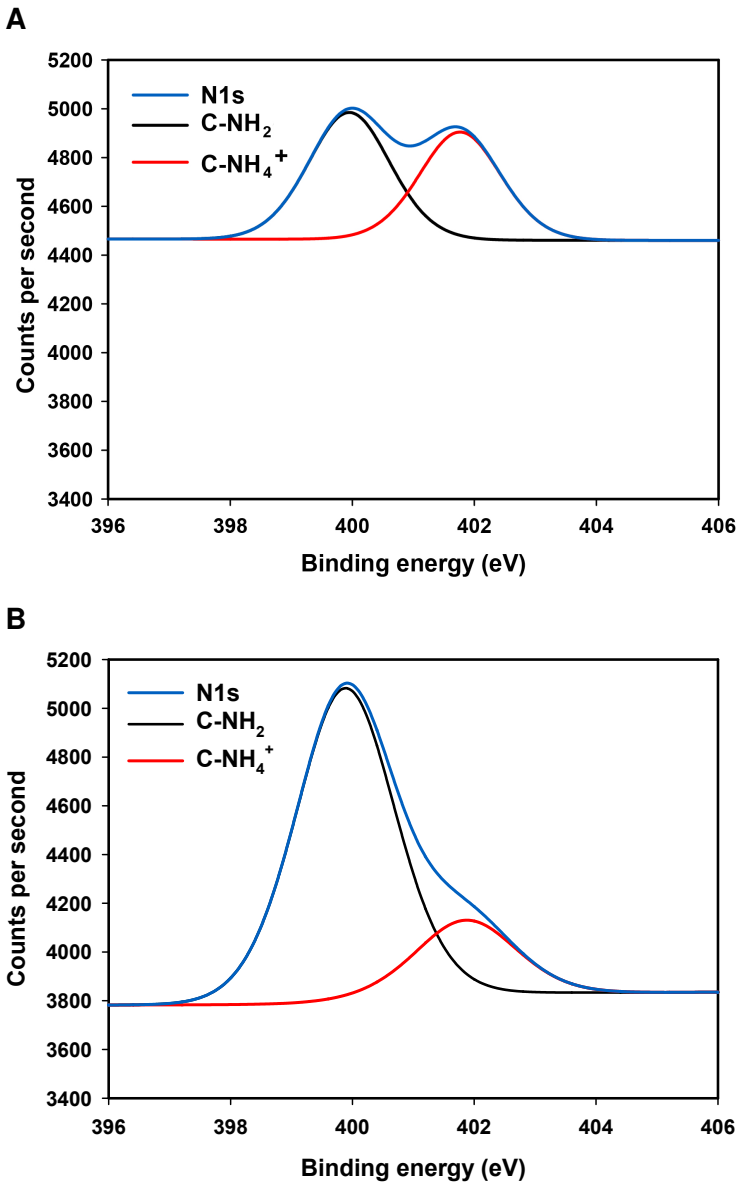

Figure 3.12: N1s high resolution spectra of bare rGO (A) and aminated rGO (B) electrodes.

of NH_2 on the surface (see section 3.1.4, Ammonium hydroxide chemisorption for more information).

The high resolution C1s spectra of both bare and aminated rGO samples are shown in figure 3.13, in the top and the bottom respectively. The spectra showed asymmetrical shapes and tailing peaks for both aminated rGO and bare rGO samples.

The C1s spectra of the bare rGO electrode can be deconvoluted into three component

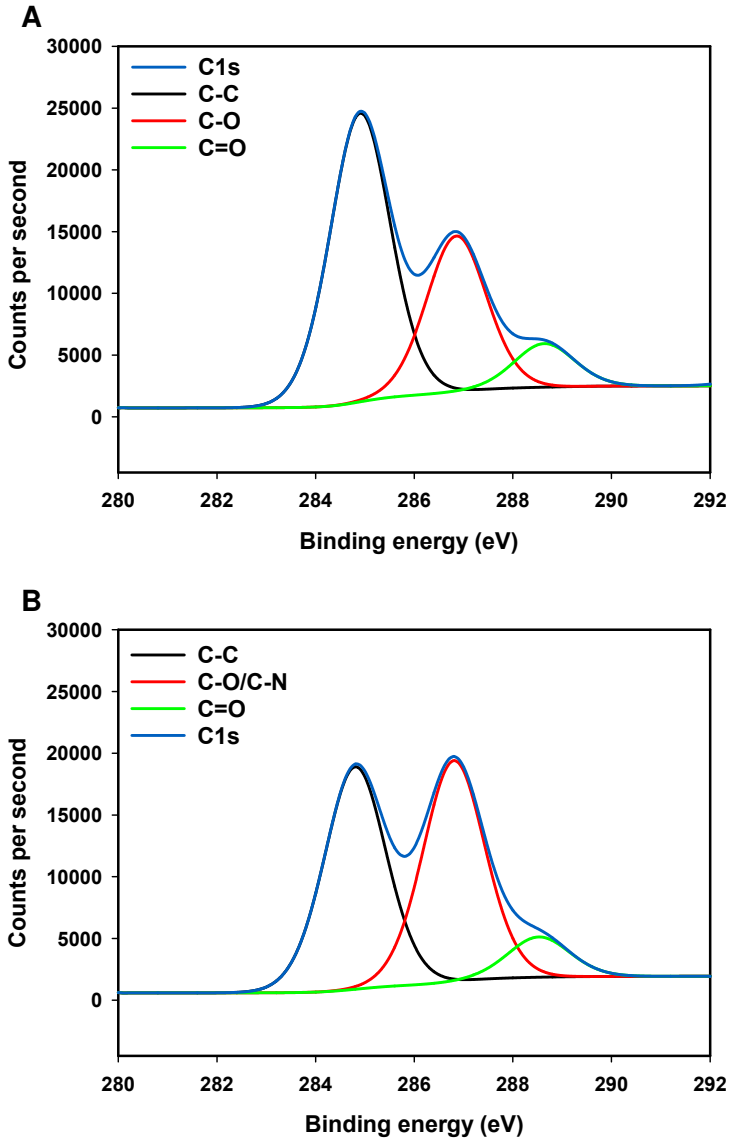

Figure 3.13: C1s high resolution spectra of bare rGO (A) and aminated rGO (B) electrodes.

peaks. The main component peak which is located at 284.80 eV corresponds to the presence of C atoms in C-C bonds (sp^3 bonded carbons) (Al-Gaashani et al., 2019). The other component peaks which are located at 286.81 eV and 288.53 ev can attribute to C-O and C=O bonds, respectively (Ederer et al., 2017; Lai et al., 2011; Stobinski et al., 2014). The C1s spectra of the aminated rGO electrode can also be deconvoluted into three component peaks. The peak at 284.90 eV represent the C-C bonds. The peak at 286.86 eV can be attributed to C-O or C-N bonds. Finally the peak at the

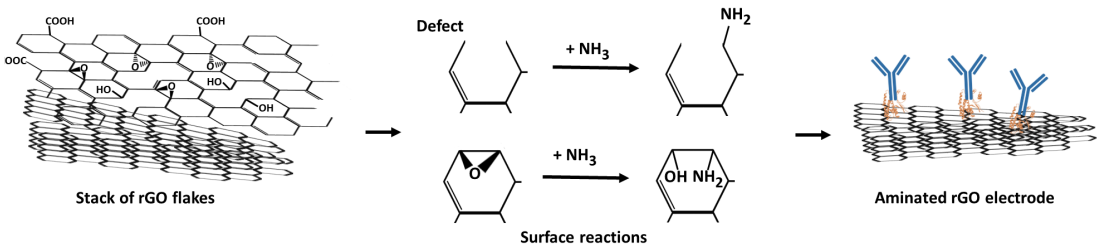

Figure 3.14: Schematic of the possible surface reactions that may occur on rGO electrode after incubation in ammonium hydroxide. These reactions would lead to the presence of amine functional groups on the surface.

higher binding energy, 288.64 eV, can be assigned to C=O bonds. Comparing these the C1s spectra of the bare rGO electrode and the aminated electrode shows that the peak which corresponds to C-C bonds decreased after amination, while the C-O/C-N peak increased and C=O remained the same. Which further confirms the presence of nitrogen atoms on the surface.

Ammonium hydroxide chemisorption

Nitrogen atoms can, in principle, be incorporated onto the surface in three ways:

- Replacing a carbon atom with a nitrogen atom
- Replacing an existing functional group by an N containing functional group (Baldovino et al., 2016; Thakur and Thakur, 2015)
- Binding a nitrogen atom to the defect sites and broken C-C bonds present in the rGO flakes (Tang and Cao, 2012; Mattson et al., 2013)

Because of the absence of high temperature and pressure, in this study it is assumed that the direct replacement of carbon by nitrogen atoms does not occur. Instead, NH_3 is assumed to react with either defects in the lattice or with acidic sites of rGO that are oxygenated functional groups namely hydroxyl, epoxide and carboxyl groups (Baldovino et al., 2016). Because the rGO SPE is made of stacked rGO flakes many

defect/vacancy sites are available for the attachment of amine groups. The presence of defects constitute instabilities of the structure of rGO, making these sites prone to bond with ammonia to stabilize the structure (Rivera et al., 2019). In the case of reactions with oxygenated functional groups, due to the lack of high temperature and suitable activators (e.g. thionyl chloride, carbodiimide or tosyl chloride), the only feasible reaction is that ammonia attacks epoxide groups as a nucleophile. In this reaction, a new bond with the carbocation adjacent to the epoxide group will form, resulting in epoxide opening, dissociation of NH_3 and forming of an amino alcohol (Mattson et al., 2013). Our XPS experiments confirm that this is the dominant amination process, as shown by the increase of the C-NH_2 component in the N1s high resolution spectra and the increase of the C-O/C-N component in the C1s spectra while the peak of C=O remained the same (figure 3.13). The above surface reactions do not affect the structure of rGO, as evidenced by the Raman spectra (figure 3.10), which show that no major defects were introduced after amination.

Besides acting as a linker for antibody, these amine groups can form hydrogen bonds with adjacent or newly formed oxygen bearing groups such as OH···N and O···HN which facilitates electron transfer by acting as electron donors to rGO and stabilizes the structure (Tang and Cao, 2011, 2012).

Scanning electron microscopy

Scanning electron microscopy (SEM) was used to characterize the morphology of the surface of the bare rGO electrode, the aminated electrode and the aminated electrode after incubation with antibody. These SEM images are presented in figure 3.15.

As can be seen in the top and the middle figures of 3.15, no changes was observed on the surface after amination process. This confirms that there were no structural changes on the surface after amination and the electrode maintained its fundamental properties during the process however SEM is not a beneficial tool to show the surface chemisorption and therefore it cannot be used to confirm the presence of nitrogen atoms on the surface. In addition it can be seen from the bottom figure of 3.15 that

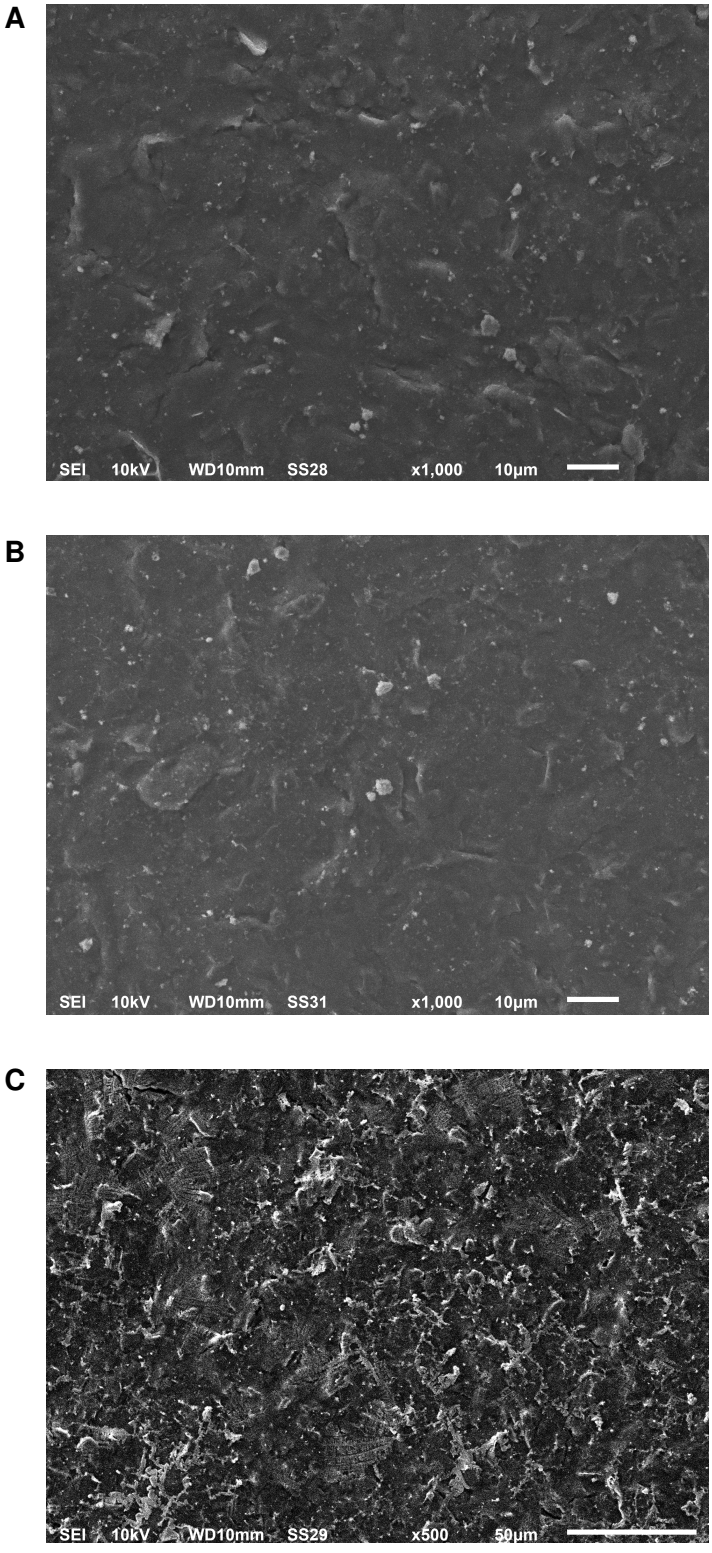

Figure 3.15: SEM images of bare rGO electrode (A), aminated rGO electrode (B) and aminated rGO electrode after being incubated in antibody (C).

there has been a change after the immobilization of the antibodies, however, SEM is not a beneficial tool to confirm the presence of biomolecules on the surface.

3.1.5 Biosensor linearity and selectivity

In order to assess the analytical performance of the biosensor, various concentrations of single stranded and double stranded MGMT gene was used to perform DPV measurement. These experiments were done under the optimal conditions achieved in 3.1.3. The DPV measurements were carried out in 10 mM PBS pH 7.4 solution containing 10 mM $K_3[Fe(CN)_6]$ and 1M KCl, as explained in details in 3.1.2. A wide range of both single and double stranded genes were used from 10 fM to 1 nM. The gene strands were diluted in TE buffer for single stranded DNA and in TE-NaCl for double stranded DNA.

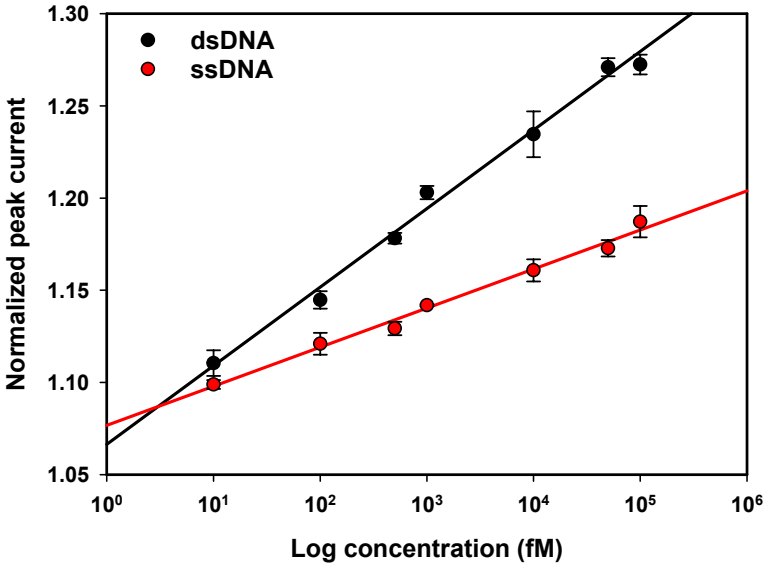

Figure 3.16: Calibration curves constructed with normalized peak currents of DPV responses as a function of the logarithm of the concentration of target ssDNA (red) and dsDNA (black). For both targets, the current increases with increase of concentration. Error bars are the standard deviation of three replicates.

The results are shown in figure 3.16, where the normalized peak currents are plotted as a function of the logarithm of the concentration and error bars are the standard deviation of three replicates. The normalized peak current increases with an increase

in the concentration, which is in agreement with the results reported by Povedano et al. (2018c) for the MGMT gene. Best fit linear models and their corresponding R^2 values are as follows:

ssMGMT:

$$y = 0.0092\ln(x) + 1.0767 \tag{3.1}$$

with R^2=0.9893 and dsMGMT:

$$y = 0.0184\ln(x) + 1.0665 \tag{3.2}$$

with $R^2 = 0.991$.

The LOD was calculated using the equation (Singh et al., 2014; Shi et al., 2018):

$$\mathrm{LOD} = 3.3\sigma/m \tag{3.3}$$

where σ is the standard deviation of the DPV response of 16 blank samples and m is the slope of the calibration curve. For ssDNA, the LOD was calculated to be 25 fM and for dsDNA it was 12 fM. To date, to the best of our knowledge only two groups reported a better LOD for the detection of DNA methylation but these groups used nanoparticles (Table 3.2).

These results indicate that the response of the biosensor is different for ssDNA compared to dsDNA. This is due to the fact that ssDNA forms a coiled shape while dsDNA makes a stretched helix shape allowing electrons to be conducted through the duplex taking advantage of the π-stacks in the duplex (Trotter et al., 2020; Gorodetsky et al., 2007; Inouye et al., 2005).

Due to the usage of hybridization, the biosensor is selective to the target gene when applied to dsDNA, but it is not selective when detecting ssDNA because it responds to the methyl group regardless of the ssDNA sequence. However, the different responses

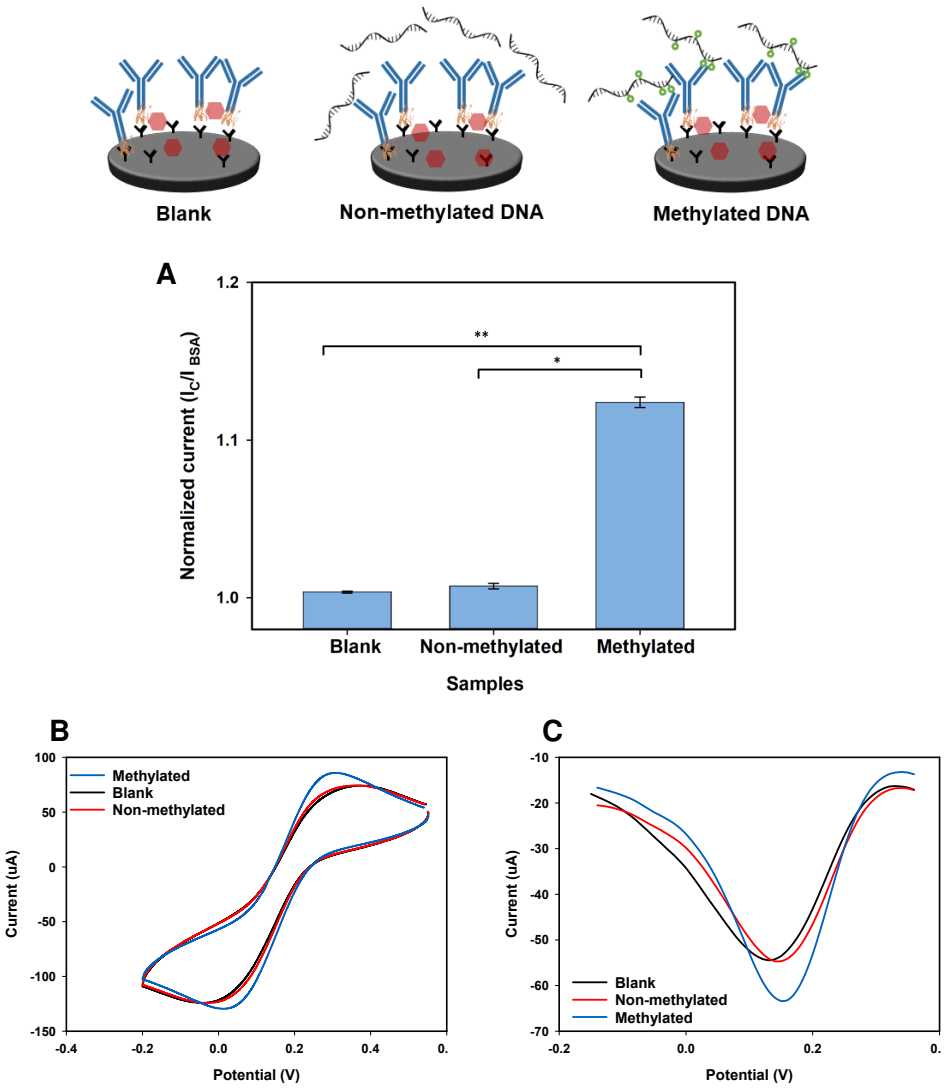

Figure 3.17: Selectivity of the proposed biosensor towards methylated DNA vs blank (buffer) and non-methylated DNA. Comparison of the voltammetric response of the biosensor in different solutions. (*p value = 00001 and **p = 0001) (A). Voltammograms corresponding to the response of the biosensor when exposed to each of the solutions used in the selectivity study (B & C).

of the sensor to dsDNA versus ssDNA can be used to achieve selectivity when applied to a sample with an unknown mixture of methylated single-stranded genes. When hybridizing the unknown mixture using the complementary target, and diluting the sample to obtain various concentrations, the formation of dsDNA (or lack thereof) can be measured.

In order to investigate the selectivity of the proposed biosensor protocol, the biosensors were incubated in blank samples, (TE-NaCl buffer containing no DNA) as well as 100 pM of methylated and non-methylated targets and the response was measured with both CV and DPV technique. All of the preparation steps and measurements for these experiments were were kept the same throughout the experiment. The selectivity results are shown in figure 3.17. The results show that there is a significant shift (Supported by a two tailed T-test analysis) after incubation in methylated DNA while no shift is observed after incubation of the sensor in blank and non-methylated DNA, indicating the selectivity of the biosensor towards the target methylated DNA.

3.1.6 Scan rate studies

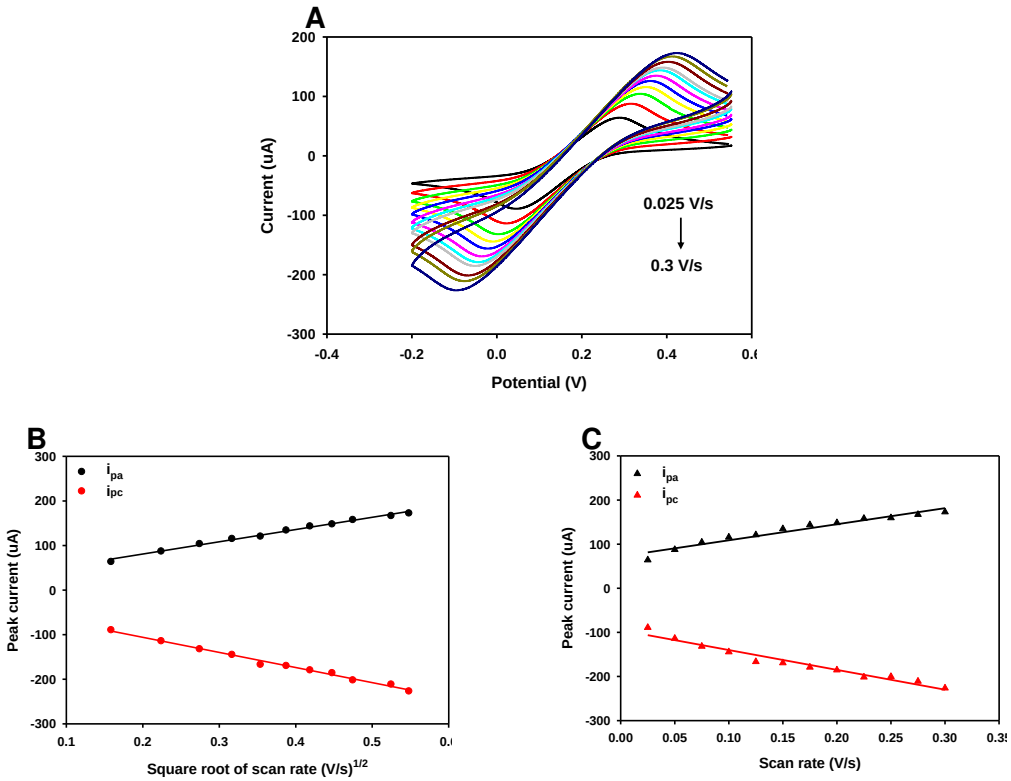

Figure 3.18: CV voltammograms of the aminated electrode under various scan rates from 0.025 V/s to 0.3 V/s (0.025, 0.05, 0.075, 0.1, 0.125, 0.15, 0.175, 0.2, 0.225, 0.275, 0.3 V/s) (A). Anodic and Cathodic peaks as a function of square root of the scan rate (B) and the scan rate (C).

Scan rate experiments of an aminated rGO electrode were performed in PBS pH 7.0 containing 10 mM $[Fe(CN)_6]$ and 1 M KCl in order to study the redox reactions on

the surface. Figure 3.18a shows the effect of varying the scan rate (0.025 to 0.3 V/s) on the voltammograms of the aminated rGO electrode where the magnitudes of both anodic (E_{pa}) and cathodic (E_{pc}) peaks currents increase linearly with the increase in the square root of the scan rate (figure 3.18b). This suggests that the electrochemical reaction is a diffusion-controlled process (Singh et al., 2013). The diffusion coefficient (D) of the redox couple from the electrolyte to the aminated electrode was calculated using Randles-Sevcik equation (Sethi et al., 2020):

$$I_p = (2.69 \times 10^5) n^{3/2} A D^{1/2} C v^{1/2} \tag{3.4}$$

Where I_p is the peak current of the aminated electrode (in A), n is the number of electrons involved (n=1), A is the surface area of the electrode (in cm^2, A=0.126 cm^2), D is the diffusion coefficient, C is the concentration of the redox species (in mM, C=10 mM) and v is the scan rate (in V/s, v=0.1 V/s, which was used throughout the paper). D is therefore calculated to be 1.17 $\times$ 10^{-6} cm^2/s.

The anodic and the cathodic peak potentials as well as the peak to peak separation (potential peak shifts, ΔE_p=$E_{pa}-E_{pc}$) increase with the scan rate (figure 3.18c). Redox couples in which the peak to peak separations show a linear relationship with the scan rate are categorized as quasi-reversible reactions (Mabbott, 1983) and it is an indication of facile charge transfer kinetics in the scan rate range (Singh et al., 2013). Therefore, the aminated electrodes provide adequate accessibility to electrons to transfer between antibody and the aminated electrode. The effective heterogeneous electron transfer rate constant (K_s) was calculated using Lavrion model (Singh et al., 2013):

$$K_s = mnFv/RT \tag{3.5}$$

Where m is the peak to peak separation (in V, m=0.362 V), n is the number of electrons involved (n=1), F is the Faraday constant (96485 J/mol), v is the scan rate (in V/s, v=0.1 V/s), R is the gas constant (8.314 J/mol.K) and T is room temperature (298 K). The K_s

value was calculated to be 1.41 s^{-1} at 0.1 V/s which indicates fast electron transfer between the amine groups and the rGO electrode.

3.1.7 Comparison with other works

The proposed biosensor are compared with other electrochemical affinity techniques reported so far for the detection of DNA methylation in table 3.2. All of these sensors use anti-5mC as their main bioreceptor.

3.1.8 Summary

In this work a novel sandwich Ab/ssDNA biosensor was developed for label-free, rapid and sensitive detection of MGMT oligonucleotide. The biosensor is based on commercially available screen-printed reduced graphene oxide (rGO) electrodes that were aminated using ammonium hydroxide solution. Amination was done in order to provide amine functional groups on the surface acting as a linker to immobilize biomolecules. Raman results suggested the presence of nitrogen atoms on the surface which further confirmed to be C-NH_2 groups via XPS. The electrochemical detection of the MGMT oligonucleotide was achieved by hybridizing the single strand synthetic oligonucleotide with its complementary sequence and capturing the methylation with antibody. Under the optimal condition, the biosensor showed a LOD of 12fM for double strand MGMT gene, without any PCR amplification, bisulfite treatment or labelling. The detection time for this biosensor was 1 hour. This is the first report on the detection of MGMT genes, using rGO electrodes. However, the reproducibility and stability of the sensor over time is still to be explored in the future. Additionally, the electrochemical performance of the aminated rGO may still be improved using elevated temperatures and pressures during ammonium hydroxide incubation. Finally, the response of the proposed technique in plasma samples needs to be tested in future studies. The proposed technique can be modified to detect other methylated target genes. This assay can form the basis for clinical applications in diagnostics and patients monitoring due to its ability to rapidly detect epigenetic biomarkers, high sensitivity and simplicity.

Electrode	Bioreceptor	Dynamic range	LOD	Technique	Reference
SPCE modified with polythiophene	Anti-5mC and Fe_3O_4/N-trimethylchitosan/gold nanocomposite	0.01-1000 pM	0.002 pM	DPV	Daneshpour et al. (2016)
SPCE	Anti-5mC immobilized on magnetic beads and biotinylated DNA probe	3.9-500 pM	1.2 pM	Amperometry	Povedano et al. (2018b)
SPCE modified with rGO and polyvinyl alcohol	Anti-5mC immobilized and DNA probe conjugated with Fe_3O_4-citric acid nanocomposites	7×10^{-4}-140.29 pM	6.31×10^{-4} pM	DPV/EIS	Khodaei et al. (2019)
rGO modified with ammuniom hydroxide	Anti5-mC and complementary DNA	0.01-100 pM	0.012 pM	DPV	This work

Table 3.2: An overview of the electrochemical affinity biosensors to date for the detection of DNA methylation, which used anti-5mC as the main bioreceptor.

3.2 PNA/Ab sensor

3.2.1 Background

The ability to detect double-stranded DNA (dsDNA) as a biomarker without denaturing it to single-stranded DNA (ss-DNA) continues to be a major challenge. In this chapter, we report a sandwich biosensor for the detection of the ds-methylated MGMT gene. The purpose of this biosensor is to achieve direct recognition of the gene sequence, as well as the presence of methylation. The biosensor is based on reduced graphene oxide (rGO) electrodes decorated with gold nanoparticles (AuNPs) and uses Peptide Nucleic Acid (PNA) that binds to the ds-MGMT gene (figure 3.19). This biosensor is named PNA/Ab, for the purpose of simplicity and clarity. PNA is an artificially synthesized nucleic acid analogue with N-(2-aminoethyl)-glycine motif backbones which are linked together via peptide bonds (D'Agata et al., 2017). PNA/Ab complexes are shown to be more stable than DNA/DNA systems with PNA probes being more efficient in hybridization with its complementary target sequence which leads to an enhanced assay sensitivity (D'Agata et al., 2017; Karimzadeh et al., 2018). Besides superior specificity towards ssDNA and RNA, PNA has shown the ability to specifically target the sequence of dsDNA by stranded invasion and form a triplex structure (Baker et al., 2006).

The reduction of GO was performed in two ways: electrochemically (ErGO) and thermally (TrGO). XPS and Raman spectroscopy, as well as voltammetry techniques, showed that the ErGO was more efficiently reduced, had a higher C/O ratio, showed a smaller crystallite size of the sp^2 lattice, and was more stable during measurement. It was also revealed that the electro-deposition of the AuNPs was more successful on the ErGO surface due to the higher At% of Au on the ErGO electrode. Therefore, the ErGO/AuNPs electrode was used to develop biosensors to detect the ds-MGMT gene. PNA, which acts as a biorecognition element, was used to form a self assembled monolayer (SAM) on the ErGO/AuNPs surface via the amine-AuNPs interaction, recognizing the ds-MGMT gene sequence by its invasion of the doublestranded DNA and the formation of a triple helix. The methylation was then detected using biotinylated-anti-

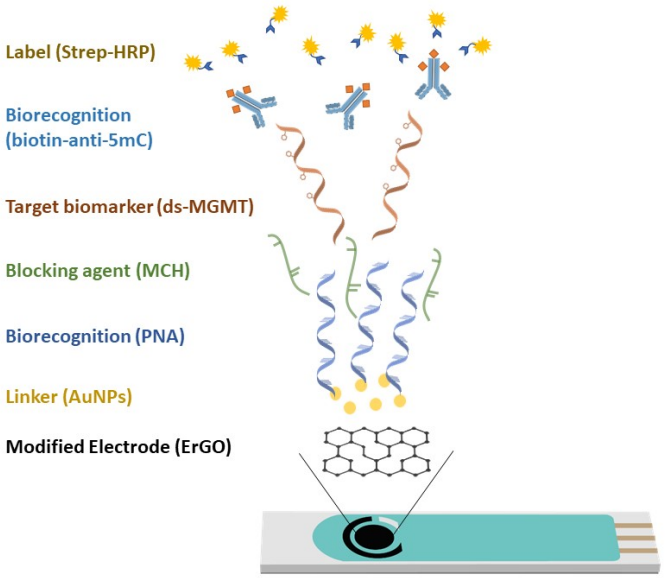

Figure 3.19: Various layers of the PNA/Ab biosensor.

5mC, which was then measured using the amperometric technique. Streptavidin-HRP was used to produce amperometric signal in the presence of hydroquinone (HQ) and H_2O_2 (Camacho et al., 2007; Dong et al., 2017). The selectivity study showed that the proposed biosensor was able to distinguish between blank, non-methylated, non-complementary, and target dsDNA spiked in mouse plasma. The LOD was calculated to be 0.86 pM with a wide linear range of 1 pM to 50 µM. To the best of our knowledge, this is the first report on using PNA to detect ds-methylated DNA.

3.2.2 Biosensor concept and preparation

With the aim of increasing the reproducibility of the SPEs, the electrodes were modified using rGO and AuNPs. The working electrodes were first drop-coated with 0.15 mg/mL of GO aqueous solution and were left to dry at room temperature for 3 h. After that, the GO layers were reduced in two different ways in order to compare the impact of the reduction techniques on the quality of rGO and AuNPs. The electrodes were either reduced electrochemically (ErGO) or thermally (TrGO). The electrochemical reduction of GO was performed using 10 successive CV scans in 10 mM PBS pH 7.4 solution containing 10 mM $K_3[Fe(CN)_6]$ and 1 M KCl over a potential range of 0.5 and -1.5

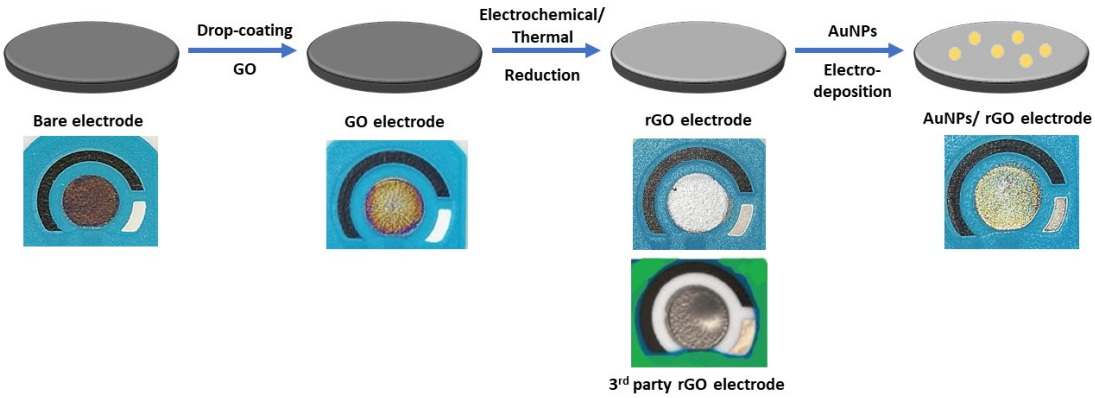

Figure 3.20: A schematic of the surface modification procedure of a screen printed electrode and the changes to the appearance of the working electrode.

V and a scan rate of 100 mV/S. Thermal reduction was performed at 250 ℃ for 1 h. After reducing GO, the AuNPs were electro-deposited on both ErGO and TrGO electrodes from 0.5 mM H_2SO_4 solution containing 1 mM $HAuCl_4$, using 5 successive CV cycles over a potential range of 1 and -1 V and a scan rate of 50 mV/s (figure 3.20). The electrochemical reduction of GO and electro-deposition of the AuNPs were both performed at room temperature.

Modified electrodes were incubated in 10 µM PNA overnight at 4 ℃ to functionalize a self assembled monolayer (SAM) on the surface of the working electrodes. On the next day, the electrodes were incubated in 1 mM aqueous solution of MCH for 5 min to minimize the nonspecific binding and then they were incubated in PBS for 1 h to stabilize the SAM. The prepared biosensors were then incubated in various concentrations of dsDNA for 1.5 h at 37 ℃, followed by incubation in biotinylated methyl binding antibody for 2 h at room temperature. Biotinylated antibody was used to detect the methylation sites on the dsDNA, and to provide binding sites for Streptavidin-HRP. Finally, to enable the amperometric detection technique, the biosensors were incubated in diluted Streptavidin-HRP for 30 min prior to the measurements. Various preparation steps of

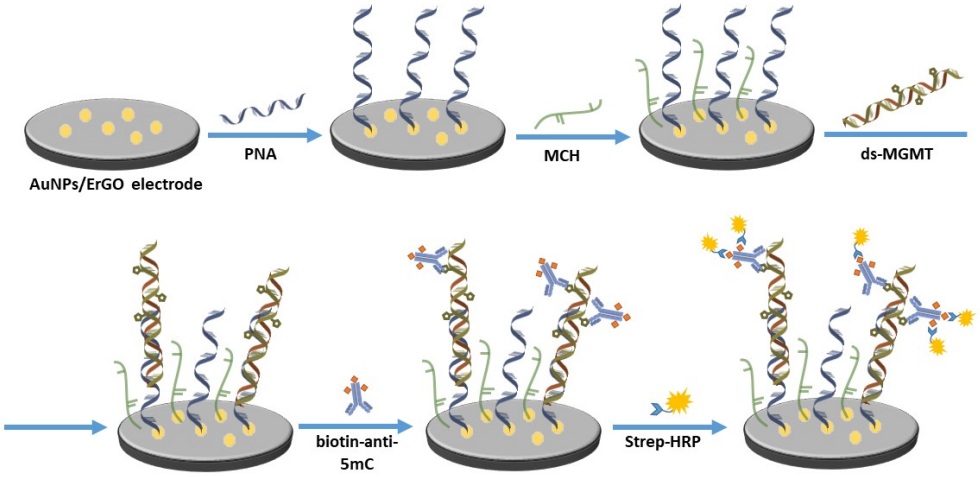

Figure 3.21: A schematic of the developed biosensor. The preparation of the AuNPs/ErGO electrode is depicted in figure 3.20.

this biosensor are depicted in figure 3.21. After each incubation step, the electrodes were rinsed with ultra-pure water. All of the incubation steps were carried out in a high humidity chamber.

3.2.3 Surface characterisation

GO reduction

GO-coated electrodes were reduced either electrochemically or thermally in order to achieve a higher reproducibility and quality. The reduction process for both ErGO and TrGO were described in Section 3.2.2. The reduction degree and the quality of the rGO modified electrodes were compared using XPS, Raman, and cyclic voltammetry techniques.

The electrochemical reduction of GO was obtained using CV scans for 10 successive cycles. The voltammograms of reducing a GO modified electrode are shown in figure 3.22. As can be seen in this figure, a large cathodic peak is located between -1.0 and -1.5 V, disappearing after several cycles. This peak can be attributed to the electrochemical reduction of the functional groups, mainly oxygenated groups which

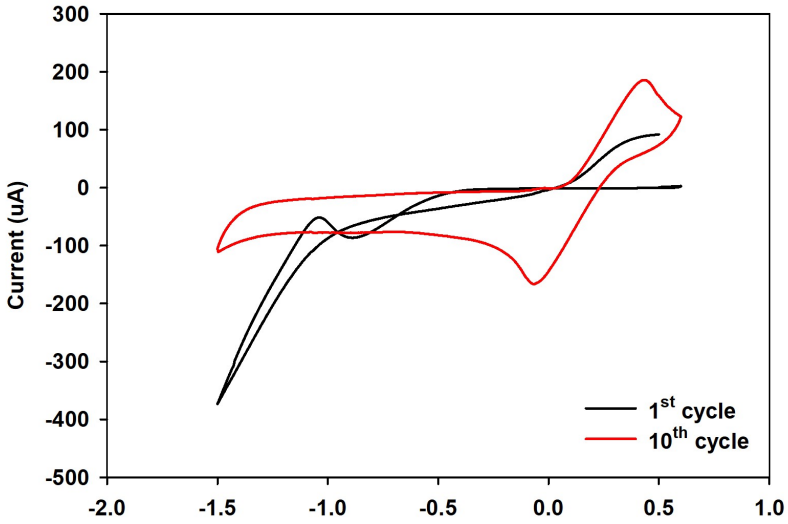

Figure 3.22: The voltammograms of the CV cycles used to electrochemically reduce GO.

are present at the GO basal plane (Wang et al., 2009; Marrani et al., 2020; Devadas et al., 2014, 2012). Therefore, after a few CV cycles, GO was reduced, rGO was obtained, and subsequently, the electric properties improved (Wu et al., 2016). The reduction of GO can also be seen from the color change in the working electrode, which changes from black to silver after reduction, consistent with a third-party rGO electrode (figure 3.20)

XPS measurements

XPS measurements were carried out in order to characterize and evaluate the chemical composition of a bare electrode and the GO-, ErGO-, and TrGO-modified electrodes. Wide scans (survey scans) as well as C1s high-resolution scans of all of the samples are shown in figures 3.23 and 3.24 respectively. Table 3.3 shows a detailed information for all of the peaks observed by the wide scan (figure 3.23), their position, FWHM, and At%.

As can be seen in figure 3.23, the survey scan spectra of all of the samples show the presence of carbon and oxygen and a trace of contaminants (Na, Cl, S, N), all less than 3% At%. The C/O ratios for the bare, GO, ErGO, and TrGO electrodes were cal-

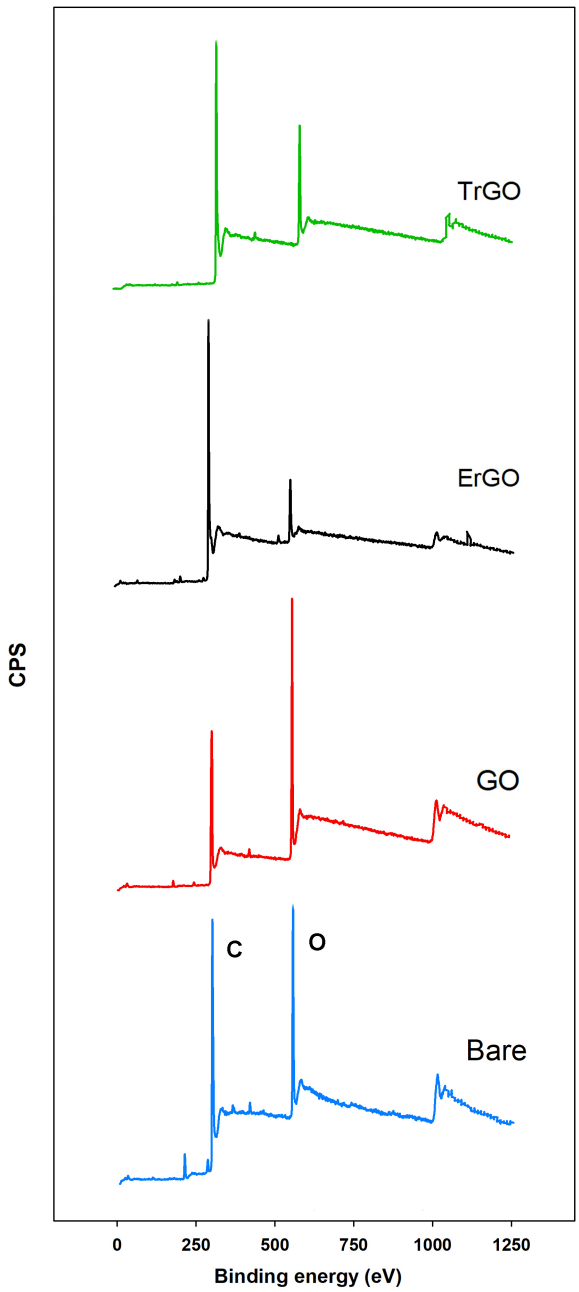

Figure 3.23: XPS wide scan spectra of a bare electrode and GO-, ErGO-, and TrGO-modified electrodes. The C/O ratios of these electrodes were 3.97, 2.49, 10.52, and 5.7, respectively.

culated to be 3.97, 2.49, 10.52, and 5.7, respectively. Schniepp et al. (2006) reported that in temperatures below 500 ℃, the C/O ratio only reached 7; however, if the temperature was increased to 750 ℃, the C/O ratio would rise to more than 13. Ren et al.

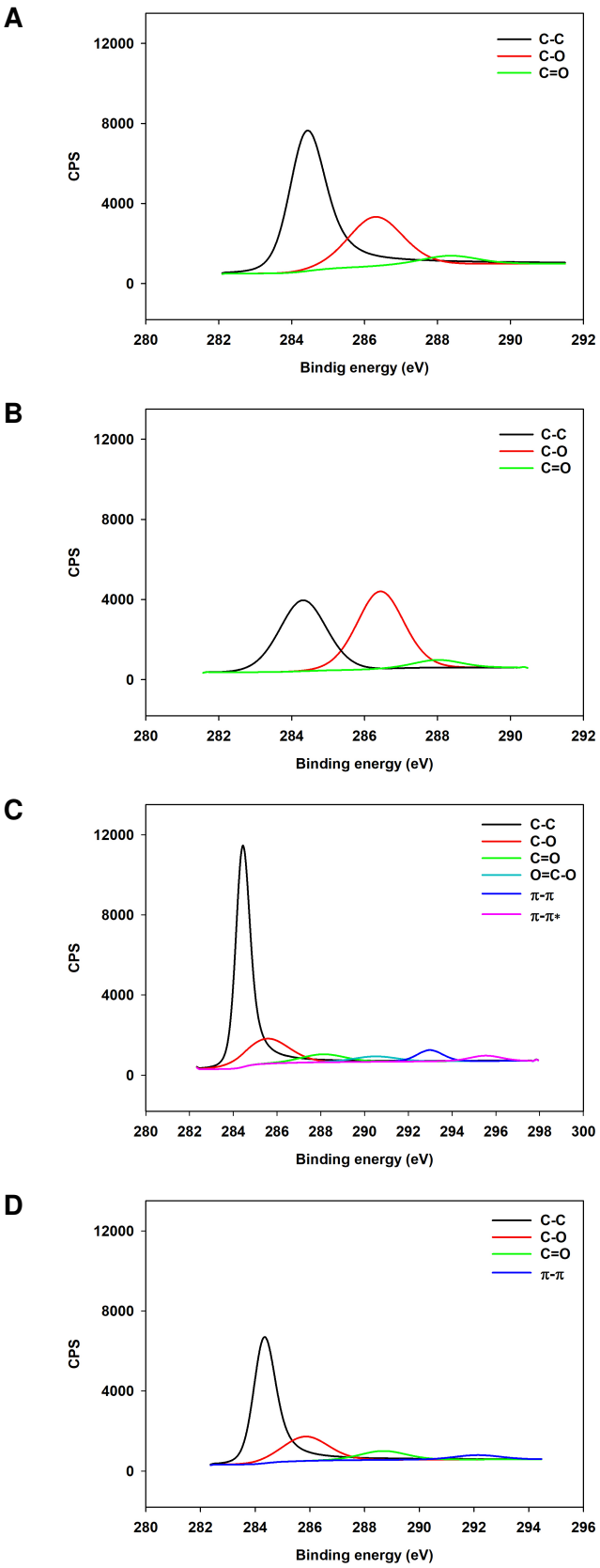

Figure 3.24: C1s high resolution spectra of a bare electrode (A) and GO (B), ErGO (C) and TrGO (D) modified electrodes.

Table 3.3: A detailed information of the XPS peaks, their positions, FWHM and At% for a bare electrode and electrodes modified with GO, ErGO and TrGO. These data are obtained from the XPS survey scans (figure 3.23).

Sample	Peak name	Position	FWHM	At%
Bare	O1s	532.10	3.31	19.26
	C1s	285.10	3.77	76.49
	N1s	400.10	3.10	1.37
	Cl2p	200.10	3.32	2.87
GO	O1s	534.37	3.01	27.98
	C1s	287.37	4.50	69.63
	N1s	402.37	3.34	1.30
	S2p	168.37	3.07	1.10
ErGO	O1s	533.33	3.89	8.57
	C1s	285.33	2.73	90.15
	Na1s	1074.33	2.87	0.44
	Cl2p	199.33	3.48	0.85
TrGO	O1s	565.37	3.88	14.65
	C1s	312.37	3.06	83.57
	N1s	430.37	3.77	1.31
	S2p	194.37	3.16	0.47

(2010) reported the C/O ratio ranging from 3.1 to 15.1, where the latter was obtained by reducing GO in 95 ℃ for 3 h using hydrazine hydrate as a reducing agent. Yang et al. (2015b) reported a C/O ratio in the range of 3.09 to 5.38 for the rGO samples that were reduced by adding $NaBH_4$ and $CaCl_2$ as catalysts and stirring for 12 h at room temperature. Chua et al. (2012) increased the C/O ratio from 3.0 to 16.0 by using thiourea dioxide ($CH_4N_2O_2S$) for 2 to 5 h at 90 ℃. Although the C/O ratio of the ErGO reported in this study was not as high as the ones reported above, the electrochemical reduction of GO does not require a high temperature or any dangerous reductants. In addition, the reduction process for each electrode took less than 5 minutes.

Figure 3.24 shows the high-resolution C1s spectra of bare, GO, ErGO, and TrGO electrodes, where all of the spectra showed asymmetrical shapes. The C1s spectra of the bare electrode (figure 3.24a) can be deconvoluted into three component peaks: a C-C peak located at 284.37 eV, a C-O peak at 286.29 eV, and a C=O peak located at

288.34 eV. The C1s spectra of the electrode covered with GO (figure 3.24b) can be deconvoluted into a C-C peak located at 286.43 eV, a C-O peak at 284.31, and a C=O peak at 288.01 eV. The GO sample exhibited the highest amount of oxygen among the samples in both the wide scan and the C1s high-resolution scan. The C1s spectra for ErGO and TrGO exhibited a few tailing peaks. As can be seen in figure 3.24c for the ErGO sample, a C-C peak is located at 284.40 eV, a C-O peak is at 285.55 eV, a C=O peak is at 288.10 eV, and a O=C-O peak is located at 290.49 eV. Two π-π peaks were also observed at 292.99 eV and 295.53 eV, respectively. The C1s spectra for the TrGO is shown in figure 3.24d. The spectra can be deconvoluted into the following peaks: a C-C peak located at 284.29 eV, a C-O peak at 285.84 eV, and a C=O peak at 288.68 eV. A π-π peak was also observed at 292.14 eV (Al-Gaashani et al., 2019; Yang et al., 2009; Krishnamoorthy et al., 2013).

Raman Spectroscopy

Raman spectroscopy was carried out for a bare electrode and GO, ErGO, and TrGO coated electrodes, and the spectrographs are shown in figure 3.25. The peaks at around 1570 cm^{-1} are G bands which are attributed to in-plane vibrations of the sp^2-bonded graphitic carbon atoms. The peaks at 1350 cm^{-1} are D bands and represent the out-of-plane vibration of the disordered structures. I_D/I_G ratio, or the intensity ratio, is normally used to evaluate disorder level, or the ratio of structural defects in the GO or rGO layers. I_D/I_G was calculated to be 0.77, 0.88, and 0.89 for bare, GO, and TrGO electrodes, respectively, but 1.15 for ErGO. The higher number in the intensity ratio of ErGO indicates that the reduction process may change the GO structure, resulting

Table 3.4: The experimental values of the peak locations, I_D/I_G ratios and the average crystallite sizes of the sp^2 lattice (L_a) of all samples.

Sample	D peak location (cm^{-1})	G peak location(cm^{-1})	I_D/I_G	L_a (nm)
Bare	1340	1570	0.77	24.99
GO	1350	1570	0.88	21.84
TrGO	1340	1570	0.89	21.60
ErGO	1350	1570	1.15	16.72

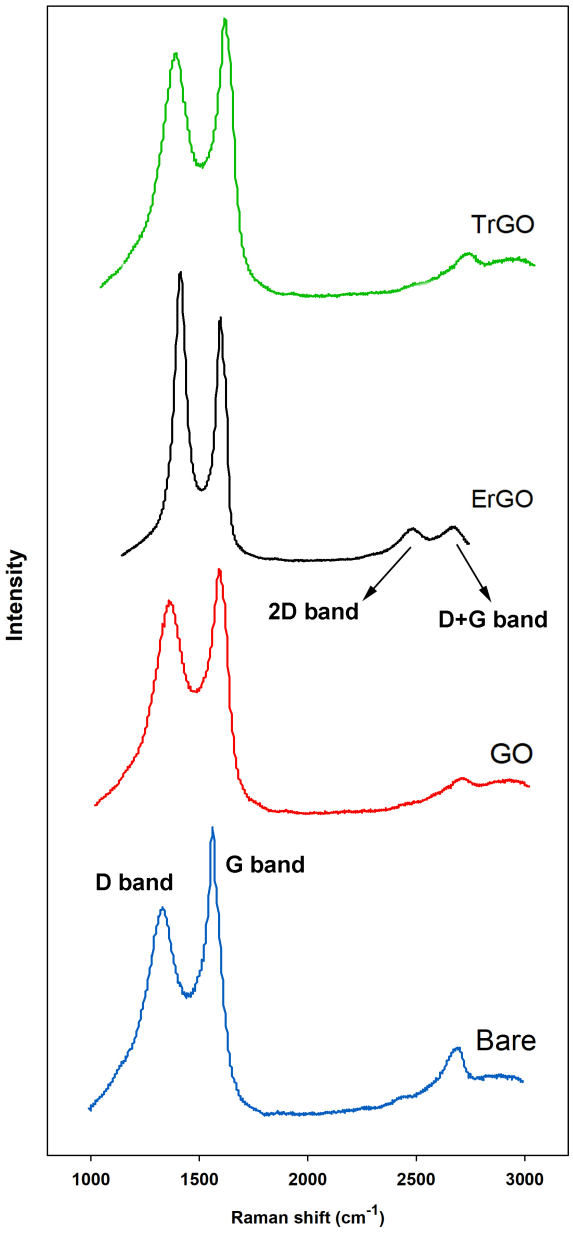

Figure 3.25: Raman spectra obtained from a bare electrode and electrodes modified with GO, ErGO, and TrGO. The ID/IG ratios were 0.77, 0.88, 1.15, and 0.89, respectively.

in an increase of defects in the structure and a decrease in the average size of the sp^2 due to the removal of the oxygenated functional groups (Lee et al., 2018; Le et al., 2020; Wu et al., 2018) which is in agreement with results from XPS spectra. A 2D band and a D + G band, which become significant in rGO, were also observed at 2680 cm^{-1} and 2910 cm^{-1}, respectively, demonstrating the restoration of the graphite structures

(Wu et al., 2018). The experimental values of the peak locations, I_D/I_G ratios, and the average crystallite sizes of the sp^2 lattice (L_a) are listed in Table 3.4. The L_a values were calculated using the equation:

$$L_a(nm) = (2.4 \times 10^{-10})\lambda_{laser}^4 (I_D/I_G)^{-1} \tag{3.6}$$

for all samples, where λ_{laser} is the laser wavelength and I_D and I_G are the intensities of the D and G Raman bands, respectively (Marrani et al., 2020).

Cyclic Voltammetry

Cyclic voltammetry was used to compare the stability of the electrodes during electrochemical measurements. 10 successive CV scans were performed for a bare electrode, an ErGO-, and a TrGO-modified electrode and the average of the anodic peak currents(i_{pa}) of the voltammograms was plotted in figure 3.26. As can be seen in this figure, the ErGO reached a higher current compared to both the TrGO and the bare electrodes. For 10 successive measurements, ErGO showed a higher stability and lower fluctuation in the peak currents.

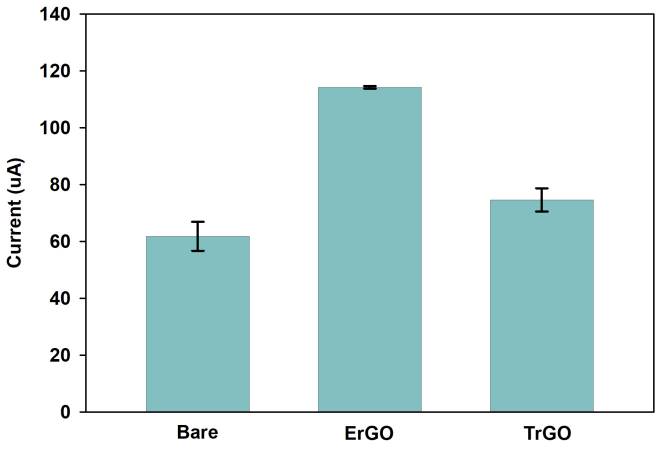

Figure 3.26: Anodic peak currents (i_{pa}) of 10 successive cycles of CV voltammograms of a bare electrode, and electrodes modified with ErGO and TrGO.

AuNPs

AuNPs were electrochemically deposited on the surface of ErGO- and TrGO-modified electrodes and were characterized using XPS and EDS spectroscopy. SEM was also used to confirm the presence of AuNPs on the surface. The electro-deposition method was described in the experimental section (see Section 2.3). figure 3.27 shows the voltammograms of the deposition process in five successive cycles with the potential range of -1 to 1 V. As can be seen in this figure, a cathodic peak is located at 0.1 V during the first scan, which can be attributed to the reduction of Au^{3+} ions to Au, as well as the seeding of the AuNPs. This peak has shifted to 0.5 V in the next cycles, indicating the easier electro-deposition of gold and the growth of the AuNPs. The Anodic peak at 0.8 V can be ascribed to the surface oxidation of the AuNPs (Devasenathipathy et al., 2014; Chiang et al., 2019; Lin et al., 2011).

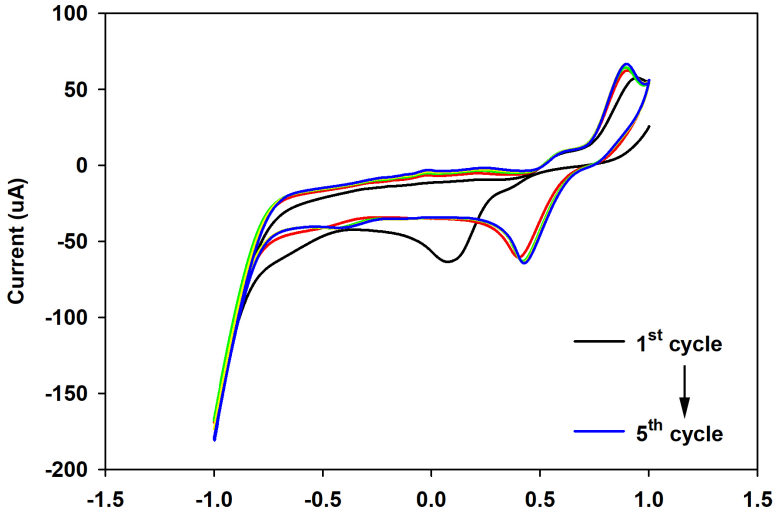

Figure 3.27: The voltammograms of 5 successive CV cycles, used to deposit AuNPs.

XPS measurements

Figure 3.23 shows a wide scan XPS spectra of a bare electrode and the GO-, ErGO-, and TrGO-modified electrodes after the immobilization of the AuNPs. These electrodes are named bare/AuNPs, GO/AuNPs, ErGO/AuNPs, and TrGO/AuNPs, respectively. The bare/AuNPs wide scan spectrum showed two Au4f peaks centered at 83.83 eV

and 87.81 eV and two Au4d peaks at 334.55 eV and 355.27 eV. A very small peak at 4.9 eV was also observed, attributed to Au5d. In the GO/AuNPs spectrum, no peaks related to the AuNPs were observed. However, the ErGO/AuNPs spectrum showed two Au4f peaks at 94.99 eV and 98.87 eV, respectively, as well as two Au4d peaks located at 351.1 eV and 369.24 eV. An Au5d and an Au5p were also observed at 16.7 eV and 67.96 eV, respectively, for this sample. Similarly, in the TrGO/AuNPs spectrum, the Au4f peaks were centered at 86.79 eV and 89.83 eV, respectively, while the Au4d peaks were observed at 341.43 eV and 359.71 eV. An Au5d peak was also observed for this sample at 5.77 eV. At% of Au for bare/AuNPs, ErGO/AuNPs, and TrGO/AuNPs were 4.16, 7.38, and 4.08, respectively. This reveals that the ErGO was a better substrate for reducing the AuNPs. Also, the ErGO/AuNPs electrode showed the highest number of AuNPs on the surface, making it the most efficient and promising electrode for further studies. Detailed information about the observed peaks, their positions, the FWHM, and At% is shown in the supplementary information in Table 3.5.

SEM and EDS

SEM and EDS were performed to characterize the surface and confirm the presence of gold nanoparticles. Figure 3.29 shows the SEM images of the ErGO electrode before and after the deposition of the AuNPs on the surface, as well as the EDS spectra of both and the area from which the spectra has been taken. Figure 3.29a shows the surface of the ErGO electrode exhibiting cracks and wrinkles of 5–20 μm. Figure 3.29b shows the surface of the ErGO/AuNPs electrode where the AuNPs are homogeneously spread on the surface. The diameter of the nanoparticles is mostly less than 100 nm. EDS spectrographs of the ErGO electrodes before and after the deposition of the AuNPs are shown in figures 3.29c and 3.29d which are in agreement with XPS data. The inset tables show the present elements, the relative concentration (Wt%), and the measurement error for each element (Σ). EDS measurements confirm the presence of the AuNPs on the surface.

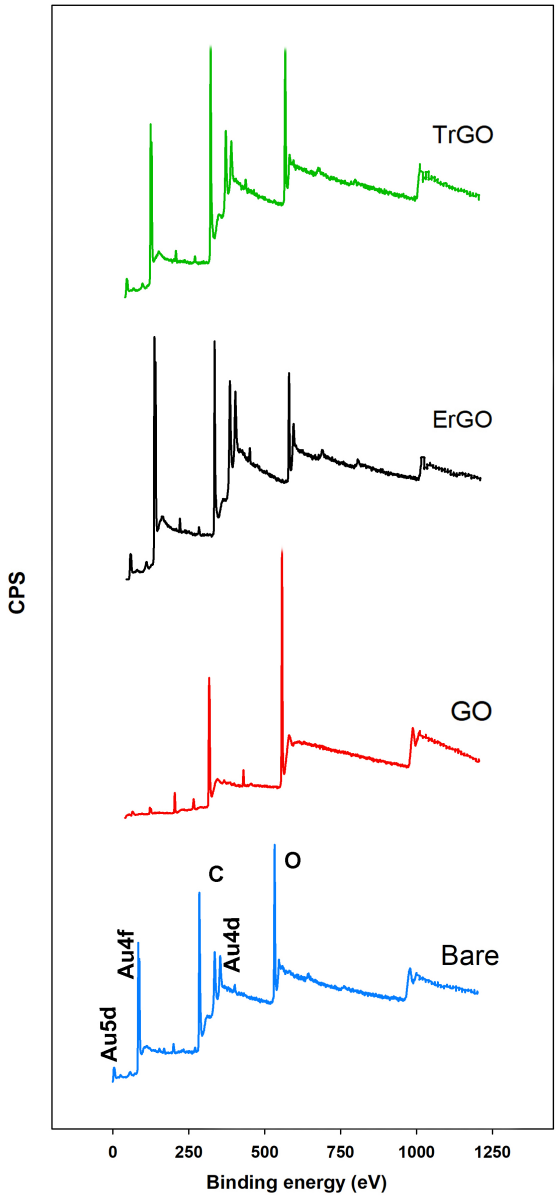

Figure 3.28: XPS spectra of the bare electrode and electrodes modified with GO, ErGO, and TrGO after the deposition of the AuNPs. The ErGO showed the highest At% for Au.

3.2.4 Assay development

Electrochemical measurements were used to evaluate the biosensor development steps and the performance of the biosensor. CV scans were performed after each preparation step and amperometric detections were conducted after the biosensors were incu-

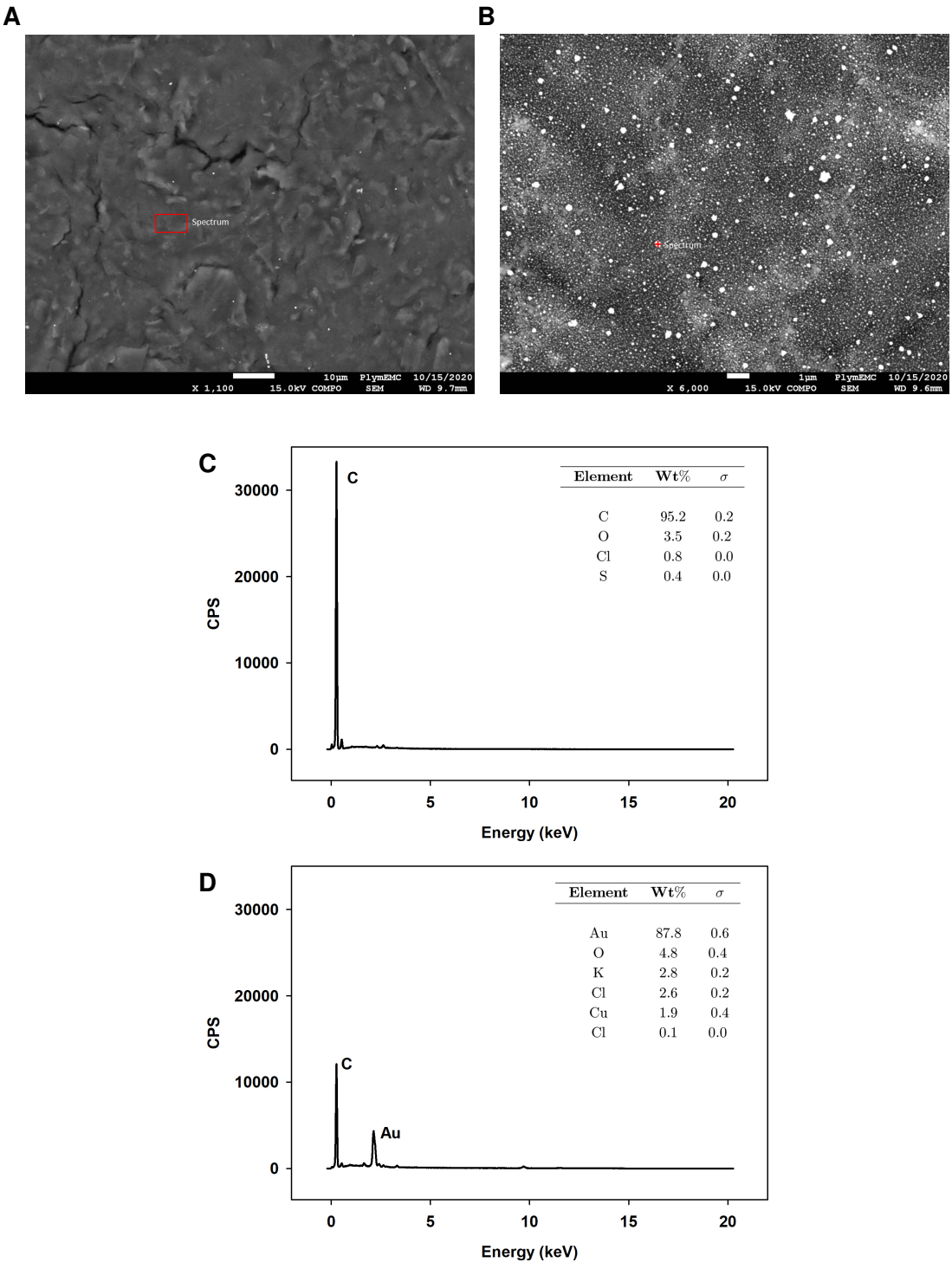

Figure 3.29: SEM images of ErGO (A) and ErGO/AuNPs (B) electrodes. EDS spectra of the ErGO(C) and ErGO/AuNPs (D) electrodes. The inset tables show the present elements, the relative concentration (Wt%) of each elements and their measurement errors (σ).

Table 3.5: A detailed information of the XPS peaks, their position, FWHM and At% for a bare electrode after the deposition of AuNPs, and electrodes modified with GO/AuNPs, ErGO/AuNPs and TrGO/AuNPs. These data are obtained from XPS survey scans (figure 3.28).

Sample	Peak name	Position	FWHM	At%
Bare/AuNPs	O1s	532.83	3.20	19.97
	C1s	284.83	3.61	72.11
	N1s	401.83	3.27	1.56
	Cl2p	199.83	3.37	1.50
	S2p	168.83	3.25	0.71
	Au4f	83.83	2.50	4.16
GO/AuNPs	O1s	531.89	3.00	29.40
	C1s	284.89	4.26	63.83
	N1s	400.89	2.84	2.76
	S2p	168.89	3.01	4.00
ErGO/AuNPs	O1s	551.00	3.26	13.25
	C1s	298.99	2.77	74.10
	N1s	418.99	3.09	2.89
	S2p	180.99	2.97	2.38
	Au4f	94.99	2.80	7.38
TrGO/AuNPs	O1s	542.79	3.43	17.65
	C1s	298.79	2.99	75.06
	N1s	408.79	3.43	1.75
	S2p	171.79	2.96	1.46
	Au4f	86.79	2.43	4.08

bated in various concentrations of ds-methylated-DNA (ds-MGMT). The ErGO/AuNPs modified electrodes were used as the working electrodes for all of the following experiments.

3.2.5 Optimization

The antigen incubation time and the Streptavidin-HRP concentration for the amperometric measurements were optimized prior to incubating the biosensor in various concentrations (figure 3.30).

The antigen incubation time was optimized by incubating at least three electrodes in the ds-methylated DNA for either 0.5, 1, 1.5, or 2 h. The results are displayed in figure

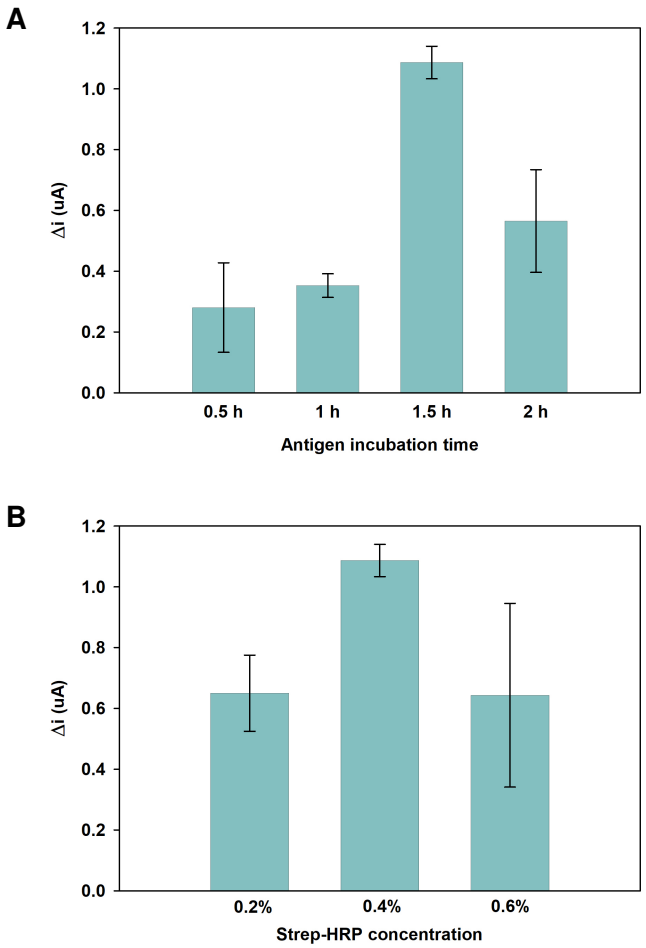

Figure 3.30: Optimization studies results. Optimizing antigen (ds-MGMT) incubation time (A) and Streptavidin-HRP concentration (B).

3.30a where it is shown that the incubation time of 1.5 h exhibits the highest difference in the current before and after adding the H_2O_2. Consequently, 1.5 h was chosen as the optimized incubation time for the antigen incubation.

The Streptavidin-HRP concentration was optimized by varying its concentration in PBS. The tested concentrations were 0.2%, 0.4%, and 0.6%, and at least three electrodes were incubated in either of these concentrations for 30 min at room temperature prior to the amperometric measurements. As can be seen in figure 3.30b, the 0.4% concentration showed the highest difference in the current before and after adding the H_2O_2. Therefore, 0.4% was chosen as the optimized Streptavidin-HRP concentration and was used in further experiments. In all of the above studies, the error bars are the standard

deviations of at least 3 electrodes.

Cyclic Voltammetry

Figure 3.31a shows the voltammograms of the various preparation steps of the biosensor (Bare, GO, ErGO, AuNPs, PNA, MCH, and ds-MGMT). As can be seen from the voltammograms, the anodic peak current (i_{pa}) of the bare electrode was first seen at 57.5 μA. After drop-coating the surface of the working electrode in GO, the i_{pa} decreased to 1.05 μA due to the non-conductive nature of GO (Marcano et al., 2010). After the electrochemical reduction of GO, the i_{pa} increased to 117.5 μA. This increase is due to the electrochemical reduction of GO and the production of rGO. RGO is electrically conductive and has a high concentration of charge carriers, mobility, and a high number of available electroactive sites on the surface, facilitating electron transfer (Pei and Cheng, 2012; Benvidi et al., 2015). After the electrochemical reduction of GO, the i_{pa} decreased to 107.2 μA by reducing the AuNPs on the rGO surface, followed by a further decrease to 73.6 μA after overnight incubation in PNA, confirming the immobilization of the AuNPs and PNA on the surface, respectively. Amine groups (N-terminal of PNA) are able to self-assemble on the AuNPs and form a SAM, decreasing the electron transfer between the electrode and the electrolyte (de la Llave et al., 2014; Olmos-Asar et al., 2014). The i_{pa} decreased once more to 63.7 after μA blocking the surface to decrease the chance of non-specific bonding. Finally, the i_{pa} slightly increased to 68.2 μA after the electrode was incubated in target ds-MGMT nucleotides, confirming the presence of the dsDNA on the surface. The dsDNA was captured by the strand invasion of PNA towards the DNA/DNA duplex and the formation of a triple helix (Hu et al., 2018; Saadati et al., 2019). Additionally, after the reduction of GO, the peak potential first shifted positively towards higher potentials, followed by a negative shift after the deposition of the AuNPs. Furthermore, a small positive shift in the peak potential was observed after the immobilization of PNA, MCH, and triple formation, which might be due to the spatial blockage and hindered electron transfer on the surface (Azimzadeh et al., 2016).

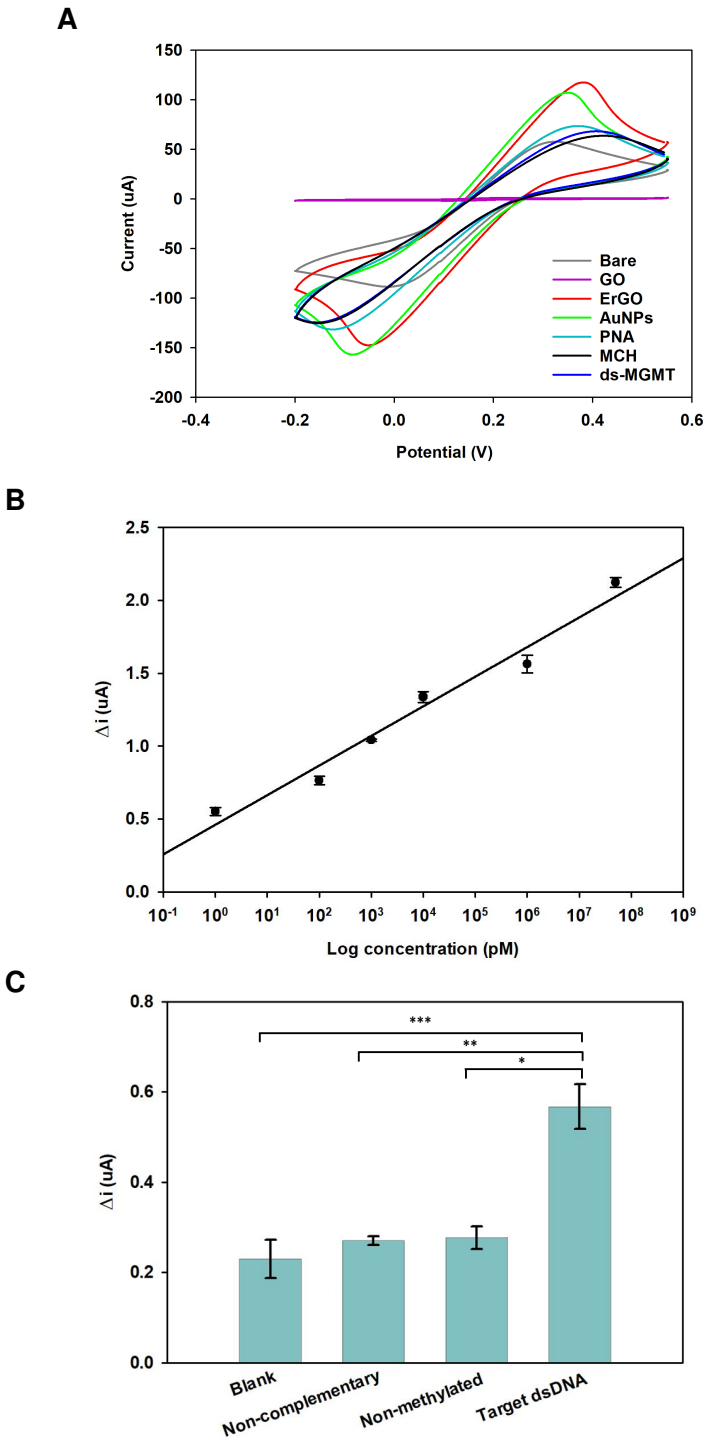

Figure 3.31: Comparison of CV voltammograms of the various preparation steps of the biosensor: Bare, GO, ErGO, AuNPs, PNA, MCH, and ds-MGMT (A). Linear regression studies for the ds-MGMT gene using the amperometric technique. Error bars are the standard deviation of at least three electrodes (B). Comparison of the amperometric response of the biosensor in different solutions: blank (mouse plasma), the ss-MGMT gene, and the ds-MGMT gene spiked in mouse plasma. (*p value = 0.0002, **p value = 0.0008 and ** p value = 0.00011) (C).

The cathodic peak currents (i_{pc}) of the CV voltammograms showed the same trend as the anodic peak current after each incubation step, with corresponding positive and negative shifts.

Linear regression

Amperometric detection was used to perform the linear regression studies. As explained in section 2.3.1, after the biosensor was incubated in Streptavidin-HRP for 30 minutes, the amperometric measurements were first preformed in HQ solution for measuring the background signal followed by the addition of H_2O_2 and measuring the reduction of HRP labels. The possible mechanism is as follows:

HRP_{Red} + H_2O_2 $\rightarrow$$HRP_{Ox}$ + H_2O

HRP_{Ox} + HQ$\rightarrow$ HRP_{Red} + BQ

BQ+H^++2 $e^-$$\rightarrow$ HQ

Where HRP_{Red} is HRP in reduced state, HRP_{Ox} is the oxidation state of HRP and BQ (ben-zoquinone) is the oxidation state of HQ.

Upon addition of H_2O_2, HRP will first react with H_2O_2 and converts to HRP_{Ox} which will then exchange electrons with HQ and produces BQ and HRP_{Red}. Then BQ receive electrons from the electrode, which electrochemically produces HQ. Recycling the HQ and BQ result in a decrease in the current which is proportional to the concentration of HRP and therefore the target biomarker on the surface (Camacho et al., 2007; Dong et al., 2017). Subsequently, the difference between the background signal and the signal from HRP reduction (Δi) was plotted as a function of logarithm of the concentration in figure 3.31b. As can be seen in this figure, the difference in current increases with an increase in the concentration, which is due to the presence of more HRP labels; this is correlated with the presence of more ds-MGMT nucleotides. The best fit linear model is:

$$y = 0.46\ln(x) + 0.20 \tag{3.7}$$

with $R^2 = 0.96$ and the linear range of 1 pM to 50 μM. The LOD was calculated to be 0.86 pM using the equation (Singh et al., 2014; Shi et al., 2018):

$$\text{LOD} = 3.3\sigma/m \tag{3.8}$$

where σ is the standard deviation of the amperometric responses of 4 blank samples and m is the slope of the calibration curve.

Selectivity

The selectivity study was performed with 100 pM of target dsDNA (ds-MGMT) non-complementary as well as non-methylated oligonucleotides spiked in mouse plasma and a blank mouse plasma sample. As can be seen in figure 3.31c, there was a significant difference (Supported by a two tailed T-test analysis) in the responses of the blank and the ds-MGMT samples. Also, the fabricated sensor was able to distinguish between the same concentration of target DNA and the non-complementary and non-methylated DNAs. The higher response of the target DNA means that the biosensor has successfully captured the target DNA, the antibodies have identified the methylated cites on the target DNA, and the reduction of HRP has taken place as described in Section 3.2.5.

3.2.6 Comparison with other works

In Table 1, the various parameters of the proposed biosensor, including the working electrode, the bioreceptor, the dynamic range, the LOD, and the measurement techniques, are compared with other electrochemical biosensors so far reported for the detection of DNA methylation. Although most of the works summarized in Table 3.6 report a better LOD than the results in this work, they all detect single-stranded DNA (ssDNA). In addition, some of the reported biosensors only detect the presence of methylation, insensitive to the gene sequence, while in this work, the presence of the methylation and the sequence of the double-stranded target gene are detected simultaneously.

Electrode	Bioreceptor	Dynamic range	LOD	Technique	Reference
Gold modified with gold nanoparticles	stem-loop-tetrahedron composite DNA	10^{-6}-10 pM	9.326×10^{-7} pM	Chronoamperometry	Chen et al. (2019)
SPCE and immuno-magnetic beads (MBs)	Anti-5mC	4.0-2.5$\times10^{2}$ pM	1 pM	Amperometry	Povedano et al. (2018a)
MoS_2 Nanosheets	FAM-labeled probe DNA	100-2$\times10^{5}$ pM	140 pM	Fluorescence	Xiao et al. (2016)
rGO modified with ammuniom hydroxide	Anti5-mC and complementary DNA	0.5-100 pM	0.012 pM	DPV	Safarzadeh et al. (2021)
SPCE modified with rGO and polyvinyl alcohol	Anti-5mC immobilized and DNA probe conjugated with Fe_3O_4-citric acid nanocomposites	7×10^{-4}-140.29 pM	6.31×10^{-4} pM	DPV/EIS	Khodaei et al. (2019)
AuNPs/ErGO	PNA and anti-5mC	1-5$\times10^{7}$ pM	0.86 pM	Amperometry	This work

Table 3.6: An overview of the other biosensors assays to date for the detection of DNA methylation, using various types of nanomaterials.

3.2.7 Summary

A biosensor for the detection of the ds-MGMT gene has been developed in this work using an ErGO/AuNPs-modified electrode. The electrochemical and thermal reductions of GO were also compared. A high C/O ratio was achieved using electrochemical reduction of GO without using any harmful reductants and in a shorter period of time compared to the techniques reported in other papers. The I_D/I_G ratios showed higher numbers of defect sites and a smaller crystallite size of sp^2 structures in ErGO. After the electro-deposition of the AuNPs, the At% of gold for the ErGO/AuNPs was higher compared to the TrGO/AuNPs. Therefore, the ErGO/AuNPs electrode was used as the base electrode to develop the biosensor. PNA was used to form a SAM layer on the surface via the amine AuNPs interaction where PNA acts as the biorecognition element. The linear range was 1 pM to 50 μM and the LOD was calculated to be 0.86 pM without any PCR amplification or bisulfite treatment. The detection time for this biosensor was 3 hours and 30 minutes. Selectivity studies showed that the biosensor is able to distinguish between blank mouse plasma, the target dsDNA, and the non-complementary and non-methylated oligonucleotides spiked in mouse plasma. However, the stability of the sensor over time and the sensor performance in human plasma is still to be explored in the future. To the best of our knowledge, this is the first report on using PNA to detect methylated DNA and to capture double-stranded methylated DNA. The sandwich design can be tailor-made to detect other methylated genes, revealing it as basis for clinical applications in diagnostics and a marking it as promising platform for detecting ds-methylated biomarkers.

Chapter 4

Conclusions and outlook

4.1 Conclusion

Glioma is an aggressive form of brain cancer that is currently difficult to diagnose and treat. It is hoped that by exploring novel, simple and non-invasive techniques for the detection or screening of life threatening diseases such as gliomas, the survival rate and the quality of life of patients will increase.

In this work two biosensors for the detection of DNA methylation as a biomarker for glioma were designed, developed and tested. The Ab/ssDNA biosensor reported in this thesis is the first biosensor to detect MGMT gene, using rGO electrodes. The PNA/Ab biosensor is the first report on direct detection of double stranded methylated DNA, with no prior preparation.

The first biosensor is based on a commercially available reduced graphene oxide (rGO) screen printed electrode, and uses anti-5mC as a bioreceptor agent and ammonium hydroxide as a linker (aminated rGO). In this biosensor, the target ssDNA was first hybridised by its complementary DNA to characterize its sequence and form a ds-DNA, which was then captured by anti-5mC on the electrode surface due to the presence of methylation. Optimization studies were done to optimize various preparation steps including the effect of BSA and protein G, amination incubation time, antibody and antigen incubation time. In addition, various techniques such as electrochemical measurements, Raman and x-ray photoelectron spectroscopy (XPS) and scanning electron microscopy (SEM) were used to characterize the electrode surface and understand possible surface reactions after amination. Finally linearity and selectivity

tests were done using voltammetric techniques. The linearity test was performed for methylated ssDNA and dsDNA, showing a different response for each of the targets with LOD of 12 fM for ssDNA and 25 fM for dsDNA. The selectivity test showed that the developed biosensor was selective towards the methylation in the target ssDNA vs. non-methylated target with the same sequence. However, this biosensor relies on the previous hybridization of the methylated DNA to select the target gene sequence, and is not selective when detecting the target in a larger pool of ssDNA strands. This is a drawback of the first biosensor.

To overcome the selectivity problem of the Ab/ssDNA biosensor and to be able to achieve simultaneous recognition of the gene sequence, as well as the presence of methylation, the PNA/Ab biosensor is developed using Peptide Nucleic Acids (PNA), as the bioreceptor agents. The PNAs are anchored on gold nanoparticles (AuNPs) which were previously electro-deposited on the ErGO surface. Similar to the Ab/ssDNA biosensor, the PNA/Ab biosensor is also based on commercially available screen printed electrodes. However, in this work the surface of the electrode was modified with rGO and AuNPs to increase the reproducibility of the commercial biosensor. Here, two types of GO reduction (Electrochemical and Thermal) were compared using various characterization techniques including XPS, SEM, EDS, Raman spectroscopy and cyclic voltammetry. After the aforementioned investigations, ErGO was used for continuing the study due to its higher reduction degree and stability during the measurements. After electro-deposition of the AuNPs, PNA was used to invade ds-MGMT genes in buffer and in mice plasma, where its methylation was captured by biotinylated antibody which was then detected by amperometric techniques using strep-HRP as the label. The LOD for this biosensor was calculated to be 0.86 pM with dynamic range of 1 pM to 50 μM.

Although both of the biosensors developed in this study were aimed to detect methylated DNA associated with glioma, but they can be re-designed to detect methylated genes with different strands, and therefore can be applicable to other diseases with

methylated DNA biomarkers.

4.2 Funding

This research was funded by EU Horizon 2020, Marie Skłodowska-Curie Actions (MSCA-ITN-ETN) AiPBAND grant number 764281. (Start date: 1 January 2018. End date: 30 June 2022)

4.3 Recommendations for future work

In this work, two different biosensors were developed, however these are just two examples of many potential biosensor designs based on graphene that can be developed and validated to quantify methylated DNA.

In terms of electrode fabrication the rGO electrodes can be printed in house in a well controlled clean-room to ensure uniformity of quality of the electrodes and improving the reproducibility of subsequent applications, which is currently a major issue in commercially available electrodes. The stability of the electrodes can also be investigated to clear their shelf life in case of mass production and storage of the electrodes. In this work, the biosensors were fabricated before their application and therefore the stability was not investigated.

Other graphene based materials can also be explored as a working electrode and be compared to the current rGO electrode. Graphene based electrode can be prepared as a 3D foam to increase its surface to volume ratio and which allows the accommodation of more biomolecules and may result in a higher sensitivity. Also, other types of biosensors can be combined with graphene and be compared with AuNPs used in this work.

In terms of biosensor fabrication and application, it would be interesting to investigate the same sensor designs reported in this work to other methylated DNAs and especially see their applications in real patients plasma or blood. Other body fluids mainly CSF can be used to detect brain tumor related DNA methylation as well. Furthermore, down or up regulation of the number of methylations on DNA strands or duplexes can

be a valuable path to look into. Also, a similar biosensor concept can be applied to other types of graphene based biosensors such as FET, SERS, plasmonic, etc and be compared with electrochemical measurement.

Finally multiplexing the biosensor to detect a combination of biomarkers at the same time and equipping the sensors to an automated sample delivery, incubation and wash system such as microfluidics will reduce possible errors and increase the reliability of the biosensor.

4.4 Publications, posters and presentations

4.4.1 Publications

- **Mina Safarzadeh**, and Genhua Pan, Detection of a Double-Stranded MGMT Gene Using Electrochemically Reduced Graphene Oxide (ErGO) Electrodes Decorated with AuNPs and Peptide Nucleic Acids (PNA), Biosensors 2022, 12(2), 98,

  https://doi.org/10.3390/bios12020098

- **Mina Safarzadeh**, Ahmed Suhail, Jagriti Sethi, Anas Sattar and Genhua Pan, A label free DNA-immunosensor based on functionalised rGO electrode for the quantification of DNA methylation, Nanomaterials 2021, 11(4), 985,

  https://doi.org/10.3390/nano11040985

- Sara Khorshidian, **Mina Safarzadeh**, Ghasem Rezaei, Behrooz Vaseghi, David Jenkins, Niroj Kumar Sahu, and Arunima Raja, Co0. 50ni0. 50-Xznx Ferrite Nanoparticle Decoration on Go Surface: Structural, Magnetic and Electrochemical Properties, MAGMA-D-22-00417,

  https://dx.doi.org/10.2139/ssrn.4071733

- Jagriti Sethi, Michiel Van Bulck, Ahmed Suhail, **Mina Safarzadeh**, Ana Perez-Castillo and Genhua Pan, A label-free biosensor based on graphene and reduced graphene oxide dual-layer for electrochemical determination of beta-amyloid biomarkers. Microchim Acta 187, 288 (2020),

https://doi.org/10.1007/s00604-020-04267-x

- Jagriti Sethi, Ahmed Suhail, **Mina Safarzadeh**, Anas Sattar, Yinghui Wei and Genhua Pan, NH2 linker for femtomolar label-free detection with reduced graphene oxide screen printed electrodes, Carbon (2021),

  https://doi.org/10.1016/j.carbon.2021.04.074

- Ahmed Suhail, Genhua Pan, Jagriti Sethi and **Mina Safarzadeh**, Label-free electrochemical biosensor for the detection of bodyfluid based biomarkers, patent application number: EP20217463.7

4.4.2 AiPBAND network events

The project aim, plans and achieved results were presented in five AiPBAND network events (In London (UK), Rome (Italy), Utrecht (the Netherlands), Catania (Italy), Leuven (Belgium)) and three webinars, as planned for in the AiPBAND proposal.

4.4.3 Conferences

- **7th International Conference on Bio-Sensing Technology**, May 2022, Poster presentation titled: Detection of a Double-Stranded MGMT Gene Using Electrochemically Reduced Graphene Oxide (ErGO) Electrodes Decorated with AuNPs and Peptide Nucleic Acids (PNA)

- **7th International Conference on Sensors and Electronic Instrumentation Advances (SEIA' 2021)**, September 2021, Oral presentation titled: Quantification of double stranded methylated DNA, using rGO and AuNPs decorated screen printed electrode.

- **31st Anniversary World Congress on Biosensors**, July 2021, Poster presentation titled: A label-free DNA-immunosensor based on aminated rGO electrode for the quantification of DNA methylation.

- **International Nanoscience Student Conference**, August 2020, poster presentation titled: A graphene-based biosensor for highly sensitive quantification of

DNA methylation

- **The 2nd World Summit on Advances in Science, Engineering and Technology**, October 2019, Oral presentation titled: Electrochemical label free detection of DNA methylation using screen-printed graphene electrodes
- **PhD micro and nano-sensors summerschool**, August 2019, poster presentation titled: Graphene based biosensors for the detection of DNA

4.5 Awards

- **Joint best poster winner**, July 2021, 31st Anniversary World Congress on Biosensors
- **University-wide 3 Minute Thesis Competition**, May 2021, 2nd place

4.6 Self-development activities

All of the network training events proposed by AiPBAND were attended. Also, PhD micro and nano-sensors summerschool was attended in order to become more exposed to the biosensors field and other relevant academic skills, such as networking. Finally, various webinars and development sessions were attended at the University of Plymouth, including "Designing an effective research poster", "Presenting at conferences", "Keeping Lab records", "Career planning for postgraduate research students", "How to transit from academia safely", "structuring your article correctly", "Open access publishing", "Unconscious bias", "Diversity in workplace" etc. I also self-learned Latex, Adobe Illustrator and Adobe In-Design. During the Covid-19 pandemic lock downs, I took various courses on Linked In learning to expand my expertise on visual communication and presentation skills as well as courses to make my job applications more effective.

4.7 Collaborative studies and placements

- A collaborative study with Dr.Sara Khorshidian was established in which the electrochemical measurements of her project were performed at the University of Ply-

mouth. In this study, various compositions of $Co_{0.50}$ $Ni_{0.50-X}$ Zn_X Ferrite nanoparticles were decorated on GO nanosheets using hydrothermal methods. The electrochemical properties of the nanocomposites were measured in $K_3[Fe(CN)_6]$ solution using CV techniques. Furthermore, the nanocomposites were used to measure the presence of paracetamol in PBS to confirm the electrochemical behaviour of the nanocomposites. The results of this study were reported in a journal paper which is listed in the publications.

- A one week placement at DTU, Denmark was done to gain experience with optical ELISA.

List of references

Abbott, N. J., Patabendige, A. A., Dolman, D. E., Yusof, S. R., and Begley, D. J. (2010). Structure and function of the blood–brain barrier. *Neurobiology of disease*, 37(1):13–25.

Ahmadi, M. and Ahour, F. (2020). An electrochemical biosensor based on a graphene oxide modified pencil graphite electrode for direct detection and discrimination of double-stranded dna sequences. *Analytical Methods*, 12(37):4541–4550.

Ahour, F., Pournaghi-Azar, M. H., Alipour, E., and Hejazi, M. S. (2013). Detection and discrimination of recombinant plasmid encoding hepatitis c virus core/e1 gene based on pna and double-stranded dna hybridization. *Biosensors and Bioelectronics*, 45:287–291.

Akbari jonous, Z., Shayeh, J. S., Yazdian, F., Yadegari, A., Hashemi, M., and Omidi, M. (2019). An electrochemical biosensor for prostate cancer biomarker detection using graphene oxide–gold nanostructures. *Engineering in Life Sciences*, 19(3):206–216.

Al-Gaashani, R., Najjar, A., Zakaria, Y., Mansour, S., and Atieh, M. (2019). Xps and structural studies of high quality graphene oxide and reduced graphene oxide prepared by different chemical oxidation methods. *Ceramics International*, 45(11):14439–14448.

Alabsi, S. S., Ahmed, A. Y., Dennis, J. O., Khir, M. M., and Algamili, A. (2020). A review of carbon nanotubes field effect-based biosensors. *IEEE Access*, 8:69509–69521.

Alix-Panabières, C. and Pantel, K. (2014). Challenges in circulating tumour cell research. *Nature Reviews Cancer*, 14(9):623–631.

Anik, Ü. (2017). Electrochemical medical biosensors for poc applications. In *Medical Biosensors for Point of Care (POC) Applications*, pages 275–292. Elsevier.

Arcella, A., Limanaqi, F., Ferese, R., Biagioni, F., Oliva, M. A., Storto, M., Fanelli, M., Gambardella, S., and Fornai, F. (2020). Dissecting molecular features of gliomas: Genetic loci and validated biomarkers. *International Journal of Molecular Sciences*, 21(2):685.

Areeb, Z., Stylli, S. S., Koldej, R., Ritchie, D. S., Siegal, T., Morokoff, A. P., Kaye, A. H., and Luwor, R. B. (2015). Microrna as potential biomarkers in glioblastoma. *Journal of neuro-oncology*, 125(2):237–248.

Asal, M., Özen, Ö., Şahinler, M., Baysal, H. T., and Polatoğlu, İ. (2018). An overview of biomolecules, immobilization methods and support materials of biosensors. *Sensor Review*.

Azimzadeh, M., Rahaie, M., Nasirizadeh, N., Ashtari, K., and Naderi-Manesh, H. (2016). An electrochemical nanobiosensor for plasma mirna-155, based on graphene oxide and gold nanorod, for early detection of breast cancer. *Biosensors and Bioelectronics*, 77:99–106.

Bai, Y., Xu, T., and Zhang, X. (2020). Graphene-based biosensors for detection of biomarkers. *Micromachines*, 11(1):60.

Baker, E. S., Hong, J. W., Gaylord, B. S., Bazan, G. C., and Bowers, M. T. (2006). Pna/dsdna complexes: site specific binding and dsdna biosensor applications. *Journal of the American Chemical Society*, 128(26):8484–8492.

Balaji, A. and Zhang, J. (2017). Electrochemical and optical biosensors for early-stage cancer diagnosis by using graphene and graphene oxide. *Cancer nanotechnology*, 8(1):10.

Baldovino, F., Quitain, A., Dugos, N. P., Roces, S. A., Koinuma, M., Yuasa, M., and Kida, T. (2016). Synthesis and characterization of nitrogen-functionalized graphene oxide in high-temperature and high-pressure ammonia. *RSC advances*, 6(115):113924–113932.

Ban, D. K., Liu, Y., Wang, Z., Ramachandran, S., Sarkar, N., Shi, Z., Liu, W., Karkisaval, A. G., Martinez-Loran, E., Zhang, F., et al. (2020). Direct dna methylation profiling with an electric biosensor. *ACS nano*, 14(6):6743–6751.

Benvidi, A., Firouzabadi, A. D., Moshtaghiun, S. M., Mazloum-Ardakani, M., and Tezerjani, M. D. (2015). Ultrasensitive dna sensor based on gold nanoparticles/reduced graphene oxide/glassy carbon electrode. *Analytical biochemistry*, 484:24–30.

Bettegowda, C., Sausen, M., Leary, R., Kinde, I., Wang, Y., Agrawal, N., Bartlett, B., Wang, H., Luber, B., Alani, R., et al. (2014). Detection of circulating tumor dna in early-and late-stage human malignancies. sci transl med. 2014; 6: 224ra24.

Bhattacharjee, R., Moriam, S., Nguyen, N.-T., and Shiddiky, M. J. (2019). A bisulfite treatment and pcr-free global dna methylation detection method using electrochemical enzymatic signal engagement. *Biosensors and Bioelectronics*, 126:102–107.

Bhattacharjee, R., Moriam, S., Umer, M., Nguyen, N.-T., and Shiddiky, M. J. (2018). Dna methylation detection: recent developments in bisulfite free electrochemical and optical approaches. *Analyst*, 143(20):4802–4818.

Bieniek, A., Terzyk, A. P., Wiśniewski, M., Roszek, K., Kowalczyk, P., Sarkisov, L., Keskin, S., and Kaneko, K. (2021). Mof materials as therapeutic agents, drug carriers, imaging agents and biosensors in cancer biomedicine: Recent advances and perspectives. *Progress in Materials Science*, 117:100743.

Bohunicky, B. and Mousa, S. A. (2011). Biosensors: the new wave in cancer diagnosis. *Nanotechnology, science and applications*, 4:1.

Bray, F., Ferlay, J., Soerjomataram, I., Siegel, R. L., Torre, L. A., and Jemal, A. (2018). Global cancer statistics 2018: Globocan estimates of incidence and mortality worldwide for 36 cancers in 185 countries. *CA: a cancer journal for clinicians*, 68(6):394–424.

Cai, C., Guo, Z., Cao, Y., Zhang, W., and Chen, Y. (2018). A dual biomarker detection platform for quantitating circulating tumor dna (ctdna). *Nanotheranostics*, 2(1):12.

Camacho, C., Matías, J. C., Chico, B., Cao, R., Gómez, L., Simpson, B. K., and Villalonga, R. (2007). Amperometric biosensor for hydrogen peroxide, using supramolecularly immobilized horseradish peroxidase on the β-cyclodextrin-coated gold electrode. *Electroanalysis: An International Journal Devoted to Fundamental and Practical Aspects of Electroanalysis*, 19(24):2538–2542.

Cardoso, A. R., Moreira, F. T., Fernandes, R., and Sales, M. G. F. (2016). Novel and simple electrochemical biosensor monitoring attomolar levels of mirna-155 in breast cancer. *Biosensors and Bioelectronics*, 80:621–630.

Carr, O., Raymundo-Pereira, P. A., Shimizu, F. M., Sorroche, B. P., Melendez, M. E., de Oliveira Pedro, R., Miranda, P. B., Carvalho, A. L., Reis, R. M., Arantes, L. M., et al. (2020). Genosensor made with a self-assembled monolayer matrix to detect mgmt gene methylation in head and neck cancer cell lines. *Talanta*, 210:120609.

Chakraborty, M. and Hashmi, M. S. J. (2017). An overview of biosensors and devices. In *Reference Module in Materials Science and Materials Engineering*. Elsevier.

Chaubey, A. and Malhotra, B. (2002). Mediated biosensors. *Biosensors and bioelectronics*, 17(6-7):441–456.

Chen, C.-M., Zhang, Q., Zhao, X.-C., Zhang, B., Kong, Q.-Q., Yang, M.-G., Yang, Q.-H., Wang, M.-Z., Yang, Y.-G., Schlögl, R., et al. (2012). Hierarchically aminated graphene honeycombs for electrochemical capacitive energy storage. *Journal of Materials Chemistry*, 22(28):14076–14084.

Chen, F., Karolak, W., Cypel, M., Keshavjee, S., and Pierre, A. (2009). Intermediate-term outcome in lung transplantation from a donor with glioblastoma multiforme. *The Journal of heart and lung transplantation*, 28(10):1116–1118.

Chen, H., Shah, A. S., Girgis, R. E., and Grossman, S. A. (2008). Transmission of glioblastoma multiforme after bilateral lung transplantation. *Journal of Clinical Oncology*, 26(19):3284–3285.

Chen, W.-x., Liu, X.-m., Lv, M.-m., Chen, L., Zhao, J.-h., Zhong, S.-l., Ji, M.-h., Hu, Q., Luo, Z., Wu, J.-z., et al. (2014). Exosomes from drug-resistant breast cancer cells transmit chemoresistance by a horizontal transfer of microrna. *PloS one*, 9(4):e95240.

Chen, X., Huang, J., Zhang, S., Mo, F., Su, S., Li, Y., Fang, L., Deng, J., Huang, H., Luo, Z., et al. (2019). Electrochemical biosensor for dna methylation detection through hybridization chain-amplified reaction coupled with a tetrahedral dna nanostructure. *ACS applied materials & interfaces*, 11(4):3745–3752.

Chen, Z. and Hambardzumyan, D. (2018). Immune microenvironment in glioblastoma subtypes. *Frontiers in immunology*, 9:1004.

Chiang, H.-C., Wang, Y., Zhang, Q., and Levon, K. (2019). Optimization of the electrodeposition of gold nanoparticles for the application of highly sensitive, label-free biosensor. *Biosensors*, 9(2):50.

Childres, I., Jauregui, L. A., Park, W., Cao, H., and Chen, Y. P. (2013). Raman spectroscopy of graphene and related materials. *New developments in photon and materials research*, 1:1–20.

Chowdhury, B., Cho, I.-H., Hahn, N., and Irudayaraj, J. (2014). Quantification of 5-methylcytosine, 5-hydroxymethylcytosine and 5-carboxylcytosine from the blood of cancer patients by an enzyme-based immunoassay. *Analytica chimica acta*, 852:212–217.

Chua, C. K., Ambrosi, A., and Pumera, M. (2012). Graphene oxide reduction by standard industrial reducing agent: thiourea dioxide. *Journal of materials chemistry*, 22(22):11054–11061.

Chung, S., Revia, R. A., and Zhang, M. (2021). Graphene quantum dots and their applications in bioimaging, biosensing, and therapy. *Advanced Materials*, 33(22):1904362.

Cialla-May, D., Schmitt, M., and Popp, J. (2019). Theoretical principles of raman spectroscopy. *Physical Sciences Reviews*, 4(6).

Colwell, N., Larion, M., Giles, A. J., Seldomridge, A. N., Sizdahkhani, S., Gilbert, M. R., and Park, D. M. (2017). Hypoxia in the glioblastoma microenvironment: shaping the phenotype of cancer stem-like cells. *Neuro-oncology*, 19(7):887–896.

Compton, R. G. and Banks, C. E. (2018). *Understanding voltammetry*. World Scientific.

Corcoran, C., Rani, S., O'Brien, K., O'Neill, A., Prencipe, M., Sheikh, R., Webb, G., McDermott, R., Watson, W., Crown, J., et al. (2012). Docetaxel-resistance in prostate cancer: evaluating associated phenotypic changes and potential for resistance transfer via exosomes. *PloS one*, 7(12):e50999.

Cottrell, S. E., Distler, J., Goodman, N. S., Mooney, S. H., Kluth, A., Olek, A., Schwope, I., Tetzner, R., Ziebarth, H., and Berlin, K. (2004). A real-time pcr assay for dna-methylation using methylation-specific blockers. *Nucleic acids research*, 32(1):e10–e10.

Crowley, E., Di Nicolantonio, F., Loupakis, F., and Bardelli, A. (2013). Liquid biopsy: monitoring cancer-genetics in the blood. *Nature reviews Clinical oncology*, 10(8):472–484.

Cui, Z., Li, D., Yang, W., Fan, K., Liu, H., Wen, F., Li, L., Dong, L., Wang, G., and Wu, W. (2022). An electrochemical biosensor based on few-layer mos 2 nanosheets for highly sensitive detection of tumor marker ctdna. *Analytical Methods*, 14(20):1956–1962.

Daneman, R. and Prat, A. (2015). The blood–brain barrier. *Cold Spring Harbor perspectives in biology*, 7(1):a020412.

Daneshpour, M., Izadi, P., Omidfar, K., et al. (2016). Femtomolar level detection of rassf1a tumor suppressor gene methylation by electrochemical nano-genosensor based on fe3o4/tmc/au nanocomposite and pt-modified electrode. *Biosensors and Bioelectronics*, 77:1095–1103.

Das, A., Pisana, S., Chakraborty, B., Piscanec, S., Saha, S. K., Waghmare, U. V., Novoselov, K. S., Krishnamurthy, H. R., Geim, A. K., Ferrari, A. C., et al. (2008). Monitoring dopants by raman scattering in an electrochemically top-gated graphene transistor. *Nature nanotechnology*, 3(4):210–215.

Das, P. M. and Singal, R. (2004). Dna methylation and cancer. *Journal of clinical oncology*, 22(22):4632–4642.

Davies, D. R. and Chacko, S. (1993). Antibody structure. *Accounts of chemical research*, 26(8):421–427.

Davis, C. D. and Uthus, E. O. (2004). Dna methylation, cancer susceptibility, and nutrient interactions. *Experimental biology and medicine*, 229(10):988–995.

de la Llave, E., Clarenc, R., Schiffrin, D. J., and Williams, F. J. (2014). Organization of alkane amines on a gold surface: Structure, surface dipole, and electron transfer. *The Journal of Physical Chemistry C*, 118(1):468–475.

Devadas, B., Madhu, R., Chen, S.-M., and Yeh, H.-T. (2014). Controlled electrochemical synthesis of new rare earth metal lutetium hexacyanoferrate on reduced graphene oxide and its application as a salicylic acid sensor. *Journal of Materials Chemistry B*, 2(43):7515–7523.

Devadas, B., Rajkumar, M., Chen, S.-M., and Saraswathi, R. (2012). Electrochemically reduced graphene oxide/neodymium hexacyanoferrate modified electrodes for the electrochemical detection of paracetomol. *Int. J. Electrochem. Sci*, 7(4):3339–3349.

Devasenathipathy, R., Mani, V., Chen, S.-M., Viswanath, B., Vasantha, V., and Govindasamy, M. (2014). Electrodeposition of gold nanoparticles on a pectin scaffold and

its electrocatalytic application in the selective determination of dopamine. *RSC Advances*, 4(99):55900–55907.

Dong, L., Li, Y., Han, C., Wang, X., She, L., and Zhang, H. (2014). mirna microarray reveals specific expression in the peripheral blood of glioblastoma patients. *International journal of oncology*, 45(2):746–756.

Dong, X.-X., Yuan, L.-P., Liu, Y.-X., Wu, M.-F., Liu, B., Sun, Y.-M., Shen, Y.-D., and Xu, Z.-L. (2017). Development of a progesterone immunosensor based on thionine-graphene oxide composites platforms: Improvement by biotin-streptavidin-amplified system. *Talanta*, 170:502–508.

Draht, M. X., Smits, K. M., Jooste, V., Tournier, B., Vervoort, M., Ramaekers, C., Chapusot, C., Weijenberg, M. P., Van Engeland, M., and Melotte, V. (2016). Analysis of ret promoter cpg island methylation using methylation-specific pcr (msp), pyrosequencing, and methylation-sensitive high-resolution melting (ms-hrm): impact on stage ii colon cancer patient outcome. *Clinical epigenetics*, 8(1):44.

Du, M., Yang, T., Zhao, C., and Jiao, K. (2012). Electrochemical logic aptasensor based on graphene. *Sensors and Actuators B: Chemical*, 169:255–260.

Duan, R. and Xi, M. (2020). A novel label-free biosensor for detection of he4 in urine based on localized surface plasmon resonance and protein g directional fixed. *Journal of Nanomaterials*, 2020.

D'Agata, R., Giuffrida, M. C., and Spoto, G. (2017). Peptide nucleic acid-based biosensors for cancer diagnosis. *Molecules*, 22(11):1951.

Ederer, J., Janoš, P., Ecorchard, P., Tolasz, J., Štengl, V., Beneš, H., Perchacz, M., and Pop-Georgievski, O. (2017). Determination of amino groups on functionalized graphene oxide for polyurethane nanomaterials: Xps quantitation vs. functional speciation. *RSC advances*, 7(21):12464–12473.

Elgrishi, N., Rountree, K. J., McCarthy, B. D., Rountree, E. S., Eisenhart, T. T., and Dempsey, J. L. (2017). A practical beginner's guide to cyclic voltammetry. *Journal of Chemical Education*, 95(2):197–206.

Elshafey, R., Tavares, A. C., Siaj, M., and Zourob, M. (2013). Electrochemical impedance immunosensor based on gold nanoparticles–protein g for the detection of cancer marker epidermal growth factor receptor in human plasma and brain tissue. *Biosensors and Bioelectronics*, 50:143–149.

Esteller, M., Garcia-Foncillas, J., Andion, E., Goodman, S. N., Hidalgo, O. F., Vanaclocha, V., Baylin, S. B., and Herman, J. G. (2000). Inactivation of the dna-repair gene mgmt and the clinical response of gliomas to alkylating agents. *New England Journal of Medicine*, 343(19):1350–1354.

Estrela, P., Bhalla, N., Jolly, P., Formisano, N., and Estrela, P. (2016). Introduction to biosensors. *Essays in Biochemistry*, 60(1):1–8.

Evron, E., Dooley, W. C., Umbricht, C. B., Rosenthal, D., Sacchi, N., Gabrielson, E., Soito, A. B., Hung, D. T., Ljung, B.-M., Davidson, N. E., et al. (2001). Detection of breast cancer cells in ductal lavage fluid by methylation-specific pcr. *The Lancet*, 357(9265):1335–1336.

Fackler, M. J., Downs, B. M., Mercado-Rodriguez, C., Cimino-Mathews, A., Chen, C., Yuan, J., Cope, L. M., Kohlway, A., Kocmond, K., Lai, E., et al. (2018). Abstract p6-03-07: An automated dna methylation assay (qm-msp) for rapid breast cancer diagnosis in underdeveloped countries.

Fackler, M. J. and Sukumar, S. (2018). Quantitation of dna methylation by quantitative multiplex methylation-specific pcr (qm-msp) assay. In *DNA Methylation Protocols*, pages 473–496. Springer.

Fadley, C. S. (2010). X-ray photoelectron spectroscopy: Progress and perspectives. *Journal of Electron Spectroscopy and Related Phenomena*, 178:2–32.

Faridbod, F. and Sanati, A. L. (2019). Graphene quantum dots in electrochemical sensors/biosensors. *Current Analytical Chemistry*, 15(2):103–123.

Farka, Z., Jurik, T., Kovar, D., Trnkova, L., and Skládal, P. (2017). Nanoparticle-based immunochemical biosensors and assays: recent advances and challenges. *Chemical Reviews*, 117(15):9973–10042.

Fatt, M. A., Horton, K. M., and Fishman, E. K. (2008). Transmission of metastatic glioblastoma multiforme from donor to lung transplant recipient. *Journal of computer assisted tomography*, 32(3):407–409.

Feng, K.-J., Yang, Y.-H., Wang, Z.-J., Jiang, J.-H., Shen, G.-L., and Yu, R.-Q. (2006). A nano-porous ceo2/chitosan composite film as the immobilization matrix for colorectal cancer dna sequence-selective electrochemical biosensor. *Talanta*, 70(3):561–565.

Ferrari, A. C. (2007). Raman spectroscopy of graphene and graphite: Disorder, electron–phonon coupling, doping and nonadiabatic effects. *Solid state communications*, 143(1-2):47–57.

Ferrari, A. C. and Basko, D. M. (2013). Raman spectroscopy as a versatile tool for studying the properties of graphene. *Nature nanotechnology*, 8(4):235–246.

Ferrari, E. (2023). Gold nanoparticle-based plasmonic biosensors. *Biosensors*, 13(3):411.

Ferrier, D. C. and Honeychurch, K. C. (2021). Carbon nanotube (cnt)-based biosensors. *Biosensors*, 11(12):486.

Fowler, J. M., Stuart, M. C., and Wong, D. K. (2007). Self-assembled layer of thiolated protein g as an immunosensor scaffold. *Analytical chemistry*, 79(1):350–354.

Frommer, M., McDonald, L. E., Millar, D. S., Collis, C. M., Watt, F., Grigg, G. W., Molloy, P. L., and Paul, C. L. (1992). A genomic sequencing protocol that yields a positive display of 5-methylcytosine residues in individual dna strands. *Proceedings of the National Academy of Sciences*, 89(5):1827–1831.

Gao, F., Fan, T., Ou, S., Wu, J., Zhang, X., Luo, J., Li, N., Yao, Y., Mou, Y., Liao, X., et al. (2018). Highly efficient electrochemical sensing platform for sensitive detection dna methylation, and methyltransferase activity based on ag nps decorated carbon nanocubes. *Biosensors and Bioelectronics*, 99:201–208.

Gazze, A., Ademefun, R., Conlan, R. S., and Teixeira, S. R. (2018). Electrochemical impedence spectroscopy enabled ca125 detection; toward early ovarian cancer diagnosis using graphene biosensors. *Journal of Interdisciplinary Nanomedicine*, 3(2):82–88.

Geim, A. K. and Novoselov, K. S. (2010). The rise of graphene. In *Nanoscience and Technology: A Collection of Reviews from Nature Journals*, pages 11–19. World Scientific.

Georgopoulos, P., Apostolidis, A., Fragkou, E., Papaioannou, M., Ioannidis, I.-E., and Markopoulou, S. (2018). Dna methylation of a panel of genes as a urinary biomarker for diagnosis of bladder cancer. *European Urology Supplements*, 17(2):e1423.

Gimple, R. C., Bhargava, S., Dixit, D., and Rich, J. N. (2019). Glioblastoma stem cells: lessons from the tumor hierarchy in a lethal cancer. *Genes & development*, 33(11-12):591–609.

Goessl, C., Krause, H., Müller, M., Heicappell, R., Schrader, M., Sachsinger, J., and Miller, K. (2000). Fluorescent methylation-specific polymerase chain reaction for dna-based detection of prostate cancer in bodily fluids. *Cancer research*, 60(21):5941–5945.

Gohring, J. T., Dale, P. S., and Fan, X. (2010). Detection of her2 breast cancer biomarker using the opto-fluidic ring resonator biosensor. *Sensors and Actuators B: Chemical*, 146(1):226–230.

Gorodetsky, A. A., Green, O., Yavin, E., and Barton, J. K. (2007). Coupling into the base pair stack is necessary for dna-mediated electrochemistry. *Bioconjugate chemistry*, 18(5):1434–1441.

Grieshaber, D., MacKenzie, R., Vörös, J., and Reimhult, E. (2008). Electrochemical biosensors-sensor principles and architectures. *Sensors*, 8(3):1400–1458.

Hamidi-Asl, E., Raoof, J. B., Ojani, R., Golabi, S. M., and Hejazi, M. S. (2013). A new peptide nucleotide acid biosensor for electrochemical detection of single nucleotide polymorphism in duplex dna via triplex structure formation. *Journal of the Iranian Chemical Society*, 10(6):1075–1083.

Han, J., Zhuo, Y., Chai, Y., Yuan, R., Zhang, W., and Zhu, Q. (2012). Simultaneous electrochemical detection of multiple tumor markers based on dual catalysis amplification of multi-functionalized onion-like mesoporous graphene sheets. *Analytica chimica acta*, 746:70–76.

Harder, B. G., Blomquist, M. R., Wang, J., Kim, A. J., Woodworth, G. F., Winkles, J. A., Loftus, J. C., and Tran, N. L. (2018). Developments in blood-brain barrier penetrance and drug repurposing for improved treatment of glioblastoma. *Frontiers in oncology*, 8:462.

Hashemi, S. A., Mousavi, S. M., Bahrani, S., Ramakrishna, S., Babapoor, A., and Chiang, W.-H. (2020). Coupled graphene oxide with hybrid metallic nanoparticles as potential electrochemical biosensors for precise detection of ascorbic acid within blood. *Analytica chimica acta*, 1107:183–192.

Heitzer, E., Auer, M., Ulz, P., Geigl, J. B., and Speicher, M. R. (2013). Circulating tumor cells and dna as liquid biopsies. *Genome medicine*, 5(8):1–11.

Heller, G., Altenberger, C., Steiner, I., Topakian, T., Ziegler, B., Tomasich, E., Lang, G., End-Pfützenreuter, A., Zehetmayer, S., Döme, B., et al. (2018). Dna methylation of microrna-coding genes in non-small-cell lung cancer patients. *The Journal of pathology*, 245(4):387–398.

Herman, J. G., Graff, J. R., Myöhänen, S., Nelkin, B. D., and Baylin, S. B. (1996). Methylation-specific pcr: a novel pcr assay for methylation status of cpg islands. *Proceedings of the national academy of sciences*, 93(18):9821–9826.

Hidayah, N., Liu, W.-W., Lai, C.-W., Noriman, N., Khe, C.-S., Hashim, U., and Lee, H. C. (2017). Comparison on graphite, graphene oxide and reduced graphene oxide: Synthesis and characterization. In *AIP Conference Proceedings*, volume 1892, page 150002. AIP Publishing LLC.

Hossain, T., Mahmudunnabi, G., Masud, M. K., Islam, M. N., Ooi, L., Konstantinov, K., Al Hossain, M. S., Martinac, B., Alici, G., Nguyen, N.-T., et al. (2017). Electrochemical biosensing strategies for dna methylation analysis. *Biosensors and Bioelectronics*, 94:63–73.

Hu, Q., Wang, Q., Kong, J., Li, L., and Zhang, X. (2018). Electrochemically mediated in situ growth of electroactive polymers for highly sensitive detection of double-stranded dna without sequence-preference. *Biosensors and Bioelectronics*, 101:1–6.

Huang, J., Zhang, S., Mo, F., Su, S., Chen, X., Li, Y., Fang, L., Huang, H., Deng, J., Liu, H., et al. (2019). An electrochemical dna biosensor analytic technique for identifying dna methylation specific sites and quantify dna methylation level. *Biosensors and Bioelectronics*, 127:155–160.

Huang, K.-J., Niu, D.-J., Sun, J.-Y., and Zhu, J.-J. (2011). An electrochemical amperometric immunobiosensor for label-free detection of α-fetoprotein based on amine-functionalized graphene and gold nanoparticles modified carbon ionic liquid electrode. *Journal of Electroanalytical Chemistry*, 656(1-2):72–77.

Huertas, C. S., Aviñó, A., Kurachi, C., Piqué, A., Sandoval, J., Eritja, R., Esteller, M., and Lechuga, L. M. (2018). Label-free dna-methylation detection by direct ds-dna fragment screening using poly-purine hairpins. *Biosensors and Bioelectronics*, 120:47–54.

Iannazzo, D., Espro, C., Celesti, C., Ferlazzo, A., and Neri, G. (2021). Smart biosensors for cancer diagnosis based on graphene quantum dots. *Cancers*, 13(13):3194.

Idris, A. O., Mamba, B., and Feleni, U. (2020). Poly (propylene imine) dendrimer:

A potential nanomaterial for electrochemical application. *Materials Chemistry and Physics*, 244:122641.

Ignatiadis, M., Lee, M., and Jeffrey, S. S. (2015). Circulating tumor cells and circulating tumor dna: challenges and opportunities on the path to clinical utility. *Clinical Cancer Research*, 21(21):4786–4800.

Inouye, M., Ikeda, R., Takase, M., Tsuri, T., and Chiba, J. (2005). Single-nucleotide polymorphism detection with “wire-like” dna probes that display quasi “on–off” digital action. *Proceedings of the National Academy of Sciences*, 102(33):11606–11610.

Jain, R. K., Di Tomaso, E., Duda, D. G., Loeffler, J. S., Sorensen, A. G., and Batchelor, T. T. (2007). Angiogenesis in brain tumours. *Nature Reviews Neuroscience*, 8(8):610.

Jayanthi, V. S. A., Das, A. B., and Saxena, U. (2017). Recent advances in biosensor development for the detection of cancer biomarkers. *Biosensors and Bioelectronics*, 91:15–23.

Jelski, W. and Mroczko, B. (2021). Molecular and circulating biomarkers of brain tumors. *International journal of molecular sciences*, 22(13):7039.

Jeong, S., Park, J., Pathania, D., Castro, C. M., Weissleder, R., and Lee, H. (2016). Integrated magneto–electrochemical sensor for exosome analysis. *ACS nano*, 10(2):1802–1809.

Jia, F., Wang, Y., Fang, Z., Dong, J., Shi, F., Zhang, W., Wang, Z., and Hu, Z. (2021). Novel peptide-based magnetic nanoparticle for mesenchymal circulating tumor cells detection. *Analytical chemistry*, 93(14):5670–5675.

Jolly, P., Tamboli, V., Harniman, R. L., Estrela, P., Allender, C. J., and Bowen, J. L. (2016). Aptamer–mip hybrid receptor for highly sensitive electrochemical detection of prostate specific antigen. *Biosensors and Bioelectronics*, 75:188–195.

Jolly, P., Zhurauski, P., Hammond, J. L., Miodek, A., Liébana, S., Bertok, T., Tkáč, J., and Estrela, P. (2017). Self-assembled gold nanoparticles for impedimetric and

amperometric detection of a prostate cancer biomarker. *Sensors and Actuators B: Chemical*, 251:637–643.

Jorio, A., Dresselhaus, M. S., Saito, R., and Dresselhaus, G. (2011). *Raman spectroscopy in graphene related systems*. John Wiley & Sons.

Josson, S., Gururajan, M., Sung, S., Hu, P., Shao, C., Zhau, H., Liu, C., Lichterman, J., Duan, P., Li, Q., et al. (2015). Stromal fibroblast-derived mir-409 promotes epithelial-to-mesenchymal transition and prostate tumorigenesis. *Oncogene*, 34(21):2690–2699.

Karimzadeh, A., Hasanzadeh, M., Shadjou, N., and de la Guardia, M. (2018). Peptide based biosensors. *TrAC Trends in Analytical Chemistry*, 107:1–20.

Kerman, K., Kobayashi, M., and Tamiya, E. (2003). Recent trends in electrochemical dna biosensor technology. *Measurement Science and Technology*, 15(2):R1.

Kersting, M., Friedl, C., Kraus, A., Behn, M., Pankow, W., and Schuermann, M. (2000). Differential frequencies of p16ink4a promoter hypermethylation, p53 mutation, and k-ras mutation in exfoliative material mark the development of lung cancer in symptomatic chronic smokers. *Journal of clinical oncology*, 18(18):3221–3229.

Khodaei, R., Ahmady, A., Khoshfetrat, S. M., Kashanian, S., Tavangar, S. M., and Omidfar, K. (2019). Voltammetric immunosensor for e-cadherin promoter dna methylation using a fe 3 o 4-citric acid nanocomposite and a screen-printed carbon electrode modified with poly (vinyl alcohol) and reduced graphene oxide. *Microchimica Acta*, 186(3):170.

Kikuyama, M., Kamisawa, T., Kuruma, S., Chiba, K., Kawaguchi, S., Terada, S., and Satoh, T. (2018). Early diagnosis to improve the poor prognosis of pancreatic cancer. *Cancers*, 10(2):48.

Konios, D., Stylianakis, M. M., Stratakis, E., and Kymakis, E. (2014). Dispersion be-

haviour of graphene oxide and reduced graphene oxide. *Journal of colloid and interface science*, 430:108–112.

Kounaves, S. P. (1997). Voltammetric techniques. *Handbook of instrumental techniques for analytical chemistry*, pages 709–726.

Kovalska, E., Lesongeur, P., Hogan, B., and Baldycheva, A. (2019). Multi-layer graphene as a selective detector for future lung cancer biosensing platforms. *Nanoscale*, 11(5):2476–2483.

Krejcova, L., Richtera, L., Hynek, D., Labuda, J., and Adam, V. (2017). Current trends in electrochemical sensing and biosensing of dna methylation. *Biosensors and Bioelectronics*, 97:384–399.

Krishnamoorthy, K., Veerapandian, M., Yun, K., and Kim, S.-J. (2013). The chemical and structural analysis of graphene oxide with different degrees of oxidation. *Carbon*, 53:38–49.

Krol, I., Castro-Giner, F., Maurer, M., Gkountela, S., Szczerba, B. M., Scherrer, R., Coleman, N., Carreira, S., Bachmann, F., Anderson, S., et al. (2018). Detection of circulating tumour cell clusters in human glioblastoma. *British journal of cancer*, 119(4):487–491.

Kros, J. M., Mustafa, D. M., Dekker, L. J., Sillevis Smitt, P. A., Luider, T. M., and Zheng, P.-P. (2015). Circulating glioma biomarkers. *Neuro-oncology*, 17(3):343–360.

Kuila, T., Bose, S., Khanra, P., Mishra, A. K., Kim, N. H., and Lee, J. H. (2011). Recent advances in graphene-based biosensors. *Biosensors and bioelectronics*, 26(12):4637–4648.

Kurdyukov, S. and Bullock, M. (2016). Dna methylation analysis: choosing the right method. *Biology*, 5(1):3.

Lai, L., Chen, L., Zhan, D., Sun, L., Liu, J., Lim, S. H., Poh, C. K., Shen, Z., and Lin, J.

(2011). One-step synthesis of nh2-graphene from in situ graphene-oxide reduction and its improved electrochemical properties. *Carbon*, 49(10):3250–3257.

Laird, P. W. (2003). Early detection: the power and the promise of dna methylation markers. *Nature Reviews Cancer*, 3(4):253.

Lam, K., Pan, K., Linnekamp, J. F., Medema, J. P., and Kandimalla, R. (2016). Dna methylation based biomarkers in colorectal cancer: A systematic review. *Biochimica et Biophysica Acta (BBA)-Reviews on Cancer*, 1866(1):106–120.

Lather, M. and Singh, P. (2020). Investigating brain tumor segmentation and detection techniques. *Procedia Computer Science*, 167:121–130.

Lauko, A., Lo, A., Ahluwalia, M. S., and Lathia, J. D. (2021). Cancer cell heterogeneity & plasticity in glioblastoma and brain tumors. In *Seminars in Cancer Biology*. Elsevier.

Le, V. H., Nguyen, T. H., Nguyen, H. H., Huynh, L. T. N., Vo, A. L., Nguyen, T. K. T., Nguyen, D. T., and Lam, V. Q. (2020). Fabrication and electrochemical behavior investigation of a pt-loaded reduced graphene oxide composite (pt@ rgo) as a high-performance cathode for dye-sensitized solar cells. *International Journal of Photoenergy*, 2020.

Lee, C.-S., Yu, S. H., and Kim, T. H. (2018). One-step electrochemical fabrication of reduced graphene oxide/gold nanoparticles nanocomposite-modified electrode for simultaneous detection of dopamine, ascorbic acid, and uric acid. *Nanomaterials*, 8(1):17.

Lee, J., Yoshida, W., Abe, K., Nakabayashi, K., Wakeda, H., Hata, K., Marquette, C. A., Blum, L. J., Sode, K., and Ikebukuro, K. (2017). Development of an electrochemical detection system for measuring dna methylation levels using methyl cpg-binding protein and glucose dehydrogenase-fused zinc finger protein. *Biosensors and Bioelectronics*, 93:118–123.

Lee, W.-H., Morton, R. A., Epstein, J. I., Brooks, J. D., Campbell, P. A., Bova, G. S., Hsieh, W. S., Isaacs, W. B., and Nelson, W. G. (1994). Cytidine methylation of regulatory sequences near the pi-class glutathione s-transferase gene accompanies human prostatic carcinogenesis. *Proceedings of the National Academy of Sciences*, 91(24):11733–11737.

Lemeshko, S., Powdrill, T., Belosludtsev, Y., and Hogan, M. (2001). Oligonucleotides form a duplex with non-helical properties on a positively charged surface. *Nucleic acids research*, 29(14):3051–3058.

Leonardi, A. A., Lo Faro, M. J., Fazio, B., Spinella, C., Conoci, S., Livreri, P., and Irrera, A. (2021). Fluorescent biosensors based on silicon nanowires. *Nanomaterials*, 11(11):2970.

Li, B., Pan, G., Avent, N. D., Lowry, R. B., Madgett, T. E., and Waines, P. L. (2015). Graphene electrode modified with electrochemically reduced graphene oxide for label-free dna detection. *Biosensors and Bioelectronics*, 72:313–319.

Li, T., Shang, D., Gao, S., Wang, B., Kong, H., Yang, G., Shu, W., Xu, P., and Wei, G. (2022). Two-dimensional material-based electrochemical sensors/biosensors for food safety and biomolecular detection. *Biosensors*, 12(5):314.

Li, X., Mo, J., Fang, J., Xu, D., Yang, C., Zhang, M., Li, H., Xie, X., Hu, N., and Liu, F. (2020). Vertical nanowire array-based biosensors: device design strategies and biomedical applications. *Journal of Materials Chemistry B*, 8(34):7609–7632.

Li, Y., Deng, L., Deng, C., Nie, Z., Yang, M., and Si, S. (2012). Simple and sensitive aptasensor based on quantum dot-coated silica nanospheres and the gold screen-printed electrode. *Talanta*, 99:637–642.

Li, Z., Lin, Z., Wu, X., Chen, H., Chai, Y., and Yuan, R. (2017). Highly efficient electrochemiluminescence resonance energy transfer system in one nanostructure: its application for ultrasensitive detection of microrna in cancer cells. *Analytical chemistry*, 89(11):6029–6035.

Liang, R.-P., Wang, Z.-X., Zhang, L., and Qiu, J.-D. (2012). A label-free amperometric immunosensor for alpha-fetoprotein determination based on highly ordered porous multi-walled carbon nanotubes/silica nanoparticles array platform. *Sensors and Actuators B: Chemical*, 166:569–575.

Lin, T.-H., Lin, C.-W., Liu, H.-H., Sheu, J.-T., and Hung, W.-H. (2011). Potential-controlled electrodeposition of gold dendrites in the presence of cysteine. *Chemical communications*, 47(7):2044–2046.

Liu, Z. and Ma, Z. (2013). Fabrication of an ultrasensitive electrochemical immunosensor for cea based on conducting long-chain polythiols. *Biosensors and Bioelectronics*, 46:1–7.

Loo, H. K., Mathen, P., Lee, J., and Camphausen, K. (2019). Circulating biomarkers for high-grade glioma.

Lu, B., Smyth, M. R., and O'Kennedy, R. (1996). Tutorial review. oriented immobilization of antibodies and its applications in immunoassays and immunosensors. *Analyst*, 121(3):29R–32R.

Ludwig, J. A. and Weinstein, J. N. (2005). Biomarkers in cancer staging, prognosis and treatment selection. *Nature Reviews Cancer*, 5(11):845–856.

Luppa, P. B., Sokoll, L. J., and Chan, D. W. (2001). Immunosensors—principles and applications to clinical chemistry. *Clinica chimica acta*, 314(1-2):1–26.

Lv, M.-m., Zhu, X.-y., Chen, W.-x., Zhong, S.-l., Hu, Q., Ma, T.-f., Zhang, J., Chen, L., Tang, J.-h., and Zhao, J.-h. (2014). Exosomes mediate drug resistance transfer in mcf-7 breast cancer cells and a probable mechanism is delivery of p-glycoprotein. *Tumor Biology*, 35(11):10773–10779.

Ma, W., Yin, H., Xu, L., Xu, Z., Kuang, H., Wang, L., and Xu, C. (2013). Femtogram ultrasensitive aptasensor for the detection of ochratoxina. *Biosensors and Bioelectronics*, 42:545–549.

Mabbott, G. A. (1983). An introduction to cyclic voltammetry. *Journal of Chemical education*, 60(9):697.

MacArthur, K. M., Kao, G. D., Chandrasekaran, S., Alonso-Basanta, M., Chapman, C., Lustig, R. A., Wileyto, E. P., Hahn, S. M., and Dorsey, J. F. (2014). Detection of brain tumor cells in the peripheral blood by a telomerase promoter-based assay. *Cancer research*, 74(8):2152–2159.

Maduraiveeran, G., Sasidharan, M., and Ganesan, V. (2018). Electrochemical sensor and biosensor platforms based on advanced nanomaterials for biological and biomedical applications. *Biosensors and Bioelectronics*, 103:113–129.

Magesa, F., Wu, Y., Tian, Y., Vianney, J.-M., Buza, J., He, Q., and Tan, Y. (2019). Graphene and graphene like 2d graphitic carbon nitride: Electrochemical detection of food colorants and toxic substances in environment. *Trends in Environmental Analytical Chemistry*, 23:e00064.

Majchrzak-Celińska, A., Paluszczak, J., Kleszcz, R., Magiera, M., Barciszewska, A.-M., Nowak, S., and Baer-Dubowska, W. (2013). Detection of mgmt, rassf1a, p15ink4b, and p14arf promoter methylation in circulating tumor-derived dna of central nervous system cancer patients. *Journal of applied genetics*, 54(3):335–344.

Majchrzak-Celińska, A., Paluszczak, J., Szalata, M., Barciszewska, A.-M., Nowak, S., Kleszcz, R., Sherba, A., and Baer-Dubowska, W. (2015). The methylation of a panel of genes differentiates low-grade from high-grade gliomas. *Tumor Biology*, 36(5):3831–3841.

Marcano, D. C., Kosynkin, D. V., Berlin, J. M., Sinitskii, A., Sun, Z., Slesarev, A., Alemany, L. B., Lu, W., and Tour, J. M. (2010). Improved synthesis of graphene oxide. *ACS nano*, 4(8):4806–4814.

Marrani, A. G., Motta, A., Palmieri, V., Perini, G., Papi, M., Dalchiele, E. A., Schrebler, R., and Zanoni, R. (2020). A comparative experimental and theoretical study of the

mechanism of graphene oxide mild reduction by ascorbic acid and n-acetyl cysteine for biomedical applications. *Materials Advances*, 1(8):2745–2754.

Mattson, E. C., Pande, K., Unger, M., Cui, S., Lu, G., Gajdardziska-Josifovska, M., Weinert, M., Chen, J., and Hirschmugl, C. J. (2013). Exploring adsorption and reactivity of nh3 on reduced graphene oxide. *The Journal of Physical Chemistry C*, 117(20):10698–10707.

Meng, F., Sun, H., Huang, Y., Tang, Y., Chen, Q., and Miao, P. (2019). Peptide cleavage-based electrochemical biosensor coupling graphene oxide and silver nanoparticles. *Analytica Chimica Acta*, 1047:45–51.

Mikeska, T. and Craig, J. M. (2014). Dna methylation biomarkers: cancer and beyond. *Genes*, 5(3):821–864.

Miller, K. D., Ostrom, Q. T., Kruchko, C., Patil, N., Tihan, T., Cioffi, G., Fuchs, H. E., Waite, K. A., Jemal, A., Siegel, R. L., et al. (2021). Brain and other central nervous system tumor statistics, 2021. *CA: a cancer journal for clinicians*, 71(5):381–406.

Müller, C., Holtschmidt, J., Auer, M., Heitzer, E., Lamszus, K., Schulte, A., Matschke, J., Langer-Freitag, S., Gasch, C., Stoupiec, M., et al. (2014). Hematogenous dissemination of glioblastoma multiforme. *Science translational medicine*, 6(247):247ra101–247ra101.

Müller Bark, J., Kulasinghe, A., Chua, B., Day, B. W., and Punyadeera, C. (2020). Circulating biomarkers in patients with glioblastoma. *British journal of cancer*, 122(3):295–305.

Munief, W.-M., Lu, X., Teucke, T., Wilhelm, J., Britz, A., Hempel, F., Lanche, R., Schwartz, M., Law, J. K. Y., Grandthyll, S., et al. (2019). Reduced graphene oxide biosensor platform for the detection of nt-probnp biomarker in its clinical range. *Biosensors and Bioelectronics*, 126:136–142.

Nemati, F., Pebdeni, A., and Hosseini, M. (2022). Chapter 13-graphene-based devices for cancer diagnosis.

Newman, J. D. and Turner, A. P. (2005). Home blood glucose biosensors: a commercial perspective. *Biosensors and bioelectronics*, 20(12):2435–2453.

Ni, Z. H., Yu, T., Lu, Y. H., Wang, Y. Y., Feng, Y. P., and Shen, Z. X. (2008). Uniaxial strain on graphene: Raman spectroscopy study and band-gap opening. *ACS nano*, 2(11):2301–2305.

Ohgaki, H. (2009). Epidemiology of brain tumors. In *Cancer Epidemiology*, pages 323–342. Springer.

Oliveira, N., Souza, E., Ferreira, D., Zanforlin, D., Bezerra, W., Borba, M. A., Arruda, M., Lopes, K., Nascimento, G., Martins, D., et al. (2015). A sensitive and selective label-free electrochemical dna biosensor for the detection of specific dengue virus serotype 3 sequences. *Sensors*, 15(7):15562–15577.

Olmos-Asar, J. A., Ludueña, M., and Mariscal, M. (2014). Monolayer protected gold nanoparticles: The effect of the headgroup–au interaction. *Physical Chemistry Chemical Physics*, 16(30):15979–15987.

Osman, D. I., El-Sheikh, S. M., Sheta, S. M., Ali, O. I., Salem, A. M., Shousha, W. G., El-Khamisy, S. F., and Shawky, S. M. (2019). Nucleic acids biosensors based on metal-organic framework (mof): paving the way to clinical laboratory diagnosis. *Biosensors and Bioelectronics*, 141:111451.

Ouyang, L., Hu, Y., Zhu, L., Cheng, G. J., and Irudayaraj, J. (2017). A reusable laser wrapped graphene-ag array based sers sensor for trace detection of genomic dna methylation. *Biosensors and Bioelectronics*, 92:755–762.

Pantel, K., Brakenhoff, R. H., and Brandt, B. (2008). Detection, clinical relevance and specific biological properties of disseminating tumour cells. *Nature Reviews Cancer*, 8(5):329–340.

Parchekani, J., Hashemzadeh, H., Allahverdi, A., Siampour, H., Abbasian, S., Moshaii, A., and Naderi-Manesh, H. (2021). Zepto molar mirna-21 detection in gold nano-islands platform toward early cancer screening. *Sensing and Bio-Sensing Research*, 34:100449.

Pei, S. and Cheng, H.-M. (2012). The reduction of graphene oxide. *Carbon*, 50(9):3210–3228.

Peng, Y., Lu, B., Deng, Y., Yang, N., and Li, G. (2022). A dual-recognition-controlled electrochemical biosensor for accurate and sensitive detection of specific circulating tumor cells. *Biosensors and Bioelectronics*, page 113973.

Petit, C., Seredych, M., and Bandosz, T. J. (2009). Revisiting the chemistry of graphite oxides and its effect on ammonia adsorption. *Journal of Materials Chemistry*, 19(48):9176–9185.

Pingarrón, J. M., Yanez-Sedeno, P., and González-Cortés, A. (2008). Gold nanoparticle-based electrochemical biosensors. *Electrochimica Acta*, 53(19):5848–5866.

Povedano, E., Gamella, M., Torrente-Rodríguez, R. M., Montiel, V. R.-V., Montero-Calle, A., Solís-Fernández, G., Navarro-Villoslada, F., Pedrero, M., Peláez-García, A., Mendiola, M., et al. (2021). Multiplexed magnetic beads-assisted amperometric bioplatforms for global detection of methylations in nucleic acids. *Analytica chimica acta*, 1182:338946.

Povedano, E., Montiel, V. R.-V., Valverde, A., Navarro-Villoslada, F., Yáñez-Sedeño, P., Pedrero, M., Montero-Calle, A., Barderas, R., Peláez-García, A., Mendiola, M., et al. (2018a). Versatile electroanalytical bioplatforms for simultaneous determination of cancer-related dna 5-methyl-and 5-hydroxymethyl-cytosines at global and gene-specific levels in human serum and tissues. *ACS sensors*, 4(1):227–234.

Povedano, E., Ruiz-Valdepenas Montiel, V., Gamella, M., Pedrero, M., Barderas, R., Pelaez-Garcia, A., Mendiola, M., Hardisson, D., Feliu, J., Yanez-Sedeno, P., et al.

(2020). Amperometric bioplatforms to detect regional dna methylation with single-base sensitivity. *Analytical chemistry*, 92(7):5604–5612.

Povedano, E., Valverde, A., Montiel, V. R.-V., Pedrero, M., Yáñez-Sedeño, P., Barderas, R., San Segundo-Acosta, P., Peláez-García, A., Mendiola, M., Hardisson, D., et al. (2018b). Rapid electrochemical assessment of tumor suppressor gene methylations in raw human serum and tumor cells and tissues using immunomagnetic beads and selective dna hybridization. *Angewandte Chemie International Edition*, 57(27):8194–8198.

Povedano, E., Vargas, E., Montiel, V. R.-V., Torrente-Rodríguez, R. M., Pedrero, M., Barderas, R., San Segundo-Acosta, P., Peláez-García, A., Mendiola, M., and Hardisson, D. (2018c). Electrochemical affinity biosensors for fast detection of gene-specific methylations with no need for bisulfite and amplification treatments. *Scientific reports*, 8(1):6418.

Prabowo, B. A., Cabral, P. D., Freitas, P., and Fernandes, E. (2021). The challenges of developing biosensors for clinical assessment: A review. *Chemosensors*, 9(11):299.

Prieto-Simon, B., Campas, M., and Marty, J.-L. (2008). Biomolecule immobilization in biosensor development: tailored strategies based on affinity interactions. *Protein and peptide letters*, 15(8):757–763.

Putzbach, W. and Ronkainen, N. J. (2013). Immobilization techniques in the fabrication of nanomaterial-based electrochemical biosensors: A review. *Sensors*, 13(4):4811–4840.

Rahman, M., Cui, D., Zhou, S., Zhang, A., and Chen, D. (2020). A graphene oxide coated gold nanostar based sensing platform for ultrasensitive electrochemical detection of circulating tumor dna. *Analytical Methods*, 12(4):440–447.

Rasheed, P. A. and Sandhyarani, N. (2017). Electrochemical dna sensors based on the use of gold nanoparticles: a review on recent developments. *Microchimica Acta*, 184(4):981–1000.

Rashid, J. I. A. and Yusof, N. A. (2017). The strategies of dna immobilization and hybridization detection mechanism in the construction of electrochemical dna sensor: A review. *Sensing and bio-sensing research*, 16:19–31.

Rasooly, A. and Jacobson, J. (2006). Development of biosensors for cancer clinical testing. *Biosensors and Bioelectronics*, 21(10):1851–1858.

Ren, P.-G., Yan, D.-X., Ji, X., Chen, T., and Li, Z.-M. (2010). Temperature dependence of graphene oxide reduced by hydrazine hydrate. *Nanotechnology*, 22(5):055705.

Reth, M. (2013). Matching cellular dimensions with molecular sizes. *Nature immunology*, 14(8):765–767.

Rivera, L., Betancur, A., Zarate, D., Torres, D. T., Hoyos, L., and Garcia, A. (2019). Reduction and simultaneous doping of graphene oxide to repel ldl in treatment of atherosclerosis disease. *arXiv preprint arXiv:1902.01850*.

Ronkainen, N. J., Halsall, H. B., and Heineman, W. R. (2010). Electrochemical biosensors. *Chemical Society Reviews*, 39(5):1747–1763.

Rostami, P., Kashaninejad, N., Moshksayan, K., Saidi, M. S., Firoozabadi, B., and Nguyen, N.-T. (2019). Novel approaches in cancer management with circulating tumor cell clusters. *Journal of Science: Advanced Materials and Devices*, 4(1):1–18.

Ruthven, D. M. (2003). Adsorption (chemical engineering). In Meyers, R. A., editor, *Encyclopedia of Physical Science and Technology (Third Edition)*, pages 251–271. Academic Press, New York, third edition edition.

Saadati, A., Hassanpour, S., de la Guardia, M., Mosafer, J., Hashemzaei, M., Mokhtarzadeh, A., and Baradaran, B. (2019). Recent advances on application of peptide nucleic acids as a bioreceptor in biosensors development. *TrAC Trends in Analytical Chemistry*, 114:56–68.

Saeed, A. A., Sánchez, J. L. A., O'Sullivan, C. K., and Abbas, M. N. (2017). Dna

biosensors based on gold nanoparticles-modified graphene oxide for the detection of breast cancer biomarkers for early diagnosis. *Bioelectrochemistry*, 118:91–99.

Safarzadeh, M., Suhail, A., Sethi, J., Sattar, A., Jenkins, D., and Pan, G. (2021). A label-free dna-immunosensor based on aminated rgo electrode for the quantification of dna methylation. *Nanomaterials*, 11(4):985.

Santangelo, A., Tamanini, A., Cabrini, G., and Dechecchi, M. C. (2017). Circulating microrna as emerging non-invasive biomarkers for gliomas. *Annals of translational medicine*, 5(13).

Santiago-Dieppa, D. R., Steinberg, J., Gonda, D., Cheung, V. J., Carter, B. S., and Chen, C. C. (2014). Extracellular vesicles as a platform for 'liquid biopsy'in glioblastoma patients. *Expert review of molecular diagnostics*, 14(7):819–825.

Schniepp, H. C., Li, J.-L., McAllister, M. J., Sai, H., Herrera-Alonso, M., Adamson, D. H., Prud'homme, R. K., Car, R., Saville, D. A., and Aksay, I. A. (2006). Functionalized single graphene sheets derived from splitting graphite oxide. *The Journal of Physical Chemistry B*, 110(17):8535–8539.

Scott, K. (2016). Electrochemical principles and characterization of bioelectrochemical systems. In *Microbial Electrochemical and Fuel Cells*, pages 29–66. Elsevier.

Sethi, J., Van Bulck, M., Suhail, A., Safarzadeh, M., Perez-Castillo, A., and Pan, G. (2020). A label-free biosensor based on graphene and reduced graphene oxide dual-layer for electrochemical determination of beta-amyloid biomarkers. *Microchimica Acta*, 187:1–10.

Shahrokhian, S. and Salimian, R. (2018). Ultrasensitive detection of cancer biomarkers using conducting polymer/electrochemically reduced graphene oxide-based biosensor: Application toward brca1 sensing. *Sensors and Actuators B: Chemical*, 266:160–169.

Shankar, G. M., Balaj, L., Stott, S. L., Nahed, B., and Carter, B. S. (2017). Liquid biopsy for brain tumors. *Expert review of molecular diagnostics*, 17(10):943–947.

Shanmuganathan, R., Basheer, N. B., Amirthalingam, L., Muthukumar, H., Kaliaperumal, R., and Shanmugam, K. (2013). Conventional and nanotechniques for dna methylation profiling. *The Journal of Molecular Diagnostics*, 15(1):17–26.

Shao, Y., Wang, J., Wu, H., Liu, J., Aksay, I. A., and Lin, Y. (2010). Graphene based electrochemical sensors and biosensors: a review. *Electroanalysis: An International Journal Devoted to Fundamental and Practical Aspects of Electroanalysis*, 22(10):1027–1036.

Sharifi, M., Avadi, M. R., Attar, F., Dashtestani, F., Ghorchian, H., Rezayat, S. M., Saboury, A. A., and Falahati, M. (2019). Cancer diagnosis using nanomaterials based electrochemical nanobiosensors. *Biosensors and Bioelectronics*, 126:773–784.

Shen, M., Rusling, J. F., and Dixit, C. K. (2017). Site-selective orientated immobilization of antibodies and conjugates for immunodiagnostics development. *Methods*, 116:95–111.

Shi, X., He, Y., Gao, W., Liu, X., Ye, Z., Liu, H., and Xiao, L. (2018). Quantifying the degree of aggregation from fluorescent dye-conjugated dna probe by single molecule photobleaching technology for the ultrasensitive detection of adenosine. *Analytical chemistry*, 90(6):3661–3665.

Shindo, D. and Oikawa, T. (2002). Energy dispersive x-ray spectroscopy. In *Analytical electron microscopy for materials science*, pages 81–102. Springer.

Siegel, R. L., Miller, K. D., and Jemal, A. (2019). Cancer statistics, 2019. *CA: a cancer journal for clinicians*, 69(1):7–34.

Silva, J. M., Dominguez, G., Garcia, J. M., Gonzalez, R., Villanueva, M. J., Navarro, F., Provencio, M., San Martin, S., Espana, P., and Bonilla, F. (1999). Presence of tumor

dna in plasma of breast cancer patients: clinicopathological correlations. *Cancer research*, 59(13):3251–3256.

Simões, F. R. and Xavier, M. G. (2017). Electrochemical sensors. *Nanoscience and its Applications*, pages 155–178.

Singh, A., Sinsinbar, G., Choudhary, M., Kumar, V., Pasricha, R., Verma, H., Singh, S. P., and Arora, K. (2013). Graphene oxide-chitosan nanocomposite based electrochemical dna biosensor for detection of typhoid. *Sensors and Actuators B: Chemical*, 185:675–684.

Singh, S., Kaushal, A., Khare, S., Kumar, P., and Kumar, A. (2014). Gold–mercaptopropionic acid–polyethylenimine composite based dna sensor for early detection of rheumatic heart disease. *Analyst*, 139(14):3600–3606.

Sonali, M. K. V., Singh, R. P., Agrawal, P., Mehata, A. K., Datta Maroti Pawde, N., Sonkar, R., and Muthu, M. S. (2018). Nanotheranostics: emerging strategies for early diagnosis and therapy of brain cancer. *Nanotheranostics*, 2(1):70.

Stevie, F. A. and Donley, C. L. (2020). Introduction to x-ray photoelectron spectroscopy. *Journal of Vacuum Science & Technology A: Vacuum, Surfaces, and Films*, 38(6):063204.

Stobinski, L., Lesiak, B., Malolepszy, A., Mazurkiewicz, M., Mierzwa, B., Zemek, J., Jiricek, P., and Bieloshapka, I. (2014). Graphene oxide and reduced graphene oxide studied by the xrd, tem and electron spectroscopy methods. *Journal of Electron Spectroscopy and Related Phenomena*, 195:145–154.

Su, S., Sun, H., Cao, W., Chao, J., Peng, H., Zuo, X., Yuwen, L., Fan, C., and Wang, L. (2016). Dual-target electrochemical biosensing based on dna structural switching on gold nanoparticle-decorated mos2 nanosheets. *ACS applied materials & interfaces*, 8(11):6826–6833.

Sullivan, J. P., Nahed, B. V., Madden, M. W., Oliveira, S. M., Springer, S., Bhere, D., Chi, A. S., Wakimoto, H., Rothenberg, S. M., Sequist, L. V., et al. (2014). Brain tumor cells in circulation are enriched for mesenchymal gene expression. *Cancer discovery*, 4(11):1299–1309.

Suresh, L., Brahman, P. K., Reddy, K. R., and Bondili, J. (2018). Development of an electrochemical immunosensor based on gold nanoparticles incorporated chitosan biopolymer nanocomposite film for the detection of prostate cancer using psa as biomarker. *Enzyme and microbial technology*, 112:43–51.

Suter, R. K., Rodriguez-Blanco, J., and Ayad, N. G. (2020). Epigenetic pathways and plasticity in brain tumors. *Neurobiology of disease*, 145:105060.

Suvarnaphaet, P. and Pechprasarn, S. (2017). Graphene-based materials for biosensors: a review. *Sensors*, 17(10):2161.

Syedmoradi, L., Esmaeili, F., and Norton, M. L. (2016). Towards dna methylation detection using biosensors. *Analyst*, 141(21):5922–5943.

Szunerits, S. and Boukherroub, R. (2018). Graphene-based biosensors. *Interface focus*, 8(3):20160132.

Tadokoro, H., Umezu, T., Ohyashiki, K., Hirano, T., and Ohyashiki, J. H. (2013). Exosomes derived from hypoxic leukemia cells enhance tube formation in endothelial cells. *Journal of Biological Chemistry*, 288(48):34343–34351.

Tahernejad-Javazmi, F., Shabani-Nooshabadi, M., and Karimi-Maleh, H. (2018). Gold nanoparticles and reduced graphene oxide-amplified label-free dna biosensor for dasatinib detection. *New Journal of Chemistry*, 42(19):16378–16383.

Tamimi, A. F. and Juweid, M. (2017). Epidemiology and outcome of glioblastoma. In *Glioblastoma [Internet]*. Codon Publications.

Tang, S. and Cao, Z. (2011). Adsorption of nitrogen oxides on graphene and graphene

oxides: Insights from density functional calculations. *The Journal of chemical physics*, 134(4):044710.

Tang, S. and Cao, Z. (2012). Adsorption and dissociation of ammonia on graphene oxides: a first-principles study. *The Journal of Physical Chemistry C*, 116(15):8778–8791.

Teles, F. and Fonseca, L. (2008). Applications of polymers for biomolecule immobilization in electrochemical biosensors. *Materials Science and Engineering: C*, 28(8):1530–1543.

Thakare, S., Shaikh, A., Bodas, D., and Gajbhiye, V. (2022). Application of dendrimer-based nanosensors in immunodiagnosis. *Colloids and Surfaces B: Biointerfaces*, 209:112174.

Thakur, A., Qiu, G., Siu-Pang, N., Guan, J., Yue, J., Lee, Y., and Wu, C.-M. L. (2017). Direct detection of two different tumor-derived extracellular vesicles by sam-aunis lspr biosensor. *Biosensors and Bioelectronics*, 94:400–407.

Thakur, V. K. and Thakur, M. K. (2015). *Chemical functionalization of carbon nanomaterials: Chemistry and applications*. CRC Press.

Thevendran, R., Foo, K. L., Hussin, M. H., Moses, E. J., Citartan, M., Prasad, H. R., and Maheswaran, S. (2022). Reverse electrochemical sensing of flt3-itd mutations in acute myeloid leukemia using gold sputtered zno-nanorod configured dna biosensors. *Biosensors*, 12(3):170.

Tian, R., Ning, W., Chen, M., Zhang, C., Li, Q., and Bai, J. (2019). High performance electrochemical biosensor based on 3d nitrogen-doped reduced graphene oxide electrode and tetrahedral dna nanostructure. *Talanta*, 194:273–281.

Tidy, C. (2018).

Tothill, I. E. (2009). Biosensors for cancer markers diagnosis. In *Seminars in cell & developmental biology*, volume 20, pages 55–62. Elsevier.

Touat, M., Duran-Peña, A., Alentorn, A., Lacroix, L., Massard, C., and Idbaih, A. (2015). Emerging circulating biomarkers in glioblastoma: promises and challenges. *Expert review of molecular diagnostics*, 15(10):1311–1323.

Trilling, A. K., Beekwilder, J., and Zuilhof, H. (2013). Antibody orientation on biosensor surfaces: a minireview. *Analyst*, 138(6):1619–1627.

Trotter, M., Borst, N., Thewes, R., and von Stetten, F. (2020). Electrochemical dna sensing–principles, commercial systems, and applications. *Biosensors and Bioelectronics*, page 112069.

Ul-Hamid, A. (2018). *A beginners' guide to scanning electron microscopy*, volume 1. Springer.

Usadel, H., Brabender, J., Danenberg, K. D., Jerónimo, C., Harden, S., Engles, J., Danenberg, P. V., Yang, S., and Sidransky, D. (2002). Quantitative adenomatous polyposis coli promoter methylation analysis in tumor tissue, serum, and plasma dna of patients with lung cancer. *Cancer research*, 62(2):371–375.

Vernon-Parry, K. (2000). Scanning electron microscopy: an introduction. *III-Vs Review*, 13(4):40–44.

Vrba, L. and Futscher, B. W. (2018). A suite of dna methylation markers that can detect most common human cancers. *Epigenetics*, 13(1):61–72.

Wan, J., Massie, C., Garcia-Corbacho, J., Mouliere, F., Brenton, J. D., Caldas, C., Pacey, S., Baird, R., and Rosenfeld, N. (2017). Liquid biopsies come of age: towards implementation of circulating tumour dna. *Nature Reviews Cancer*, 17(4):223–238.

Wang, C., Liu, Y., Chen, R., Wang, X., Wang, Y., Wei, J., Zhang, K., and Zhang, C. (2022). Electrochemical biosensing of circulating microrna-21 in cerebrospinal fluid of medulloblastoma patients through target-induced redox signal amplification. *Microchimica Acta*, 189(3):1–9.

Wang, J. (2002). Electrochemical nucleic acid biosensors. *Analytica chimica acta*, 469(1):63–71.

Wang, J. (2006). Electrochemical biosensors: towards point-of-care cancer diagnostics. *Biosensors and Bioelectronics*, 21(10):1887–1892.

Wang, J. (2012). Electrochemical biosensing based on noble metal nanoparticles. *Microchimica Acta*, 177(3-4):245–270.

Wang, J. and Bettegowda, C. (2017). Applications of dna-based liquid biopsy for central nervous system neoplasms. *The Journal of Molecular Diagnostics*, 19(1):24–34.

Wang, L. (2017). Early diagnosis of breast cancer. *sensors*, 17(7):1572.

Wang, S., Wang, R., Sellin, P., and Zhang, Q. (2004). Dna biosensors based on self-assembled carbon nanotubes. *Biochemical and biophysical research communications*, 325(4):1433–1437.

Wang, X., Cheng, S., Wang, X., Wei, L., Kong, Q., Ye, M., Luo, X., Xu, J., Zhang, C., and Xian, Y. (2021a). ph-sensitive dye-based nanobioplatform for colorimetric detection of heterogeneous circulating tumor cells. *ACS sensors*, 6(5):1925–1932.

Wang, Y.-H., Song, Z., Hu, X.-Y., and Wang, H.-S. (2021b). Circulating tumor dna analysis for tumor diagnosis. *Talanta*, 228:122220.

Wang, Z., Zhou, X., Zhang, J., Boey, F., and Zhang, H. (2009). Direct electrochemical reduction of single-layer graphene oxide and subsequent functionalization with glucose oxidase. *The Journal of Physical Chemistry C*, 113(32):14071–14075.

Wei, L., Wang, P., Yang, Y., Luo, R., Li, J., Gu, X., Zhan, Z., Dong, Y., Song, W., and Fan, R. (2018). Facile synthesis of nitrogen-doped reduced graphene oxide as an efficient counter electrode for dye-sensitized solar cells. *Journal of Nanoparticle Research*, 20(4):110.

Welch, N. G., Scoble, J. A., Muir, B. W., and Pigram, P. J. (2017). Orientation and characterization of immobilized antibodies for improved immunoassays. *Biointerphases*, 12(2):02D301.

Westphal, M. and Lamszus, K. (2015). Circulating biomarkers for gliomas. *Nature Reviews Neurology*, 11(10):556–566.

Whitehead, C. A., Kaye, A. H., Drummond, K. J., Widodo, S. S., Mantamadiotis, T., Vella, L. J., and Stylli, S. S. (2020). Extracellular vesicles and their role in glioblastoma. *Critical reviews in clinical laboratory sciences*, 57(4):227–252.

WHO (2018).

Wu, B., Zhao, N., Hou, S., and Zhang, C. (2016). Electrochemical synthesis of polypyrrole, reduced graphene oxide, and gold nanoparticles composite and its application to hydrogen peroxide biosensor. *Nanomaterials*, 6(11):220.

Wu, J.-B., Lin, M.-L., Cong, X., Liu, H.-N., and Tan, P.-H. (2018). Raman spectroscopy of graphene-based materials and its applications in related devices. *Chemical Society Reviews*, 47(5):1822–1873.

Xiao, L., Xu, L., Gao, C., Zhang, Y., Yao, Q., and Zhang, G.-J. (2016). A mos2 nanosheet-based fluorescence biosensor for simple and quantitative analysis of dna methylation. *Sensors*, 16(10):1561.

Xu, R., Rai, A., Chen, M., Suwakulsiri, W., Greening, D. W., and Simpson, R. J. (2018). Extracellular vesicles in cancer—implications for future improvements in cancer care. *Nature reviews Clinical oncology*, 15(10):617–638.

Yanez-Sedeno, P. and Pingarron, J. (2005). Gold nanoparticle-based electrochemical biosensors. *Analytical and bioanalytical chemistry*, 382(4):884–886.

Yang, C., Denno, M. E., Pyakurel, P., and Venton, B. J. (2015a). Recent trends in carbon nanomaterial-based electrochemical sensors for biomolecules: A review. *Analytica chimica acta*, 887:17–37.

Yang, D., Velamakanni, A., Bozoklu, G., Park, S., Stoller, M., Piner, R. D., Stankovich, S., Jung, I., Field, D. A., Ventrice Jr, C. A., et al. (2009). Chemical analysis of graphene oxide films after heat and chemical treatments by x-ray photoelectron and micro-raman spectroscopy. *Carbon*, 47(1):145–152.

Yang, H., Ren, J., Zhao, M., Chen, C., Wang, F., and Chen, Z. (2022). Novel electrochemical immunosensor for o6-methylguanine-dna methyltransferase gene methylation based on graphene oxide-magnetic nanoparticles-β-cyclodextrin nanocomposite. *Bioelectrochemistry*, 146:108111.

Yang, W., Ratinac, K. R., Ringer, S. P., Thordarson, P., Gooding, J. J., and Braet, F. (2010). Carbon nanomaterials in biosensors: should you use nanotubes or graphene? *Angewandte Chemie International Edition*, 49(12):2114–2138.

Yang, Y., Fu, Y., Su, H., Mao, L., and Chen, M. (2018). Sensitive detection of mcf-7 human breast cancer cells by using a novel dna-labeled sandwich electrochemical biosensor. *Biosensors and Bioelectronics*, 122:175–182.

Yang, Y., Mao, G., Ji, X., and He, Z. (2020). Dna-templated quantum dots and their applications in biosensors, bioimaging, and therapy. *Journal of materials chemistry B*, 8(1):9–17.

Yang, Z.-z., Zheng, Q.-b., Qiu, H.-x., Jing, L., and Yang, J.-h. (2015b). A simple method for the reduction of graphene oxide by sodium borohydride with cacl2 as a catalyst. *New Carbon Materials*, 30(1):41–47.

Yekula, A., Yekula, A., Muralidharan, K., Kang, K., Carter, B. S., and Balaj, L. (2020). Extracellular vesicles in glioblastoma tumor microenvironment. *Frontiers in immunology*, 10:3137.

Yildizhan, Y., Vajrala, V. S., Geeurickx, E., Declerck, C., Duskunovic, N., De Sutter, D., Noppen, S., Delport, F., Schols, D., Swinnen, J. V., et al. (2021). Fo-spr biosensor calibrated with recombinant extracellular vesicles enables specific and sensitive detection directly in complex matrices. *Journal of extracellular vesicles*, 10(4):e12059.

Yüce, M. and Kurt, H. (2017). How to make nanobiosensors: surface modification and characterisation of nanomaterials for biosensing applications. *RSC advances*, 7(78):49386–49403.

Zachariah, M. A., Oliveira-Costa, J. P., Carter, B. S., Stott, S. L., and Nahed, B. V. (2018). Blood-based biomarkers for the diagnosis and monitoring of gliomas. *Neuro-oncology*, 20(9):1155–1161.

Zafar, Z., Ni, Z. H., Wu, X., Shi, Z. X., Nan, H. Y., Bai, J., and Sun, L. T. (2013). Evolution of raman spectra in nitrogen doped graphene. *Carbon*, 61:57–62.

Zhang, H., Fan, M., Jiang, J., Shen, Q., Cai, C., and Shen, J. (2019). Sensitive electrochemical biosensor for micrornas based on duplex-specific nuclease-assisted target recycling followed with gold nanoparticles and enzymatic signal amplification. *Analytica chimica acta*, 1064:33–39.

Zhang, K., Xie, M., Zhou, B., Hua, Y., Yan, Z., Liu, H., Guo, L.-n., Wu, B., and Huang, B. (2013). A new strategy based on aptasensor to time-resolved fluorescence assay for adenosine deaminase activity. *Biosensors and Bioelectronics*, 41:123–128.

Zhang, L., Mazouzi, Y., Salmain, M., Liedberg, B., and Boujday, S. (2020). Antibody-gold nanoparticle bioconjugates for biosensors: synthesis, characterization and selected applications. *Biosensors and Bioelectronics*, 165:112370.

Zhao, C., Wang, H., Xiong, C., and Liu, Y. (2018). Hypoxic glioblastoma release exosomal vegf-a induce the permeability of blood-brain barrier. *Biochemical and biophysical research communications*, 502(3):324–331.

Zhao, H., Qu, Y., Yuan, F., and Quan, X. (2016). A visible and label-free colorimetric sensor for mirna-21 detection based on peroxidase-like activity of graphene/gold-nanoparticle hybrids. *Analytical Methods*, 8(9):2005–2012.

Zhou, L., Wang, K., Sun, H., Zhao, S., Chen, X., Qian, D., Mao, H., and Zhao, J. (2019). Novel graphene biosensor based on the functionalization of multifunctional

nano-bovine serum albumin for the highly sensitive detection of cancer biomarkers. *Nano-Micro Letters*, 11(1):20.

Zhou, W., Apkarian, R., Wang, Z. L., and Joy, D. (2006). Fundamentals of scanning electron microscopy (sem). In *Scanning microscopy for nanotechnology*, pages 1–40. Springer.

Zhou, X., Pu, Q., Yu, H., Peng, Y., Li, J., Yang, Y., Chen, H., Weng, Y., and Xie, G. (2021). An electrochemical biosensor based on hemin/g-quadruplex dnazyme and pdru/pt heterostructures as signal amplifier for circulating tumor cells detection. *Journal of Colloid and Interface Science*, 599:752–761.

Zhu, Y., Murali, S., Cai, W., Li, X., Suk, J. W., Potts, J. R., and Ruoff, R. S. (2010). Graphene and graphene oxide: synthesis, properties, and applications. *Advanced materials*, 22(35):3906–3924.